Stabilization of magnetic islands in tokamaks by localized heating and current drive

Stabilization of magnetic islands in tokamaks by localized heating and current drive

A numerical approach

Stabilisatie van magnetische eilanden in tokamaks door toepassing van lokale verwarming en stroomaandrijving

Proefschrift

ter verkrijging van de graad van doctor aan de Technische Universiteit Eindhoven, op gezag van de rector magnificus, prof.dr.ir. C.J. van Duijn, voor een commissie aangewezen door het College voor Promoties in het openbaar te verdedigen op maandag 23 mei 2011 om 14.00 uur

door

Diego De Lazzari

geboren te Treviso, Italië

Dit proefschrift is goedgekeurd door de promotoren:

prof.dr. N.J. Lopes Cardozo
en
prof.dr. W.J. Goedheer

Copromotor:
dr. E. Westerhof

Ai miei Genitori

Contents

1   Introduction

1.1   The growing demand for energy

The sustainability of the contemporary economy depends mainly on the availability of fossil fuels. In 2007 [Priddle et al., 2009] about 81.4% of the total annual energy consumption, estimated as 12 billion tonnes of oil equivalent, was covered by oil (34%), coal (26.5%) and natural gas (20.9%). The present level of consumption leads to the progressive depletion of these resources.

The rapid growth of the world population (predicted to reach 10 billion people within 2050) and the growth of the economy of developing countries leads to an even further increase in the energy demand. The International Energy Agency [Priddle et al., 2009; International Energy Agency, 2009] predicts a growth of 57% in world energy consumption, in the period $2004 - 2030$. The increase will be much greater (95%) in the non-OECD countries[1] than in the OECD countries (24%). The total estimated consumption for 2030 is about 18 billion tonnes of oil equivalent, as shown in figure 1.2(b). The environmental impact due to the massive consumption of fossil fuels, namely the production of greenhouse gases which is directly related with the global warming [Bernstein et al., 2007], sets a further constraint.

A solution is expected to come from the development of alternative, sustainable, CO_2-free energy sources. Several examples of alternative sources are available, namely solar, wind, hydro, bio and nuclear energy. None of these represents yet a ultimate, reliable substitute of fossil fuels. Table 1.1 shows that in order to produce 1 GWyr electric power, the size of a power plant (or the amount of raw material) required, may differ by several orders of magnitude depending on the primary energy source. Renewable energy sources, in principle inexhaustible and environmentally friendly, are available in almost any place around the world. The energy density produced by each unit, such as solar panels or wind turbines, is rather modest i.e. large areas are required. This makes these sources very suitable for a decentralized distribution of electricity. Nuclear power plants, presently exploiting the principle of nuclear fission, provide high concentration of energy but they suffer of a low social acceptance due to the risk of major accidents, to long-lived nuclear waste and to the proliferation of fissile material. In addition to this, the world reserves of uranium are not well known and the use of breeders to close the fuel cycle, in alternative to the storage of exhausted fuel as such, is still under development.

The picture drawn so far addresses the necessity of a diversified energy system, in which the weight of fossil energy is slowly reduced in favour of more sustainable solutions from an economical and environmental point of view. In this mixed energy scenario all possible sources are implemented, so that the risks and negative impacts of all sources can be limited. The capability of developing a sustainable energy infrastructure

---

[1]The so called "developing countries", not belonging to the Organization for Economic Cooperation and Development (OECD)

Energy source	Fuel needed for a 1000MW power plant, during one year	Approximate land use for a 1000MW plant (km2)	Comments
Biomass	30,000 km2 of woods	30,000	
Wind	2700 wind turbines of 1.5MW	490	
Solar PV	23 km2 of solar panels	23	placed in a country near the equator
Biogas	60 million pigs	600	pigs are held for food, energy is extra.
Gas	1.2 km3	1	
Oil	1,400,000 tons	1	10,000,000 oil barrels or 100 oil tankers
Coal	2,500,000 tons	1+ mines	26,260 train waggon loads
Nuclear fission	35 tons of uranium oxide	1+ mines	from 210 tons of uranium ore
Fusion	100 kg deuterium and 150 kg tritium	1+ mines	from 2850 m3 of sea water and 10 tons of lithium ore

Figure 1.1: Fuel requirements for different energy sources. In the table [Westra et al., 2005], the fuel use is shown for a $1,000$ MW power plant for one year (total output about $7,000$ million kWh). Clearly, wind, solar and biomass need a lot of space. Fission and fusion stand out as they require only very modest amounts of fuel.
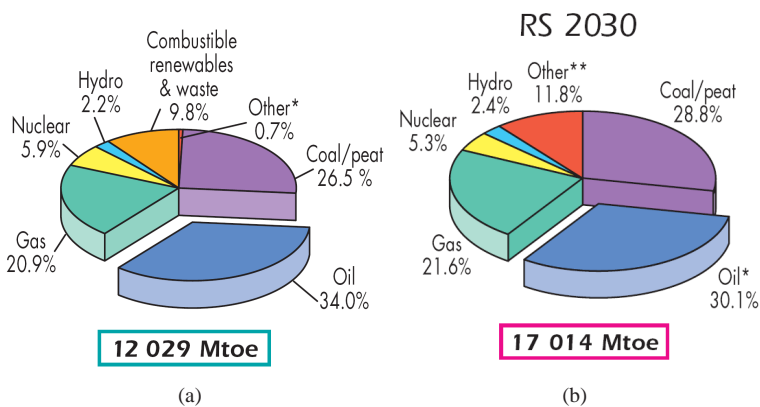
Figure 1.2: (a) Fuel shares of total primary energy supply (TPES) in 2007 and (b) in 2030, based on current climate-policy frameworks [Priddle et al., 2009].

will strongly depend on the improvement of existing technologies and on the efficiency with which the energy is distributed and consumed.

Fusion power is usually not taken into account in energy scenarios up to 2050, as it is expected that fusion will not be commercially available before 2040 - 2050. The enor-

mous potential of this technology lies in the combination of a very high energy density and higher environmental safety as compared to nuclear fission. Nuclear fusion technology can also be coupled, as neutron source, to the traditional nuclear fission reactor in order to reduce the nuclear waste and avoid the issues related with chain reactions [Bethe, 1979; Gerstner, 2009]. This type of sub-critical reactor could overcome some of the above mentioned criticism concerning the use of nuclear fission.

1.2   Introduction to nuclear fusion

Nuclear fusion, the merging of light atomic nuclei to form heavier ones, is the process powering the sun and stars. In the core of the sun, the temperature (≈ 1.3 keV) and the density ($\approx 1.5 \times 10^5$ kg m^{-3}) are sufficiently high to allow the positively charged nuclei to overcome the Coulomb barrier and reach distances of the order of 10^{-15} m, where the nuclear attractive force becomes dominant. At these temperatures, well above typical ionization energies (13.6 eV in the hydrogen case), the fusion reactants exist in the plasma state and they are confined by the gravitational force.

The most promising fusion reaction for a first generation nuclear power plant is the fusion of the hydrogen isotopes deuterium (D) and tritium (T)

$$D + T \rightarrow He(3.5\text{MeV}) + n(14.1\text{MeV}), \tag{1.1}$$
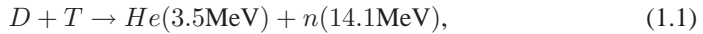
producing an α particle, a neutron and a total (kinetic) energy of 17.6 MeV. Compared with other possible fusion reactions, such as D-D or D-^{3}He, the D-T reaction shows the highest reaction rate, $\langle \sigma v \rangle$, for energies between 50 to 80 keV (see figure 1.3(a)). The reaction rate is calculated by averaging the cross section over the reactant thermal distribution. To determine the requirements for a net energy output, the fusion power density is calculated [Wesson, 2004] as

$$P_{\text{DT}} = \frac{1}{4} \overline{n^2 \langle \sigma v \rangle} k E_{\text{DT}} \quad \text{MWm}^{-3}, \tag{1.2}$$

where $n = 2n_{\text{D}} = 2n_{\text{T}}$ is the fuel ion density and E_{DT} the total reaction energy. The bar indicates the average over the plasma volume. Since 80% of the energy delivered in the D-T reaction is carried by neutrons, escaping from the plasma, only α particles can be involved in the heating process. In present day tokamaks the α-power is usually small and in steady state external heating, P_{aux} is supplied to balance the rate of energy loss from the plasma. The break even point is said to be reached when $P_{\text{DT}} = P_{\text{aux}}$. The power density lost from the plasma is defined as the total plasma energy density devided by the energy confinement time τ_{E},

$$P_{\text{L}} = \frac{3 \overline{nT}}{\tau_{\text{E}}} \quad \text{MWm}^{-3}, \tag{1.3}$$

where T refers to the plasma temperature. The "ignition" is reached when the power produced by α-particles is sufficient to sustain the plasma, such that $P_\alpha \geq P_{\text{L}}$. This

inequality, leads to a figure of merit for ignition requirements, $n\tau_E$, depending only on the temperature. This parameter has a optimum for $T \approx 30\,\text{keV}$, as shown in figure 1.3(b). As the energy confinement time scales also with the temperature, the optimal temperature for ignition is further reduced to $10-20\,\text{keV}$. In this range the DT reaction rate is proportional to T^2 and the triple product of ion density, temperature and energy confinement time is a constant. The ignition condition, known as "Lawson" criterion [Lawson, 1957] is,

$$nT\tau_E \geq 3 \times 10^{21}\text{m}^{-3}\,\text{s keV}\,. \qquad (1.4)$$

(a)   (b)
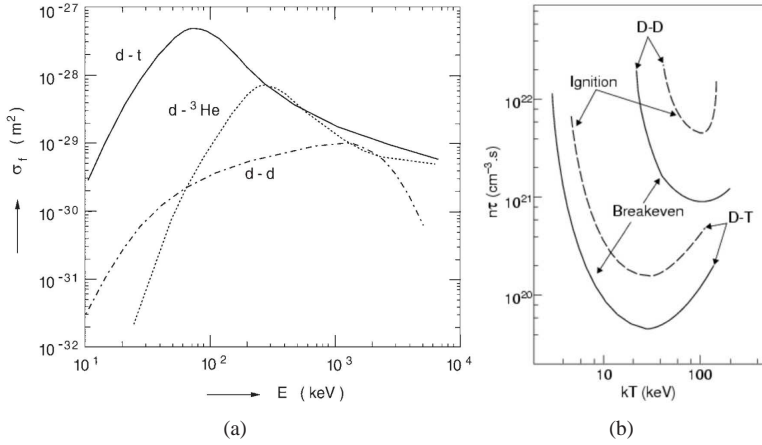
Figure 1.3: In (a) the cross section for deuterium-tritium, deuterium-deuterium and deuterium-^{3}He reaction is shown. At lower energies the probability that a fusion reactor will take place is much higher for a D-T reaction. In (b) the ignition and the break-even criteria, for deuterium-tritium and deuterium-deuterium reactions, are compared.

A different approach to nuclear energy

The most remarkable advantages in the use of nuclear fusion concern the inherent safety of the reaction, the lack of long-lived radioactive waste and the fuel availability. In first place a fusion reactor needs to be continuously fueled, in order to be sustained. This reduces significantly the issues related with power plant accidents, namely explosion or radioactive leakage. An uncontrolled increase in fusion fuel would lead to the plasma being extinguished as it cannot be sustained when the plasma density is too high. In second place, it is noticed that both the fuel and the products of a fusion reaction are not radioactive. The nuclear waste produced by a fusion reactor consists of the radioactive tritium and the in-vessel materials activated by high neutron energy. After ≈ 100 years,

the level of radioactivity calculated for a decommissioned reactor is estimated to be comparable to that of coal ashes. The only radioactive isotope occurring during the reaction is tritium, with a half-life of about 12.3 years. This is produced by a neutron-induced fission reaction from lithium, exploiting the neutrons released by the D-T reaction:

$$Li^6 + n \rightarrow T + He^4 + 4.8\text{MeV}. \tag{1.5}$$

In a 1GWyr power plant the annual amount of tritium and deuterium required is very limited, estimated to be about 150 kg. Last but not least, nuclear fusion does not produce greenhouse gases. The third main advantage of nuclear fusion regards the abundance of fuel, deuterium and lithium. Deuterium can be extracted from the sea water, in principle without limits. Known land reserves of lithium are sufficient to satisfy the world energy consumption for about 1000 years. These resources are distributed all over the planet, overcoming in this way the present geopolitical tensions related to the control over oil or uranium reserves. A final note concerns the economical feasibility of a reactor taking into account the costs of design and construction. This is a difficult estimate, considering that the technology is still under development. Using near term technology, the Power Plant Conceptual Study (PPCS) [Maisonnier et al., 2005] calculates the cost of a kWh as 5 to 9 eurocents for a 5 GW plant.

Plasma confinement

On earth, the high density and the gravitational confinement occurring in the sun are not achievable. It is possible though, to increase the temperature. The method generally exploited in order to keep energy and particles in the plasma, and hence to limit the outward energy and particle fluxes, is the magnetic confinement. This is achieved by generating a high (toroidal) magnetic field so that the charged ions of fusion fuel follow spiral orbits around the field lines. The fuel is therefore trapped along the field lines and can be heated to the required temperature by external means. Magnetic confinement has been proposed in a number of different configurations. The most successful is known as Tokamak [Wesson, 2004] (**To**roidal'naya **ka**mera s **ma**gnitnymi **k**atushkami), i.e. toroidal chamber with magnetic coils (see figure 1.4).

In a tokamak the main magnetic field is produced in the toroidal direction by a set of coils surrounding a toroidal vacuum vessel. A current flowing trough the plasma, in the toroidal direction, provides a further magnetic field in the poloidal direction and heats the plasma. This current is driven by the toroidal electric field induced by means of a transformer. As the current in the primary transformer circuit is ramped up, a varying magnetic flux in the transformer's core is produced, inducing in turn a toroidal electric field in the secondary transformer circuit, i.e. the plasma.

In the central region, the temperature can reach 15 keV, about 10 times the temperature in the core of the sun. Further details are given in the following chapter. The tokamak has proven to be the most promising machine currently available, to achieve ignition. The Joint European Tokamak (JET), currently the world largest tokamak, obtained a record peak fusion power in a D-T plasma of 16 MW. This corresponded to a measured energy
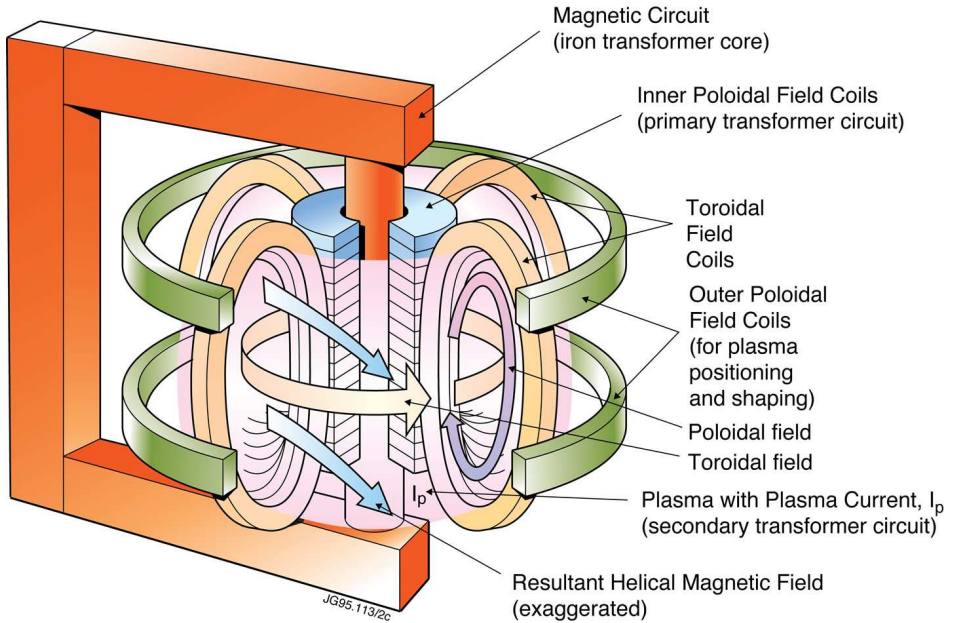
Figure 1.4: Tokamak concept (property of EFDA-JET)

multiplication factor Q of approximately 0.7. The parameter $Q = P_{\mathrm{DT}}/P_{\mathrm{aux}}$ is the ratio of fusion power to input heating power. These experiments have opened the way to future nuclear fusion experimental reactors such as ITER [Shimada et al., 2007], presently being built in France. ITER, aims to demonstrate the technical feasibility of nuclear fusion, is designed to achieve a Q of about 10.

1.3 Introduction to the topic of the thesis

From an ideal confinement to magnetic islands

The combination of the toroidal and poloidal component of the magnetic field results in helical field lines, which form toroidal, magnetic surfaces. For a plasma in equilibrium (magnetic pressure is balanced by the plasma pressure), no pressure gradient along field lines is allowed, leading to isobaric magnetic surfaces. As the heat transport along the field lines is very fast, the surfaces are also isothermal. The number of toroidal windings necessary for a field line to complete a poloidal orbit is defined with the parameter q, also known as safety factor. When q is an irrational number the field line is ergodic, i.e. it covers the entire toroidal surface. For rational values of $q = m/n$ the field line closes upon itself after m toroidal and n poloidal windings, respectively. These surfaces, in particular at low rational q, are critical with respect to magnetic field perturbations. As

a consequence, the magnetic configuration, ideally structured as a set of nested surfaces, is prone to reconnection phenomena, resulting generally in a loss of particle and energy confinement.
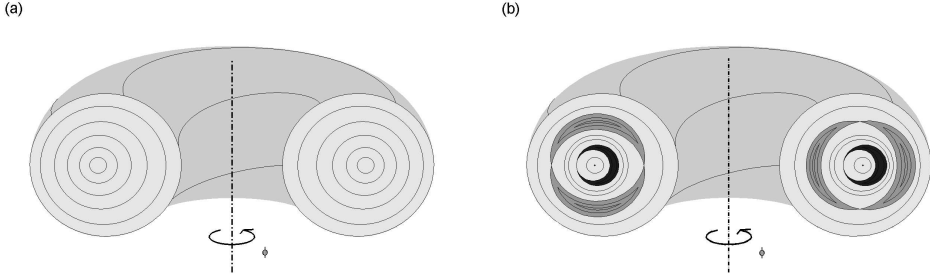
Figure 1.5: In (a) a set of unperturbed nested magnetic surfaces is shown while in (b) the effect of the reconnection at the rational surfaces $q = 1$ and $q = 2$ results in a set of magnetic islands [de Bock, 2007].

This thesis is focused on a particular type of magnetic instability called "tearing mode", responsible for a new, non-symmetric magnetic topology, characterized by a chain of "magnetic islands" (see Chapter 3). In a magnetic island a field line is displaced radially by a distance which is comparable with the island width (see figure 1.5). The size of an island can reach a considerable fraction of the plasma cross section (up to 50% for a $2/1$ island). The result is an enhancement of the radial particle and energy flux over the island region and consequently a flattening of the temperature profile which can strongly limit the performance of a tokamak. When the perturbation is particularly large, it may lead to a "disruption" [Schüller, 1995], a sudden termination of the plasma as a whole where the confined energy is transferred to the wall (up to ≈ 2 MJ/m^2, in JET) with the risk of melting or vaporization of the plasma facing components. The "energy quench" is followed by a rapid loss of plasma current ($\approx 10^2$ up to 10^3 MA/s), referred also as "current quench", which induces enormous forces in vessel components ($\approx 10^6$ N, in JET). This can affect the vessel integrity. It is therefore important to improve the understanding and the control of tearing modes in order to achieve the requirements for performance and safety of a tokamak reactor.

Analogy with Hamiltonian dynamics

The problem underlying magnetic reconnection is very broad and can be referred to as "break up" of invariant tori in a perturbed Hamiltonian system. A general review of these topics can be found in [Arnold, 1963; Berry, 1978] while in [Rosenbluth et al., 1966; Hazeltine and Meiss, 1991] the destruction of magnetic surfaces is specifically treated. To illustrate the analogy the case of a conservative, integrable, dynamical system with N degrees of freedom is presented here, which is defined by the canonical equations of

motion,

$$p = -\frac{\partial H}{\partial q}, \quad q = \frac{\partial H}{\partial p} \quad (p = p_1, \ldots, p_N; q = q_1, \ldots, q_N) \qquad (1.6)$$

with Hamiltonian $H(\mathbf{p}, \mathbf{q})$. This is in fact the formalism used to describe the field line equations in a tokamak, given in equation (2.8). The state of a system is given by the canonical coordinates $\{\mathbf{p}, \mathbf{q}\}$ in the $2N$-dimensional phase space, where $\mathbf{q}$ represents the spatial coordinate and $\mathbf{p}$ the related momenta. Being conservative and integrable, the system has N independent constants of motion $I(\mathbf{p}, \mathbf{q})$ such that,

$$\sum_k \frac{\partial I_i}{\partial q_k} \frac{\partial I_j}{\partial p_k} - \frac{\partial I_i}{\partial p_k} \frac{\partial I_j}{\partial q_k} = 0, \quad i \neq j, \qquad (1.7)$$

a property called involution. The Hamiltonian $H(\mathbf{p}, \mathbf{q})$ is one of these constants. It can be shown that, for bound motion in which the region of accessible phase space is finite, the set of constants of motion describes N-dimensional tori in phase space. These tori are said invariant because an orbit starting in one torus remains bound to that torus. An appropriate choice of N irreducible paths γ_i, such that they cannot be shrunk to zero, allows to define a preferred set of constant of motion J_i,

$$J_i = \int_{\gamma_i} \mathbf{p} \cdot \mathbf{dq}, \qquad (1.8)$$

called action variables, and their related angles ϕ_i. A relevant quantity for the following discussion is the frequency vector of the torus ω, which can be defined as

$$\omega_i(J) = \frac{\partial \phi_i}{\partial t} = \frac{\partial H}{\partial J_i}(\mathbf{J}), \quad i = 1, N. \qquad (1.9)$$

It is found that, for most part of the orbits, the frequency vector is "incommensurable", i.e. no integer vector $\mathbf{m}$ exists, such that $\mathbf{m} \cdot \omega = 0$, with $\mathbf{m} \neq 0$. The trajectories are then called conditionally periodic and they cover densely the torus. This means that a point moving on the torus never returns to its original position. When the frequency is commensurable, the orbit closes upon itself after $\mathbf{m}$ windings on the torus. The exceptional class of periodic orbits is particularly important for stability analysis of quasi-integrable systems, since these orbits are generally broken, when a small perturbation is applied. The work by [Birkhoff, 1927] proved that, instead of a complete circle of fixed points, the perturbed orbits evolve into a finite even number of fixed points, half of them representing a stable point (elliptic type) and half of them representing an unstable point (hyperbolic type) as shown in figure 1.6. Stable points are surrounded by closed invariant curves while the unstable points are connected between each other by curves called "separatrices". In a two-dimensional torus the overall configuration can be defined as a "chain of islands".

This thesis

Magnetic islands and their evolution have been studied extensively for nearly four decades [Furth et al., 1963; Rutherford, 1973]. Despite this long standing effort the complete sup-
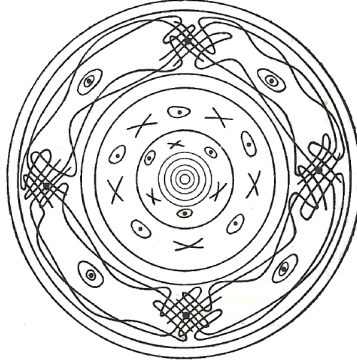
Figure 1.6: Break-up of invariant, rational tori [Berry, 1978].

pression of tearing modes (in modern tokamaks) has been achieved only ten years ago
[Gantenbein et al., 2000; Isayama et al., 2000; La Haye et al., 2002]. This outstanding
result was obtained by means of electron cyclotron waves (ECW) which allow to deposit
highly localized power at the island location. The EC power generates a current per-
turbation either inductively, through a temperature perturbation, or non-inductively by
direct current drive. Qualitatively, this means that the effect of the localized EC power on
magnetic islands is twofold: it increases the local stability, to make the island formation
more difficult, and it compensates for the effect of the temperature flattening inside the
island region by a local increase of the temperature and by inducing a current across the
island. This thesis addresses in particular the stabilizing effect of these techniques, usu-
ally referred as Electron Cyclotron Resonance Heating (ECRH) and Electron Cyclotron
Current Drive (ECCD). The aim of the study can be summarized as follows:

- To include new insights in the model for the evolution of a tearing mode by a close
  comparison of the stabilizing contributions of the local heating and the current
  drive;

- To extend the above mentioned model to a generalized geometry of the magnetic
  island;

- To provide accurate predictions on the power requirements for the stabilization
  of the mode. This requires the application of the model to realistic, machine-
  dependent scenarios and has a particular relevance for ITER design.

In order to analyze the problem completely it is necessary to take into account both
the geometry of the tearing instability, which depends on the perturbed magnetic equi-
librium of the plasma and the parameters determining the EC power deposition, which
can be calculated by means of beam-tracing codes. The approach to the topic has been
therefore both theoretical and numerical. The theoretical approach relies on the model
developed by Rutherford in 1973. Assuming a simplified description of both the mag-
netic equilibrium and the magnetic perturbation in the vicinity of the mode, the model

leads to the well known equation for the evolution of the magnetic island width, called the "Rutherford" equation. The equation relates the growth of the island width to the different helical current perturbations occurring in the island region. The main merit of the "Rutherford" model has been the capability to reproduce accurately experimental results, despite its relative simplicity: effects related with toroidicity, as well as with the geometry of the tokamak or any other feature "far" from the resonant surface are in fact usually neglected. The EC the power deposition profile is assumed to be Gaussian, characterized by the width of the profile, the position of the peak (along the radial and angular directions) and a possible modulation of the power. All numerical evaluations have been performed with MatLab.

The problem is generally non-trivial because we deal at the same time with quantities which are constant over the magnetic surfaces (they will be called flux functions) and highly localized ones, such as the EC power. In second place the geometry of a tearing mode, even in a simplified model, can be deformed by second order effects or by relaxing some of the assumptions underlying the model.

The thesis is structured as follows. Chapter 2 introduces the background on tokamak physics, necessary for a general understanding of the thesis. The theory of magnetic islands, their topological properties and the temporal evolution are extensively discussed in chapter 3. In chapter 4, the focus is drawn on the relative merits of ECRH and ECCD. This chapter answers to the following questions:

- Is it possible to identify a set of relevant parameters in the expression for the contribution of ECRH and ECCD to the Rutherford equation, in order to determine their relative importance for island suppression?

- Why has ECRH been experimentally observed to be the dominant effect for island suppression in small size tokamaks such as TEXTOR and T-10 while it appears negligible on middle-large size tokamaks (DIII-D, JT-60, ASDEX)?

- To what extent can the results of the analysis be applied to the experimental data?

In chapter 5 an extension of the previously discussed model allows the treatment of asymmetries in the island shape and discuss their effect on the previous predictions. The interest in this topic has been justified by the experimental evidence, since asymmetric islands have been found in ASDEX-Upgrade, DIII-D and in JT-60U. This chapter addresses the following questions:

- How can the magnetic perturbation due to tearing modes be reformulated consistently, such that second order effects due to shear flow, temperature gradient and "amplitude deformations" are taken into account?

- How do these perturbations in the island topology affect the evolution of the mode and, in particular, the contribution of ECRH and ECCD?

- In the previous literature [Lazzaro and Nowak, 2009; Urso et al., 2010] island deformations are found to have a sizable effect on the island evolution. Can these statements be confirmed or refuted?

Chapter 6 addresses the requirements for NTM suppression by an extensive analysis of the parameter η_{NTM}. This is defined as the ratio between the maximum in the driven current density, responsible for the stabilization of the mode and the maximum in the bootstrap current density, the main drive of the mode destabilization. A particular emphasis is given to the optimization of the parameters determining NTM stability in ITER ECRH system. The chapter answers to the following questions:

- Why is η_{NTM} found not to be a suitable parameter to investigate the requirements for NTM stabilization?

- What is the criterion for NTM stabilization that merges in a coherent theoretical framework the numerous (and contrasting) experimental measurements performed in different tokamaks?

- Which conclusions can be drawn for the ITER ECRH system?

In the last chapter, conclusions and perspectives considered in the thesis are summarized.

References

Arnold VI. Small denominators and problems of stability of motion in classical and celestial mechanics. *Russian Mathematical Surveys* **18**(6), 85 (1963).

Bernstein L et al. Climate change 2007: Synthesis Report. Technical report, Intergovernmental Panel on Climate Change, 2007.

Berry MV. Regular and irregular motion. *AIP Conference Proceedings* **46**, 16 (1978).

Bethe HA. The fusion hybrid. *Physics Today* **32**(5), 44–51 (1979).

Birkhoff GD. On the periodic motions of dynamical systems. *Acta Mathematica* **50**, 359 (1927).

de Bock MFM. *Understanding and controlling plasma rotation in tokamaks*. PhD thesis, Technische Universiteit Eindhoven, 2007.

Furth HP, Killeen J, and Rosenbluth MN. Finite-resistivity Instabilities of a sheet pinch. *Phys. Fluids* **6**, 459 (1963).

Gantenbein G, Zohm H, Giruzzi G, Günter S, Leuterer F, Maraschek M, Meskat J, Yu Q, ASDEX Upgrade Team, and ECRH-Group (AUG)l. Complete suppression of neoclassical tearing modes with current drive at the electron-cyclotron-resonance frequency in ASDEX Upgrade Tokamak. *Phys. Rev. Lett.* **85**(6), 1242 (2000).

Gerstner E. Nuclear energy: The hybrid returns. *Nature* **460**, 25 (2009).

Hazeltine RD and Meiss JD. *Plasma Confinement*. Addison-Wesley, 1991.

International Energy Agency. How the energy sector can deliver on a climate agreement in Copenhagen. Technical report, IEA, 2009. Special early excerpt of the World Energy Outlook 2009.

Isayama A et al. Complete stabilization of a tearing mode in steady state high-β_p H-mode discharges by the first harmonic electron cyclotron heating/current drive on JT-60U. *Plasma Phys. Control. Fusion* **42**(12), L37 (2000).

La Haye RJ, Günter S, Humphreys DA, Lohr J, Luce TC, Maraschek ME, Petty CC, Prater R, Scoville JT, and Strait EJ. Control of neoclassical tearing modes in DIII–D. *Phys. Plasmas* **9**(5), 2051 (2002).

Lawson JD. Some criteria for a power producing thermonuclear reactor. *Proc. Phys. Soc. B* **70**, 6 (1957).

Lazzaro E and Nowak S. ECCD control of dynamics of asymmetric magnetic islands in a sheared flow. *Plasma Phys. Control. Fusion* **51**, 035005 (2009).

Maisonnier D et al. A conceptual study of commercial fusion power plants. Technical report, EFDA European fusion development agreement, 2005. Final Report of the European Fusion Power Plant Conceptual Study (PPCS).

Priddle R et al. Key world energy statistics. Technical report, International Energy Agency, 2009.

Rosenbluth MN, Sagdeev RZ, and Taylor JB. Destruction of magnetic surfaces by magnetic field irregularities. *Nucl. Fusion* **6**, 297 (1966).

Rutherford PH. Nonlinear growth of tearing mode. *Phys. Fluids* **16**(11), 1903 (1973).

Schüller FC. Disruptions in tokamaks. *Plasma Phys. Control. Fusion* **37**, A135 (1995).

Shimada M et al. Progress in the ITER physics basis. *Nucl. Fusion* **47**, s1 (2007).

Urso L, Zohm H, Isayama A, Maraschek M, Poli E, ASDEX Upgrade Team, and JT-60 Team. ASDEX Upgrade–JT-60U comparison and ECRH power requirements for NTM stabilization in ITER. *Nucl. Fusion* **50**, 025010 (2010).

Wesson J. *Tokamaks*. Oxford University Press, third edition, 2004.

Westra MT et al. Energy, powering your world. Technical report, FOM-Institute for Plasma Physics Rijnhuizen, 2005.

2 Tokamak physics

The study of the tearing mode instability involves a number of different basic physical concepts, concerning the magnetic confinement, the transport and the use of external heating systems to control and suppress the mode. This chapter is meant to introduce a common theoretical framework, the tokamak physics, in which each of these topics is addressed separately. This constitutes the necessary background to the theory of magnetic islands, treated in the following chapters.

2.1 Magnetic confinement

Motion of a single particle in a magnetic field

A charged particle p in a constant uniform magnetic field moves freely in the direction parallel to the field, while in the perpendicular direction the Lorentz force $F = q\mathbf{v} \times \mathbf{B}$, forces the particle to gyrate around the field line with the characteristic cyclotron frequency $\omega_c = q_p B/m_p$. Here $\mathbf{B}$ is the confining magnetic field, while q, v and m are the charge, the velocity, and the mass of the particle, respectively. The radius of this
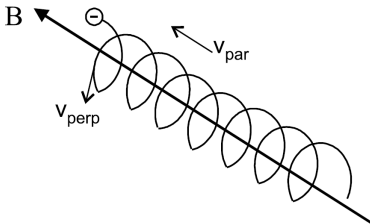
Figure 2.1: Cartoon of a charged particle gyrating around a magnetic field line.

circular motion (or gyro-radius) is known as the Larmor radius and is given by $r_L = m_p v_\perp/q_p B$, where $v_\perp$ is the magnitude of the perpendicular velocity. For a 10 keV plasma in a magnetic field $B = 5$ T, a typical value of the electron and the ion gyroradius is $r_{Le} \approx 5 \times 10^{-5}$ m and $r_{Li} =\approx 2 \times 10^{-3}$ m, respectively. In the direction parallel to the magnetic field, the particle moves with a velocity $v_\parallel$ which is of the order of the thermal speed, $v_{Tp} = (k_B T_p/m_p)^{1/2}$, T being the temperature of the particle distribution and k_B the Boltzmann constant. This implies that, in a fusion plasma with density $n \simeq 10^{20}$ m^{-3}, the mean free path covered by a particle before experiencing a collision, $L_p = v_{Tp}/\nu_p$, is about 10 km for electrons and ions, ν_p being the particle collision rate. The comparison of L_p and r_{Lp} shows how the tokamak enforces a good perpendicular confinement while, along the magnetic field, particles are free to flow for a distance much larger than any linear magnetic device. The transport parallel and perpendicular to a straight magnetic field caused by collisions, fast parallel motions and the finite size of the Larmor radii is denoted as classical transport. To prevent parallel losses, the magnetic field can be bent,

for example by means of a toroidal set of magnetic coils, in order to create a closed toroidal configuration. Due to the curvature and the gradient of the toroidal magnetic field, a vertical drift of the particle orbits arises, which acts in opposite direction for positive and negatively charged particles. The vertical electric field established by this vertical charge separation, leads to an outward radial drift ($\mathbf{E} \times \mathbf{B}$ -drift), the direction thereof being independent of the charge of the particles. As a result, the plasma would be expelled from a torus with a purely toroidal field. In order to counterbalance the charge separation, a poloidal magnetic field is introduced. By adding a small poloidal field the particles still move mainly in the toroidal direction, but they now cover the entire poloidal cross section before returning near the initial position. Ions and electrons still have a vertical drift associated with them but this now cancels in the upper and lower halves of the torus with the effect that there is no net drift. The vertical drift along the flux surfaces leads in particular to particle orbits on closed drift surfaces, which are slightly shifted horizontally with respect the flux surfaces.

The curvature of the field lines and the variation in the field strength is also responsible for distinct classes of particles which can be distinguished into trapped and passing particles, as shown in figure 2.2. Trapped particles bounce backward and forward between the two turning points [Wesson, 2004]. The mirror force responsible for the trap-
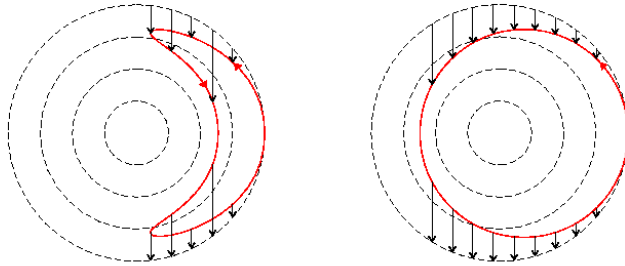
Figure 2.2: Poloidal projection of typical charged particle orbits in a tokamak. The particles experience a vertical drift (strongly exaggerated for purpose of illustration) dependent upon their velocity parallel to the magnetic field [Pinches, 1996]

ping is a consequence of the parallel gradient of the magnetic field $\nabla B_\parallel$ which acts on the perpendicular component of particle velocity $v_\perp$ as

$$F = -\mu \nabla B_\parallel \text{ , with } \quad \mu = \frac{\frac{1}{2}mv_\perp^2}{B} \text{ .} \tag{2.1}$$

The magnetic moment μ is an adiabatic invariant, being almost constant in a slowly varying magnetic field. Recalling that the magnetic field is minimal at the midplane, where the

perpendicular velocity is defined as $v_{0,\perp}$, the magnetic momentum conservation yelds,

$$\frac{v_\perp^2}{B} = \frac{v_{0,\perp}^2}{B_{\min}} \, ,$$ (2.2)

where $v_\perp$ can be conveniently calculated at the bounce point ($v_\parallel = 0$) by using the energy conservation $v_\perp = v_{0,\perp} + v_{0,\parallel}$, to obtain

$$\frac{B_{\mathrm{b}}}{B_{\min}} = \frac{v_{0,\parallel}^2}{v_{0,\perp}^2} \, .$$ (2.3)

Equation (2.3) determines the trapping condition for a particle. Particles with a sufficiently large $v_{0,\parallel}/v_{0,\perp}$, such that B_{b} exceeds the maximum magnetic field at a given magnetic surface, can flow around the torus following the helical path of the field lines. The trapped particles have insufficient parallel kinetic energy compared with their perpendicular energy to penetrate into the high-field side of the torus and are consequently located in the outer low-field side of the tokamak. They bounce backwards and forwards between their mirror points experiencing a continual vertical drift due to the combined effects of field curvature and gradient. The projection of these orbits on the poloidal plane, shows a "banana" shape.

Collisional transport in a toroidal geometry, where the excursion of the particle orbits from the flux surfaces, determined by drifts, is much larger than the Larmor radius, is denoted as "neoclassical" transport. In this transport model, the step size in the diffusion processes is defined by the banana width.

Magnetic confinement in a tokamak

In the previous chapter, the tokamak plasma was introduced as an axially symmetric system with closed magnetic surfaces, in which the magnetic field is a combination of a dominant toroidal field produced by external coils and of a poloidal field induced by a current flowing in the plasma [Braams and Stott, 2002; Wesson, 2004]. The toroidal geometry can be generally described by a set of coordinates $\{r, \theta, \phi\}$ where r, θ and ϕ are the radial coordinate, the poloidal and the toroidal angles, respectively as illustrated in figure 2.3(a) for the case of a circular cross section. The combination of the toroidal field B_ϕ and the poloidal field B_θ gives rise to magnetic field lines which have a helical trajectory around the torus as shown in figure 2.3(b). A measure of the pitch of the helical field lines is the safety factor q (introduced in section 1.3). Owing to the axisymmetric property, the equilibrium does not depend on the toroidal angle ϕ, meaning that the magnetic field lines lie on nested toroidal magnetic surfaces. The basic condition for plasma equilibrium requires that the magnetic force balances the force due to the plasma pressure, that is $\mathbf{j} \times \mathbf{B} = \nabla p$. This implies that magnetic surfaces coincide with surfaces of constant pressure, $\mathbf{B} \cdot \nabla p = 0$ and that current lines lie on magnetic surfaces, $\mathbf{j} \cdot \nabla p = 0$. The ratio of plasma pressure and magnetic pressure, known as the parameter $\beta \equiv 2\mu_0 p / B^2$, is a measure for the quality of plasma confinement.

(a)
(b)
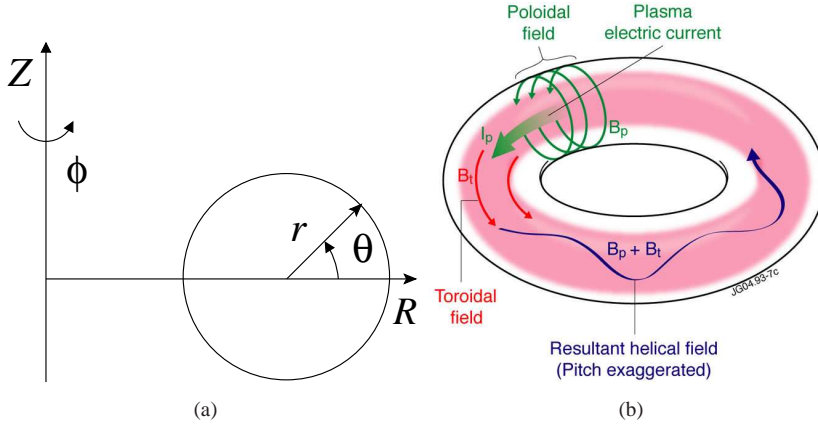
Figure 2.3: In figure (a) a set of toroidal coordinates is represented while in (b) the main components of the magnetic field and the resulting field lines are shown.

It is customary to label magnetic surfaces by the radial coordinate r or by introducing a toroidal flux function χ, which is proportional to the toroidal flux contained within the surface. A flux representation of the total magnetic field can be formulated as,

$$\mathbf{B} = \frac{1}{R}\left(\nabla\chi \times \nabla\theta + \nabla\phi \times \nabla\psi\right) \tag{2.4}$$

where R is the major radius of the torus, θ the poloidal angle and ψ the poloidal flux function. The two terms in equation (2.4) correspond to the toroidal and the poloidal components of the field, respectively. More generally [Hazeltine and Meiss, 1991] any function f that is constant along fields lines, i.e. $\mathbf{B} \cdot \nabla f \equiv 0$ is called a "flux label". Reformulating the safety factor in terms of magnetic fluxes $q = d\chi/d\psi$, it is possible to rewrite equation (2.4),

$$\mathbf{B} = \frac{1}{R}\nabla\psi \times \nabla(q\theta - \phi) = \frac{1}{R}\nabla\psi \times q\nabla\xi\,, \tag{2.5}$$

where a new helical angle $\xi = \theta - \frac{1}{q}\phi$ has been defined. When q varies along the radial direction, the field is said to have magnetic shear. On a "rational surface" with $q = m/n$, where m and n are integers, the field lines close upon themselves after m toroidal and n poloidal revolutions. Using equation (2.4) it can easily be shown that the field line orbits are described by a Hamiltonian system [White, 2001]. Magnetic field line equations are defined as, $d\chi/d\phi = (\mathbf{B} \cdot \nabla\chi)/(\mathbf{B} \cdot \nabla\phi)$ and $d\theta/d\phi = (\mathbf{B} \cdot \nabla\theta)/(\mathbf{B} \cdot \nabla\phi)$ or by

substituting **B**,

$$\frac{d\chi}{d\phi} = \frac{\nabla\chi \cdot (\nabla\psi \times \nabla\phi)}{(\nabla\chi \times \nabla\theta) \cdot \nabla\phi}$$
$$\frac{d\theta}{d\phi} = \frac{\nabla\theta \cdot (\nabla\psi \times \nabla\phi)}{(\nabla\chi \times \nabla\theta) \cdot \nabla\phi}. \tag{2.6}$$

Since the gradient of the poloidal flux function $\nabla\psi$ can be written in a general form as

$$\nabla\psi = \partial_\chi\psi\nabla\chi + \partial_\theta\psi\nabla\theta + \partial_\phi\psi\nabla\phi, \tag{2.7}$$

equation (2.6) reduces to

$$\frac{d\chi}{d\phi} = -\frac{\partial\psi}{\partial\theta}; \quad \frac{d\theta}{d\phi} = \frac{\partial\psi}{\partial\chi}. \tag{2.8}$$

This is a Hamiltonian representation of the field lines where $\psi(\chi,\theta,\phi)$ is the Hamiltonian, χ the action, θ the angle and ϕ the time coordinate.

2.2 From banana orbits to the bootstrap current

In a high temperature, low collisional plasma, when a trapped particle can complete at least one bounce orbit before suffering a collision, the plasma is said to be in the banana regime. The width of a banana orbit $w_b \approx \epsilon^{1/2}r_{\mathrm{L}\theta_i}$ is typically of the order of several centimetres for ions where $\epsilon = r/R$ is the local inverse aspect ratio for minor radius r, R is the major radius and $r_{\mathrm{L}\theta_i} = (2m_i k_B T_i/e^2 B_\theta)^{1/2}$ is the ion poloidal gyroradius. It can be shown [Wesson, 2004] that a fraction $\epsilon^{1/2}$ of the particles are trapped into such orbits. In the cylindrical limit, corresponding to a very small inverse aspect ratio approximation, the fraction of trapped particles becomes negligible, as expected.

The number of trapped particles following a banana orbit is proportional to the density. Observing the region between two adjacent field lines (see the figure 2.4), it is noted that a particle imbalance between the "inner leg" of green orbit and the "outer leg" of the pink orbit, owing to a finite density gradient, results in a net, toroidal momentum or, "banana" current,

$$J_{\mathrm{banana}} = -e\epsilon^{1/2}(\epsilon^{1/2}v_T)w_b\frac{dn}{dr}, \tag{2.9}$$

where the term $\epsilon^{1/2}v_T$ represents the typical parallel velocity of the trapped particles and n is the plasma density. Both trapped ions and trapped electrons carry such a current. A momentum source to passing particles results from collisions with the trapped particles carrying this net toroidal momentum. In steady state these momentum sources are balanced by a momentum exchange between the passing ions and electrons requiring a difference in average, toroidal velocities of these species. This represents the bootstrap current. An heuristic derivation of the bootstrap current density, valid for negligible temperature gradients and small (yet non negligible) inverse aspect ratio can be argued from the balance of the momentum exchange (expressed as the variation of the momentum
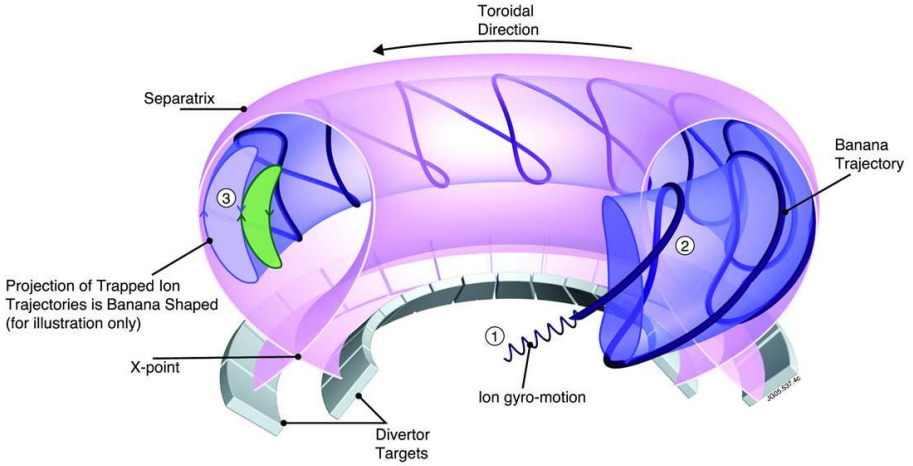
Figure 2.4: Charged particles travel in tight "gyro-orbits" around magnetic field lines. In some cases, due to the gradient of the magnetic field, their trajectory traces out banana-shape orbits (property of EFDA-JET).

density in time) between the passing electrons and the passing ions, $\nu_{\mathrm{ei}} m_e J_{\mathrm{BS}}/e$ with the momentum exchange between the passing and trapped electrons $\approx (\nu_{\mathrm{ee}}/\epsilon) m_e J_{\mathrm{Banana}}/e$. Here ν_{ee} is the collision frequency between passing and trapped electrons, ν_{ei} is the collision frequency between passing ions and passing electrons while e and m_e are the electron charge and mass, respectively. Under the assumption $\nu_{\mathrm{ee}} \simeq \nu_{\mathrm{ei}}$, the previous argument implies that the bootstrap current differs from the "banana" current by a factor $1/\epsilon$. A more elaborate analysis, for small ϵ values, leads to the following expression for the bootstrap current,

$$J_{\mathrm{BS}} \simeq -\frac{\sqrt{\epsilon}n}{B_\theta}\left[2.44(T_i + T_e)\frac{1}{n}\frac{\partial n}{\partial r} + 0.69\frac{\partial T_e}{\partial r} - 0.42\frac{\partial T_i}{\partial r}\right] \qquad (2.10)$$

where $T_{\mathrm{i,e}}$ is the electron and ion temperature. In the limit $\epsilon = 1$, when most of the particles are trapped, the bootstrap current is driven by the pressure gradient,

$$J_{\mathrm{BS}} \simeq -\frac{1}{B_\theta}\frac{\partial p}{\partial r} \, . \qquad (2.11)$$

Such a current exists independently of the externally driven toroidal current. At high β it can become a significant fraction of the total parallel current density $J_\parallel$.

2.3   Electron cyclotron waves

The plasma in a tokamak is partly heated by means of ohmic heating due to the induced plasma current. This method is generally limited by two factors, the capability of inducing a current while maintaining the plasma stable and the reduction of the plasma resistivity as the temperature increases. From MHD stability the current limit [Shimada et al., 2007] is taken as equivalent to $q_a \gtrsim 2$ where $q_a \approx 2\pi(aB_\phi/\mu_0 I)(a/R)k$ is the value of the safety factor at the plasma edge $r = a$, k being the vertical elongation. In the case of ITER, the current limit is approximately 15 MA. This limitation of Ohmic heating motivated the use of auxiliary heating systems in order to enhance plasma performance up to the ignition condition.

Among the most successful methods commonly applied, neutral beam injection (NBI) and radio frequency (or microwave frequency) heating are briefly described. In the first method an energetic beam of charged particles is neutralized and injected into the plasma core where the beam is ionized and the energy transferred by collisions to the bulk plasma. In the second method, energy is transferred to the plasma by means of electromagnetic waves, through resonant interaction with the cyclotron motion (or harmonics of it) of the ions or electrons. Depending on the resonance frequency we can distinguish between Ion Cyclotron Resonance Heating (ICRH) and Electron Cyclotron Resonance Heating (ECRH), respectively. The use of Electron Cyclotron Waves (ECW) [Bornatici et al., 1983; Prater, 2004], has proved to be of particular importance both for plasma heating and as a means to locally drive non inductive toroidal current. In the following EC waves will be presented in more detail.
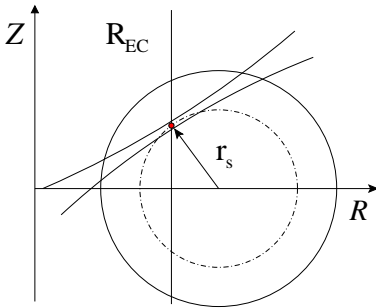
Figure 2.5: Cartoon showing the ECW injection at the resonance radius R_{EC}. In the following chapters we will refer more often to the resonance radius as the distance r_s, from the axis with respect to the poloidal cross section.

The non-relativistic cyclotron frequency for an electron gyrating around a magnetic field line is defined as, $\omega_{ce} = \frac{eB}{m_e}$, or, numerically, as $f_{ce} = \omega_{ce}/2\pi \simeq 28 \cdot B[T]$GHz. In the range of interest, this implies a frequency of the order of 100 GHz and consequently a wavelength in the millimetre range. Electron cyclotron waves are injected from vacuum and propagate as a narrow, well-defined beam, with high power density. The absorption of the EC waves in the plasma is limited around a resonance layer where the cyclotron frequency or an harmonic thereof, equates the wave frequency [Westerhof, 2008]. Approximating the magnetic field with its (dominant) toroidal component, the position of this layer for the n_{th} harmonic at frequency ω is $R_{EC} = R(neB_\phi/m_e\omega - 1)$. The com-

bination of a thin resonant layer and a narrow beam defines a small plasma volume where the EC power is deposited. This allows to manipulate locally the pressure and the current density.

Electron cyclotron waves can drive a non-inductive current (ECCD) in a toroidal plasma [Ohkawa, 1976; Fisch and Boozer, 1980]. For an electron moving in the plasma the resonance occurs at a Doppler shifted frequency $\omega = n\omega_{ce}/\gamma + k_\parallel v_\parallel$ where γ is the relativistic factor, $k_\parallel$ and $v_\parallel$ are the parallel components of the wave vector and the velocity, respectively. Injecting electron cyclotron waves at a given toroidal angle (oblique injection) allows to select a population of resonant electrons with a certain $v_\parallel$. Electron cyclotron absorption results in an increase of the perpendicular energy of resonant electrons and hence to a lower collisionality (see figure 2.6-a). The collision rate decreases as v^{-3}. This creates an asymmetry in the electron distribution function, i.e. an excess of electrons moving in the direction of $v_\parallel$. This corresponds to a net current in the opposite (toroidal) direction, known as the Fish-Boozer current. When trapped particles are
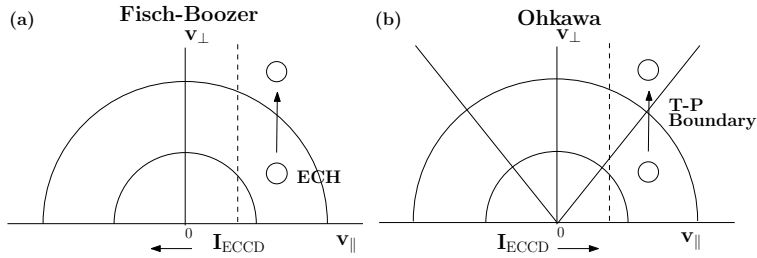
Figure 2.6: (a) Schematic illustration [Prater, 2004] in velocity space of electron cyclotron current drive by the Fisch-Boozer process and (b) by the Ohkawa process. The acronym "T-P" stays for Trapped-Passing boundary.

involved, EC-induced velocity excursions might move electrons from the passing region to the trapped region as shown in figure 2.6-b. In steady state the flux of electrons, in-out of the trapped region is balanced, but the detrapping process is symmetric in $v_\parallel$ while the trapping process is asymmetric for a finite $k_\parallel$. This generates a net electrical current flowing in the opposite direction with respect to the Fish-Boozer current which is known as Ohkawa current.

References

Bornatici M et al. Electron cyclotron emission and absorption in fusion plasmas. *Nucl. Fusion* **23**, 1153 (1983).

Braams CM and Stott PE. *Nuclear Fusion: Half a Century of Magnetic Confinement Fusion Research*. Institute of Physics Publishing, 2002.

Fisch NJ and Boozer AH. Creating an asymmetric plasma resistivity with waves. *Phys. Rev. Lett.* **45**, 720 (1980).

Hazeltine RD and Meiss JD. *Plasma Confinement*. Addison-Wesley, 1991.

Ohkawa T. Steady state operation of tokamaks by rf heating. Ga-a13847, General Atomic, 1976.

Pinches SD. *Nonlinear interaction of fast particles with alfvén waves in tokamaks*. PhD thesis, University of Nottingham, 1996.

Prater R. Heating and current drive by electron cyclotron waves. *Phys. Plasmas* **11**(5), 2349 (2004).

Shimada M et al. Progress in the ITER physics basis. *Nucl. Fusion* **47**, s1 (2007).

Wesson J. *Tokamaks*. Oxford University Press, third edition, 2004.

Westerhof E. Electron cyclotron waves. *Fusion Sci. Tech.* **53**(2T), 202 (2008).

White RB. *The theory of toroidally confined plasmas*. Imperial College Press, 2001.

3 The theory of magnetic islands

3.1 Introduction

Magneto hydrodynamic (MHD) instabilities are one of the major limiting factors to achieve high confinement [Hazeltine and Meiss, 1991; Biskamp, 1993; Wilson, 2008]. They can be broadly distinguished in terms of the characteristic time scale with which they evolve in the plasma. Here two main categories are introduced, ideal and resistive instabilities. Ideal instabilities are modes which occur for a perfectly conducting plasma, growing on the fast Alfvén time scale, $\tau_a = a/(B/\sqrt{\mu_0 \rho})$, where a, μ_0 and ρ are the plasma minor radius, the permeability of free space and the mass density, respectively. In a tokamak these instabilities can lead to a rapid loss of confinement, (a so called plasma disruption) in a few microseconds [Wesson, 2004]. The appearance of ideal instabilities sets therefore a limit in the achievable plasma pressure and current, which is usually referred to as the ideal β limit [Sauter et al., 1997]. The latter is defined, for monotonic q profiles and neglecting the effects owing to the wall or other instabilities as $\beta_N \equiv \beta(\%)/(I[MA]/a[m]B[T]) \approx 4l_i$ where l_i is the internal plasma inductance. The ideal β limit has been reached in most of the tokamaks for short discharges, while for discharges lasting several confinement times, τ_E, the achievable β is limited by the excitation of resistive instabilities. Unlike ideal instabilities, these can change the topology of the magnetic field. Tearing instabilities, in particular, reconnect magnetic flux-surfaces to form chains of magnetic islands, allowing field lines to drift radially, for a distance of the order of the island width. These modes evolve during the initial, linear phase on an hybrid time scale $\tau_H \propto \tau_a^{2/5} \tau_r^{3/5}$ where $\tau_r = \mu_0 a^2/\eta$ is the resistive time scale, for a finite resistivity η. In a tokamak τ_H is of the order of 10ms, justifying the term "hybrid" since $\tau_a \ll \tau_H \ll \tau_r$. In the non-linear phase they evolve on the slow local resistive time scale. More details will be given in the following section.

A magnetic island effectively "short-circuits" magnetic surfaces by making a path for heat and particles to radially transit the island region without crossing the equilibrium magnetic field. As a consequence of heat and particle transport along the field lines, temperature and pressure inside the island are found to be locally flattened. This results in a loss of energy and particle confinement. According to the "belt" model [Sauter et al., 1997] the degradation in energy confinement due to this flattening is predicted to range from a few percent up to 50% for a large island (see figure 3.1). In addition a magnetic island slows the plasma rotation because of the radial magnetic field fluctuation imposed at the resistive wall. As the island tends to rotate with the plasma, it induces eddy currents on the wall whose magnetic field opposes the island perturbation. At high frequencies the resistive wall behaves like a perfect conductor but as the plasma rotation is slowed, the oscillating magnetic field penetrates further into the wall, increasing the drag. This leads eventually to mode locking and to disruptions [La Haye, 2006a].

This chapter provides a theoretical framework for the description of tearing mode
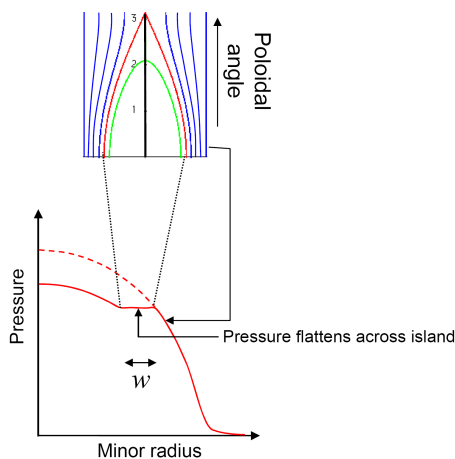
Figure 3.1: Flattening of the pressure and temperature profiles across the island, along the radial direction. The degradation in energy confinement due to this flattening is predicted to range from a few percent up to 50% for a large island.[Wilson, 2008]

instabilities. We shall begin with a brief introduction of the magnetic reconnection process, in order to describe the geometrical properties of the perturbed magnetic topology and afterwards, the temporal evolution of the mode. A particular emphasis is given to the mechanisms driving the so called neoclassical tearing mode, appearing at high β, even when the plasma is linearly stable.

3.2 Resistive MHD and magnetic reconnection

Tearing modes are macroscopic, resistive instabilities which affect the whole plasma. It is natural therefore to investigate them using the magnetohydrodynamical approximation, which effectively treats the plasma as a single-fluid. The model combines the Maxwell equations with the equations of fluid dynamics [Goedbloed and Poedts, 2004]. As general assumptions, the quasi-neutrality condition is required for the fluid while the magnetic field must be sufficiently strong to enforce a small Larmor radius to the particle orbits; furthermore viscosity and heat conduction are neglected. With these premises, the MHD equations describing a plasma in presence of a finite resistivity η, can be written as,

$$\frac{d\rho}{dt} = -\rho\nabla \cdot \mathbf{v} \qquad \text{(Continuity)}, \qquad (3.1)$$

$$\rho\left(\frac{d\mathbf{v}}{dt}\right) = \mathbf{J} \times \mathbf{B} - \nabla p \quad \text{(Momentum)}, \qquad (3.2)$$

$$\frac{dp}{dt} = -\gamma p\nabla \cdot \mathbf{v} \qquad \text{(Internal energy)}, \qquad (3.3)$$

$$\frac{\partial B}{\partial t} = -\nabla \times \mathbf{E} \qquad \text{(Faraday's law)}, \qquad (3.4)$$

where,

$$\mathbf{E} = -\mathbf{v} \times \mathbf{B} + \eta \mathbf{J} , \qquad \text{(Ohm's law)} , \qquad (3.5)$$

$$\mathbf{J} = \frac{\nabla \times \mathbf{B}}{\mu_0} \qquad \text{(Ampere's law)} , \qquad (3.6)$$

$$\nabla \cdot \mathbf{B} = 0 \qquad \text{(Absence of magnetic monopole)} . \qquad (3.7)$$

In equations (3.1), (3.2) and (3.3) the definition of convective derivative,

$$\frac{d}{dt} \equiv \left(\frac{\partial}{\partial t} + \mathbf{v} \cdot \nabla \right) ,$$

has been used. The parameter γ denotes the ratio of specific heats. It is noticed here that, in equation (3.6), the displacement current has been neglected, assuming for most plasma phenomena non-relativistic velocities $v \ll c$. Substituting equations (3.5) and (3.6) in equation (3.4) the following expression for the evolution of the magnetic field is obtained,

$$\frac{\partial B}{\partial t} = \nabla \times (\mathbf{v} \times \mathbf{B}) + \frac{\eta}{\mu_0} \nabla^2 \mathbf{B} . \qquad (3.8)$$

The first term on the rhs of equation (3.8), describes the convection of the magnetic field by the plasma flow. When the first term is dominant, the magnetic flux is frozen into the plasma and the topology of the magnetic field cannot change. On the other hand, when the diffusive term is not negligible, the topology of the magnetic field is free to change. The relative magnitude of the two terms on the right-hand side of equation (3.8) is conventionally measured in terms of the Lundquist number:

$$S = \frac{\mu_0 v_{\mathrm{a}} L}{\eta} \qquad (3.9)$$

where v_{a} is the Alfven speed and L the characteristic length-scale of the plasma. If S is much larger than unity then convection dominates, and the frozen flux constraint prevails, while, in the opposite limit, the diffusion dominates, and the coupling between the plasma flow and the magnetic field is weak.

In a tokamak the condition $S \gg 1$ is typically satisfied. This leads to the conclusion that in most part of the plasma the resistivity plays no role and the plasma itself can be treated as a perfectly conducting fluid. In this limit the resistive model described above reduces to the so called ideal MHD. In the "resistive layer", where the instability occurs, the effect of the magnetic diffusion is responsible for the magnetic reconnection of the field lines, as shown in figure 3.2. Here the ideally stable magnetic topology breaks towards a new equilibrium with a lower magnetic energy.

In order to describe the geometry and, later, the temporal evolution of a tearing mode, a few further simplifications are made, leading to the so called "reduced MHD" [Biskamp, 1993; White, 2001]. In first place a large aspect ratio is assumed, such that $\epsilon = a/R \ll 1$. This reduces the problem from a three dimensional to a two dimensional one. Secondly a strongly magnetized plasma in the toroidal direction is introduced, such
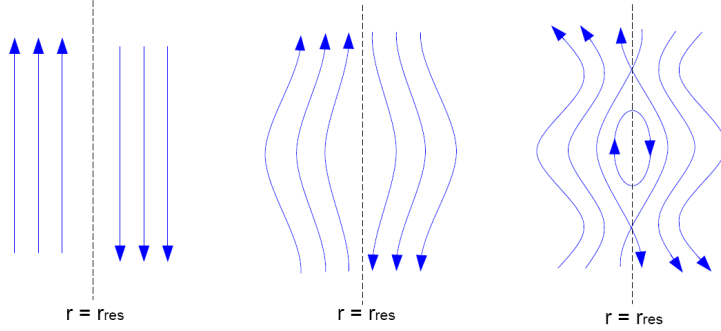
Figure 3.2: Cartoon [Urso, 2009] describing the reconnection of the field lines in a slab geometry, around the resonant radius, due to a finite resistivity.

that $\mathbf{B} \simeq B_\phi \mathbf{e}_\phi$, where to the lowest order $B_\phi = \mathrm{const}$. The plasma motion is therefore highly anisotropic, such that strong local gradients are allowed only in the poloidal plane. As a consequence, along the toroidal direction $v_\phi \ll 1$. Introducing the vector potential $\mathbf{A}$ and the scalar potential φ in the Faraday's law (3.4) and substituting the electrical field from Ohm's law (3.5) the following expression,

$$\frac{\partial \mathbf{A}}{\partial t} = \mathbf{v} \times \mathbf{B} + \eta J - \nabla \varphi, \tag{3.10}$$

is obtained. Consider now the poloidal component of equation (3.10). It is noted that the term $\partial_t A_\perp$ is negligible since $B_\phi = (\nabla_\perp \times \mathbf{A}_\perp) \cdot \mathbf{e}_\phi$ is approximately constant. The subscript $\perp$ denotes the direction perpendicular to the toroidal field. In addition resistive instabilities are driven by the parallel current $J_\parallel \simeq J_\phi$, so that $J_\perp$ can also be negligible. This leads to an expression for the poloidal velocity,

$$\mathbf{v}_\perp = \frac{\mathbf{e}_\phi \times \nabla \varphi}{B_\phi} . \tag{3.11}$$

Equation (3.11) satisfies the condition $\nabla \cdot \mathbf{v} = 0$, indicating the incompressibility of the flow. It is noticed that the incompressibility holds when the perturbed plasma moves with a speed $v \ll v_a$ and $v \ll v_s$ where v_s is the sound speed. Recalling the poloidal flux function ψ and using equation (3.11) it is possible to reformulate the parallel component of equation (3.10) as,

$$\frac{1}{R} \frac{\partial \psi}{\partial t} = \nabla_\parallel \varphi + \eta J, \tag{3.12}$$

where the operator $\nabla_\parallel$, defined as,

$$\nabla_\parallel \equiv \frac{\mathbf{B} \cdot \nabla}{B_\phi} , \tag{3.13}$$

is the gradient along the perturbed magnetic field lines of the island and the current density J can be written as $J \simeq J_\phi = \nabla_\perp^2 \psi$. It is remarked that, the relation $\psi = -RA_\phi$ is used in order to substitute the flux function ψ to the parallel component of the vector potential A_ϕ.

The equation for the potential φ is obtained by considering the ϕ-component of the curl of the equation of motion (3.2),

$$\frac{\partial \mathcal{U}}{\partial t} = -\mathbf{v} \cdot \nabla \mathcal{U} + \mathbf{B} \cdot \nabla J \,, \tag{3.14}$$

where $\mathcal{U} = \nabla_\perp^2 \Phi$ is the plasma vorticity, $\Phi = \varphi/B_\phi$ being the stream function. Equations (3.12) and (3.14) for the two scalar quantities ψ and Φ, along with the definition of the magnetic field and equation (3.11) are a closed set, known as reduced MHD equations.

Having described the mathematical framework of the problem, we will focus on the consequences of the mode, namely the creation of a magnetic island. In the next section the geometrical aspects of the problem will be discussed, while in section 3.4 the temporal evolution of the instability will be treated.

3.3 Topology of the mode

A magnetic island can be seen as a closed helical flux tube, bounded by the separatrix, with its typical X-point in the poloidal cross section. The magnetic axis of the island is represented by a field line which closes upon itself after m toroidal and n poloidal windings, respectively. The projection of this field line on the poloidal plane is called O-point. In order to describe the region in the vicinity of a magnetic island chain, it
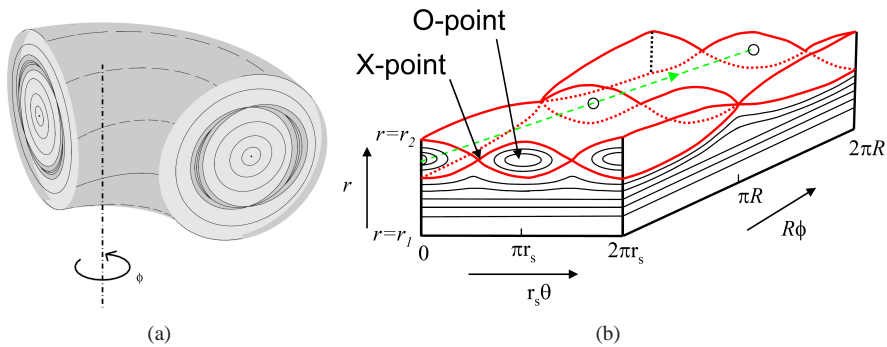
Figure 3.3: Magnetic surface reconnection forming a magnetic island, described in a toroidal geometry (a) [de Bock, 2007]. In slab geometry (b) the annulus of plasma has been cut along the poloidal and toroidal direction and unfolded [Wilson, 2008].

is customary to introduce the slab approximation. The toroidal annulus, adopting a large aspect ratio approximation, can be "unfolded" along the toroidal direction into a cylinder, and then along the poloidal direction as shown in figure 3.3(b). The approximation is valid in the limit of a small island, the width being negligible with respect to the minor radius a. In the model, the coordinate system $\{x, \theta, \phi\}$ will be used as a set of cartesian coordinates, $x = r - r_s$ being the distance from the resonant surface, θr_s and ϕR being the poloidal and the toroidal direction, respectively. Taking into account the helical character of the tearing perturbation, it is convenient to recall the helical angle ξ (introduced in chapter 2), such that $m\xi = m\theta - n\phi$. The unit vector $\mathbf{e}_\phi$ is directed perpendicularly to the green dashed line connecting the O-points, representing the locus of points where $\xi = 0$. The large aspect ratio approximation and the definition of ξ, allow to write the following relation,

$$\nabla \xi = \nabla \theta + \frac{n}{m} \nabla \phi = \frac{\mathbf{e}_\theta}{r_s} + \frac{n}{m} \frac{\mathbf{e}_\phi}{R} \approx \frac{\mathbf{e}_\theta}{r_s} \,, \tag{3.15}$$

leading to the conclusion that the ξ-direction of the helical angle can be approximated with the θ-direction. In the following treatment we will make use of the coordinate system $\{x, \xi, \phi\}$. Along with this set of toroidal coordinates, it is customary to introduce the equilibrium helical flux function,

$$\psi_{h,0} = \psi - \frac{n}{m} \chi \,, \tag{3.16}$$

defining the helical field $B_{h,0} \equiv \frac{1}{R} \nabla \psi_{h,0} \times \nabla \xi$ which vanishes at the rational surface, $\nabla \psi_{h,0}|_{r_s} = 0$. When the small-amplitude approximation is assumed, equation (3.16) can be approximated near the resonant surface by its lowest term from a Taylor expansion such that,

$$\psi_{h,0} \approx -\frac{x^2}{2} \frac{q_s'}{q_s} \frac{\partial \psi}{\partial x} \bigg|_{r_s} \,, \tag{3.17}$$

where $\psi'|_{r_s} = RB_p|_{r_s}$ and q_s' denotes the magnetic shear at the rational surface. In the Taylor approximation, the constant zero order term $\psi_{0,h}(r_s)$ has been neglected, since it does not affect fields lines. The perturbed helical flux function can be written then as $\psi_h = \psi_{h,0} + \psi_{h,1}$, where $\psi_{h,1}$ represents the perturbation to the equilibrium helical flux function. In the following, the subscript h will be dropped for simplicity. Being a periodic function in θ and ϕ, the function ψ_1 can be written as a Fourier series,

$$\psi_1 = \sum_{m_0, n_0} \tilde{\psi}_{m_0, n_0} e^{i(m_0 \theta - n_0 \phi)} \,, \tag{3.18}$$

where the dominant contribution to ψ_1 is provided by the resonant harmonic, such that the approximation to the first leading order is

$$\psi_1 = \tilde{\psi}_1(r) e^{(i(m\theta - n\phi))}.$$

The expression for ψ_1 can be further simplified by neglecting the radial dependence of $\tilde{\psi}_1$, near the rational surface. This last assumption, known as the constant-$\tilde{\psi}_1$ approximation is valid for small islands, whose width is much smaller than the tokamak minor

radius. In order to simplify the notation, in the rest of the chapter $\tilde{\psi}_1(r_s) \equiv \tilde{\psi}$ is defined. The equation of the field lines in the vicinity of the magnetic island can then be formulated as,

$$\Omega = 8\frac{x^2}{w^2} + \mathrm{sign}(\psi_0'')\cos(m\xi)\,, \tag{3.19}$$

where the flux label $\Omega = \frac{\psi_h}{\mathrm{sign}(\psi_0'')\tilde{\psi}}$ was introduced and

$$w = 4\left(\frac{\tilde{\psi}}{|\psi_0''|}\right)^{1/2}\,, \tag{3.20}$$

represents the width of the island. It is noted that in a typical tokamak equilibrium, with a monotonically increasing q-profile, the shear profile is such that ψ_0'' is negative. This property sets the O-point at $x = 0$, $\xi = 0$, leading to $\Omega = -1$ while the X-point falls at $x = 0$, $\xi = \pm\pi$, for $\Omega = 1$. Flux labels $-1 \leq \Omega < 1$ refer to the region inside the island while, the locus of points such that $\Omega = 1$ is called separatrix. Externally to the separatrix, $\Omega > 1$, the helical flux function is an invariant of the perturbed field lines. This condition remains valid only when the perturbation had a single helicity. In case of multiple helicities ergodic regions or stochasticity can occur near the separatrix.

Having defined the flux coordinates $\{\psi, \xi, \phi\}$, it is worth introducing the flux surface average operator $\langle f \rangle \equiv \{f\}/\{1\}$, [Fitzpatrick, 1995; Hegna and Callen, 1997] where the curly bracket is defined as,

$$\{f(\sigma, \Omega, \xi)\} \equiv \oint \frac{\mathrm{d}\xi}{2\pi}\frac{w}{4\sqrt{2}}\frac{f(\sigma, \Omega, \xi)}{\sqrt{\Omega + \cos(m\xi)}}\,, \tag{3.21}$$

for $\Omega > 1$ and,

$$\{f(\sigma, \Omega, \xi)\} \equiv m\int_{-\tilde{\xi}}^{\tilde{\xi}}\frac{\mathrm{d}\xi}{2\pi}\frac{w}{4\sqrt{2}}\frac{\frac{1}{2}[f(\sigma, \Omega, \xi) + f(-\sigma, \Omega, \xi)]}{\sqrt{\Omega + \cos(m\xi)}}, \tag{3.22}$$

for $\Omega \leq 1$, with $\tilde{\xi} = \arccos(-\Omega)/m$ and $\sigma = \mathrm{sign}(r - r_s)$. An important property, which will be used in the next section is that the flux surface average annihilates the operator $\nabla_\parallel \equiv \mathbf{B}\cdot\nabla$, i.e.

$$\langle\nabla_\parallel\rangle = 0. \tag{3.23}$$

3.4 Derivation of the Rutherford equation

In order to solve the non-linear stability problem for a magnetic island, the external and the internal regions, with respect to the island separatrix, are treated separately. In the "outer region", which comprises most of the plasma, non-linear, non-ideal, and inertial effects are negligible. Neglecting the inertia term $\partial\mathcal{U}/\partial t = 0$ and linearizing the vorticity equation in (3.14), a differential equation for $\psi_1(r)$ [Biskamp, 1993] is obtained. In

cylindrical geometry this equation can be written as,

$$\frac{1}{r}\frac{\partial}{\partial r}r\frac{\partial \psi_1}{\partial r} - \left(\frac{m^2}{r^2} + \frac{\partial J_{0,\parallel}/\partial r}{\frac{B_\theta}{\mu_0}\left(1 - \frac{nq}{m}\right)}\right)\psi_1 = 0 \, . \tag{3.24}$$

Equation (3.24) shows clearly the resonant nature of the tearing mode instability, since
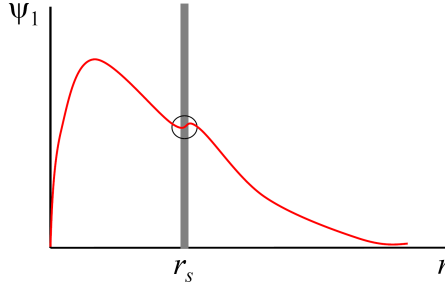
Figure 3.4: Trend of the amplitude of the flux perturbation, ψ_1, in cylindrical geometry [Wilson, 2008].

the third term on the equation (3.24) diverges at $q = m/n$, and the important role played by the equilibrium density gradient at the rational surface. It can be shown [Biskamp, 1993] that only low m modes can be unstable. Integrating equation (3.24) over the ideal-MHD region until the right-hand boundary, $r = r_s^+$ and the left-hand boundary, $r = r_s^-$, $\psi_1(r)$ is found to have a gradient discontinuity across the rational surface. It is customary to characterize this jump of the logarithmic derivative of ψ_1 across the island with the so called tearing stability index Δ_0'. In the limit of a small island, the tearing stability index is written as

$$\Delta_0' = \lim_{\varepsilon \downarrow 0} \frac{\psi_1'(r_s + \varepsilon) - \psi_1'(r_s - \varepsilon)}{\psi_1(r_s)} \, , \tag{3.25}$$

where $r_s \gg \varepsilon \gg w$. It is remarked here that Δ_0' represent the jump in the derivative of the outer solution. As $r_s \gg \varepsilon$, this is calculated in the limit of $\varepsilon \to 0$. Δ_0' is a global property of the plasma, depending only on the equilibrium and on the boundary conditions. It can be interpreted as a measure for the free energy available in the plasma to drive a tearing mode. According to [Hegna and Callen, 1994], the change in magnetic energy in the presence of an island is given by:

$$\delta W = -\frac{1}{4}r_s\psi_0^2\Delta_0' \, . \tag{3.26}$$

In the internal region, non-ideal, non-linear effects, and plasma inertia can all be important. In order to obtain a smooth solution for $\psi(r)$ over the entire range, the inner solution must be asymptotically matched to the outer solution calculated above. As $\varepsilon \gg$

w, the step in the derivative of the *internal* solution can be calculated in the limit of $\varepsilon \to \infty$,

$$\Delta_0' = \lim_{\varepsilon \uparrow \infty} \frac{\psi_1'(\varepsilon) - \psi_1'(-\varepsilon)}{\psi_1(r_s)} . \tag{3.27}$$

The argument, despite the apparent contradiction, has a large importance in the following discussion, as shown in equation (3.31). For a finite size island, the matching is calculated at the separatrix, for $\varepsilon = w/2$. As a consequence equation (3.27) is modified as follows,

$$\Delta'(w) = \frac{\psi_1'(r_s + w/2) - \psi_1'(r_s - w/2)}{\psi_1(r_s)} . \tag{3.28}$$

An analytical solution can be derived in the simplified geometry introduced in the previous section.

According to the linear tearing mode theory, for $\Delta_0' > 0$ the mode is growing exponentially within the resistive layer of width δ, with a linear growth rate γ. These quantities are approximately dependent on the Lundquist number as, $\gamma \propto S^{-3/5}$ and $\delta \propto S^{-2/5}$. In the non-linear regime the growth slows down, eventually leading to a saturated state. When the non-linear effects are reducing the island growth well before the saturation level or when the island width becomes larger than the thin resistive layer, the linear model is no longer valid and a non-linear approach should be applied. It is also noted that, due to the narrow width of the resistive layer, only the non-linear stage is accessible to experimental measurements.

When the island exceeds the resistive layer width, the inertia becomes negligible and the equation of motion degenerates to the equilibrium equation $\mathbf{B} \cdot \nabla J = 0$ so that J is by definition a flux function: $J(\psi)$. From Ampère's law, relating the perturbation of the helical flux to the parallel current density perturbation $J_{1,\parallel}(\psi)$, it follows that,

$$\frac{1}{R} \nabla^2 \psi_1 = \mu_0 J_{1,\parallel}(\psi) . \tag{3.29}$$

To obtain the m-th Fourier harmonic, equation (3.29) is multiplied with the phase factor $\cos(m\xi)$ and integrated over ξ. In addition, integrating over x in the inner region and using the approximation $\nabla^2 \psi_1 \approx \partial^2 \psi_1 / \partial x^2$, one obtains

$$\frac{1}{R} \int_{-\infty}^{\infty} \mathrm{d}x \oint \mathrm{d}\xi \, \frac{\partial^2 \psi_1}{\partial x^2} \cos(m\xi) = \int_{-\infty}^{\infty} \mathrm{d}x \oint \mathrm{d}\xi \, \mu_0 J_{1,\parallel}(\psi) \cos(m\xi). \tag{3.30}$$

Now the left hand side can be evaluated and matched to the linear exterior solution with the result of

$$\frac{1}{R} \int_{-\infty}^{\infty} \mathrm{d}x \oint \mathrm{d}\xi \, \frac{\partial^2 \tilde{\psi}}{\partial x^2} \cos^2(m\xi) = \frac{\pi}{R} \Delta_0' \tilde{\psi} . \tag{3.31}$$

As a result we arrive at the following basic equation for the tearing mode, relating Δ_0' to the total perturbed helical current flowing in the island region,

$$\Delta_0' \tilde{\psi} = 2\mu_0 R \int_{-\infty}^{\infty} \mathrm{d}x \oint \frac{\mathrm{d}\xi}{2\pi} \cos(m\xi) J_{1,\parallel} . \tag{3.32}$$

33

In order to connect the perturbation of the parallel current density $J_{1,\parallel}$ with the time rate of change of the helical flux perturbation $\partial\psi_1/\partial t$, the flux surface average of equation (3.12),

$$\frac{1}{R}\left\langle\frac{\partial\psi_1}{\partial t}\right\rangle = \eta J_{1,\parallel}(\psi) + \langle\nabla_\parallel\varphi\rangle\,,\tag{3.33}$$

is used. It is noticed that the term depending on the electrostatic potential, $\nabla_\parallel\varphi$, vanishes. To derive the last statement, it is sufficient to recall the definition of $\nabla_\parallel$ given in equation (3.13) and the surface average property in equation (3.23) so that $\langle\nabla_\parallel\varphi\rangle = 0$ is obtained. The right hand side of equation (3.30) can now be rewritten by substitution of $J_{1,\parallel}$ from equation (3.33). In addition, the previous literature suggests a change of coordinates, $\{\xi, x\}$ to $\{\xi, \Omega\}$, in order to make explicit the Ω-dependence of the flux surface average $\langle\partial\psi_1/\partial t\rangle$. Rearranged in this way, the above mentioned integration in (3.30) is performed over the flux label Ω, from the O-point to infinity,

$$\begin{aligned}
\Delta_0'\tilde{\psi} &= 2\mu_0 R\int_{-1}^{\infty}\mathrm{d}\Omega\left[\frac{1}{\eta R}\left\langle\frac{\partial\psi_1}{\partial t}\right\rangle\right]\oint\frac{\mathrm{d}\xi}{2\pi}\frac{\cos(\xi)}{d\Omega/d\xi} \tag{3.34}\\
&= \frac{2\mu_0}{\eta}\frac{\partial\tilde{\psi}}{\partial t}\int_{-1}^{\infty}\mathrm{d}\Omega\,\langle\cos(m\xi)\rangle\oint\frac{\mathrm{d}\xi}{2\pi}\frac{\cos(\xi)}{d\Omega/d\xi}\,.
\end{aligned}$$

From the definition of the island width (3.20), it is possible to rearrange the equation (3.34) such that the linear stability index Δ_0' is related with the resistive time scale $\tau_{\mathrm{r}} = \mu_0 r_{\mathrm{s}}^2/\eta$ and the time derivative of the island width. The amplitude of the perturbation $\tilde{\psi}$ can be formulated as

$$\tilde{\psi} = \frac{w^2}{16}\psi_0''\quad\text{and}\quad\frac{d\tilde{\psi}}{dt}\frac{1}{\tilde{\psi}} = \frac{2}{w}\frac{dw}{dt}\,,\tag{3.35}$$

resulting in the well known Rutherford equation,

$$r_{\mathrm{s}}\Delta_0' = g_1\frac{\tau_{\mathrm{r}}}{r_{\mathrm{s}}}\frac{dw}{dt}\,.\tag{3.36}$$

Both the left and right hand sides are dimensionless and g_1 is a numerical coefficient related to the island geometry,

$$g_1 = \frac{4}{w}\int_{-1}^{\infty}\mathrm{d}\Omega\frac{\left(\oint\frac{\mathrm{d}\xi}{2\pi}\frac{\cos(\xi)}{d\Omega/dx}\right)^2}{\oint\frac{\mathrm{d}\xi}{2\pi}\frac{1}{d\Omega/dx}}\approx 0.82\,.\tag{3.37}$$

Despite the appearance, g_1 does not depend on w as $\mathrm{d}\Omega/\mathrm{d}x$ also scales as $1/w$. This equation is equivalent to the one used in Chapter 5 where the radial coordinate is normalized. As it was mentioned in the previous section, the equation (3.36) predicts the island to grow linearly in time for $\Delta_0' > 0$, as long as Δ_0' is independent of w, i.e. for sufficiently small islands. For finite size island, Δ_0' is typically observed to decrease linearly with w: $\Delta'(w) \simeq \Delta_0' - \alpha w$. The island is seen to saturate at a finite size such that $\Delta'(w) = 0$ and all available free energy of the originally unstable equilibrium has been exhausted.

3.5 Neoclassical tearing modes and the modified Rutherford equation

Neoclassical tearing modes (NTMs) are magnetic islands destabilized by a helically perturbed bootstrap current, introduced in chapter 2. Unlike the classical tearing modes, occurring when the plasma current profile is linearly unstable, such that the tearing mode has a lower magnetic energy than the original plasma, the NTM is a high-β phenomenon, linearly stable ($\Delta'_0 < 0$) and non-linearly unstable. The main reason for a perturbation in the bootstrap current nearby the island, originates from the effect of the magnetic island on the local pressure. For conventional profiles of safety factor and pressure gradient, a "seed" island can flatten locally the pressure, because of the rapid parallel transport along the field lines which makes the pressure approximately a flux function. As a result the bootstrap current inside the island is removed while in the outer region the pressure gradient is maintained and so is the current. The helical perturbation of the bootstrap current reinforces the seed, i.e. it destabilizes the equilibrium.

The inclusion of the helical perturbation of the bootstrap current, along with a number of other effects (treated separately in the following paragraphs), leads to a generalized formulation of the Rutherford equation (GRE). The model is based on the generalization of the flux surface averaged Faraday-Ohm's law (3.33), relating the time rate of change of the helical flux perturbation, i.e. the helical electric field, to the parallel current density perturbations with the same helicity,

$$\frac{1}{R}\left\langle \frac{\partial \psi_1}{\partial t} \right\rangle = \eta_0 \left(J_{1,\parallel}(\psi) - \sum_i J_{1,i}(\psi) \right) + \eta_1(\psi) \left(J_0 - \sum_i J_{0,i} \right) . \tag{3.38}$$

The helical perturbation of the parallel current density and any non-inductive contribution therein are indicated with $J_{1,\parallel}(\psi)$ and $J_{1,i}(\psi)$, respectively. In equation (3.38), $\eta_1(\psi)$ represents a possible helical perturbation to the resistivity as a consequence of heating (or cooling) inside the island, while J_0 and $J_{0,i}$ represent the total equilibrium current density and every non-inductive contribution to the latter, respectively. A final note concerns the resistivity η, denoted here with η_0, to be distinguished from its perturbation η_1.

In analogy with the procedure used in the previous section the generalized Rutherford equation appears as,

$$0.82 \frac{\tau_r}{r_s} \frac{dw}{dt} = r_s \Delta'(w) + r_s \sum_i \Delta'(J_{1,i}) + r_s \Delta'(\eta_1) , \tag{3.39}$$

where the second term on the right hand side, accounts for corrections to the classical tearing mode equation, due to all possible non-inductive perturbations and the final term due to the inductive helical perturbation of the parallel current density. The general contribution from a non-inductive helical current perturbation can be written as,

$$\Delta'(J_{1,i}) = -\frac{16\mu_0 L_q}{B_p \pi w^2} \int_{-\infty}^{\infty} dx \oint d\xi J_{1,i} \cos(m\xi) . \tag{3.40}$$

Here the formula for the island width in equation (3.20) was used in place of $\tilde{\psi}$ while the second derivative of the equilibrium flux function was replaced as $|\psi_0''| = RB_{\mathrm{p}}/L_{\mathrm{q}}$, $L_{\mathrm{q}} = q/(\partial q/\partial r)$ being the q scale length. In the following subsections a number of effects contributing to the generalized Rutherford equation will be described.

Effect of bootstrap current gap

In the island region, for $-1 \leq \Omega \leq 1$, the bootstrap current is negligible, such that the current density perturbation $J_{1,\mathrm{BS}}(\Omega) = -J_{0,\mathrm{BS}}|_{r_{\mathrm{s}}}$. Substituting $J_{1,\mathrm{BS}}$ in place of $J_{1,i}$ in equation (3.40) and integrating within the island separatrix, where the perturbation is localized, the expression

$$\Delta'_{\mathrm{BS}} = \frac{16\mu_0 L_{\mathrm{q}}}{\pi B_{\mathrm{p}} w^2} \int_{-1}^{1} \mathrm{d}\Omega \oint \mathrm{d}\xi J_{0,\mathrm{BS}} \frac{\cos(m\xi)}{\partial\Omega/\partial x} , \tag{3.41}$$

is obtained. Using the approximation for $J_{0,\mathrm{BS}}$ given in equation (2.10),

$$g_1 \frac{\tau_{\mathrm{r}}}{r_{\mathrm{s}}} \frac{dw}{dt} = r_{\mathrm{s}}\Delta' + \frac{L_{\mathrm{q}}}{L_{\mathrm{p}}} \frac{r_{\mathrm{s}}}{w} \beta_{\mathrm{p}} \sqrt{\epsilon} c_{\mathrm{neo}} , \tag{3.42}$$

where $L_{\mathrm{p}} = -p/(\partial p/\partial r)$ is the pressure scale length while the geometrical coefficient c_{neo} is expressed as

$$c_{\mathrm{neo}} = \frac{8}{\pi} \int_{-1}^{1} \mathrm{d}\Omega \oint \mathrm{d}\xi \frac{\cos(m\xi)}{\partial\Omega/\partial x} = 32/3\pi . \tag{3.43}$$

The inclusion of the bootstrap term implies that the width of the island reaches a stable point at $w = w_{\mathrm{sat}}$, where $dw/dt = 0$, as shown in figure 3.5. This relation shows that the saturated width grows with β_{p} producing consequently a progressive degradation of the confinement. In particular for low m-modes, the width reaches a size comparable to the resonant radius. The tearing instability appears therefore to limit severely the achievable performances of a tokamak, eventually terminating the discharge in a disruption. The divergence of $\Delta'_{\mathrm{BS}} \propto 1/w$ indicates that the mode should always be unstable. Experimentally nonetheless, it is observed that NTMs are destabilized only above a certain threshold island. This suggests that, in the limit of small island size, further mechanisms should exist accounting for the stability of the mode. Two such mechanisms are related to the influence of radial diffusion in competition with parallel transport and to finite orbit width effects. The flattening of the temperature, density and pressure inside the island, is based on the assumption that the perpendicular transport $\chi_\perp$ is negligible with respect to the parallel transport $\chi_\parallel$. When the island reaches a critical value w_χ, the two transport time scales become comparable and the pressure is not flattened any longer. As a consequence an island below the critical width cannot drive an NTM. A corrected formulation for the bootstrap term is,

$$r_{\mathrm{s}}\Delta_{\mathrm{BS}} = c_{\mathrm{neo}} \frac{L_{\mathrm{q}}}{L_{\mathrm{p}}} \frac{r_{\mathrm{s}}}{w} \beta_{\mathrm{p}} \sqrt{\epsilon} \left(\frac{w^2}{w^2 + w_\chi^2} \right) , \tag{3.44}$$

where the critical island w_χ is [Wilson, 2008]

$$w_\chi = \sqrt{\frac{RqL_{\mathrm{q}}}{m}} \left(\frac{\chi_\perp}{\chi_\parallel}\right)^{1/4} \; .$$

Effect of polarization

The second effect, still debated, concerns the polarization current correction [Wilson et al., 1996; Waelbroeck et al., 2001], due to the island rotation. This appears to be dominant in particular in the limit of small islands. An island propagates at frequency ω in the frame of the plasma flow, resulting in a fluctuation of the electric field. Because the electron banana width is small for electrons, trapped electrons respond to the local electric field. In contrast, the ion banana orbits are much wider leading to an average response to the fluctuating electric field. The different responses of trapped electrons and trapped ions results in the so-called perpendicular ion polarization current, which is not divergence free. Since the charge neutrality needs to be maintained, the electrons respond with a parallel current to make the total current divergence free. The latter can be either stabilizing or destabilizing depending on the sign of ω, but is generally expected to be stabilizing. An often used approximation for this term is [Wilson, 2008],

$$r_{\mathrm{s}}\Delta'_{\mathrm{pol}} = -c_{\mathrm{neo}} \frac{L_{\mathrm{q}}}{L_{\mathrm{p}}} \frac{r_{\mathrm{s}}}{w} \beta_{\mathrm{p}} \sqrt{\epsilon} \left(\frac{w_{\mathrm{pol}}^2}{w^2}\right) \; , \qquad (3.45)$$

where the polarization width is $w_{\mathrm{pol}} = (L_{\mathrm{q}}/L_{\mathrm{p}})^{1/2} w_b$, w_b being the banana width. The generalized Rutherford equation now appears as

$$g_1 \frac{\tau_{\mathrm{r}}}{r_{\mathrm{s}}} \frac{dw}{dt} = r_{\mathrm{s}}\Delta' - c_{\mathrm{neo}} \frac{L_{\mathrm{q}}}{L_{\mathrm{p}}} \frac{r_{\mathrm{s}}}{w} \beta_{\mathrm{p}} \sqrt{\epsilon} \left(\frac{w^2}{w^2 + w_\chi^2} - \frac{w_{\mathrm{pol}}^2}{w^2}\right) \; , \qquad (3.46)$$

the trend thereof is shown by the blue curve of figure 3.5.

Effect of an external perturbation field

In this subsection the effect of an external perturbation field on the NTM evolution is briefly described. For a detailed theory of perturbation fields, we refer to [Fitzpatrick et al., 1991; Fitzpatrick, 1993, 1998; de Bock, 2007].

Resonant magnetic perturbation fields, generated outside the plasma (or the island region) by external currents, have a remarkable influence on magnetic island stability. Due to the conservation of the magnetic flux in a conducting fluid, a plasma counterbalances the effect of an external field by inducing shielding currents, in accordance to Lenz' law. In analogy with the previous sections, the perturbation field is modeled as a helical flux function expressed by a Fourier series. The (m, n) Fourier component of this field induces a shielding current with the same helicity, which flows parallel to the magnetic field on the (m, n) resonant surface. It follows that the dominant contributions
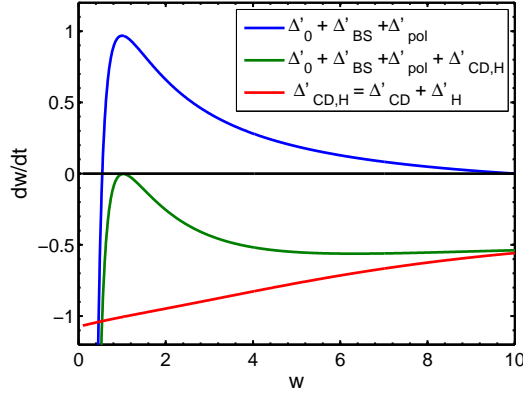
Figure 3.5: Cartoon illustrating the phase-space diagram of the island width, in arbitrary units. The blue curve represents the evolution of an NTM as described by the rhs of equation (3.46). The red solid curve refers to the stabilizing contribution of the current drive and the local heating. The suppression of the mode, by means of current drive and local heating, is illustrated by the green curve. Since $dw/dt \leq 0$ for every value of the width, the island is said to be fully suppressed.

of the perturbation field are represented by the resonant harmonics, as in equation (3.18). The shielding currents, in turn, modify the equilibrium at the rational surface and induce a finite electromagnetic torque on the corresponding mode. The effect of this torque is to reduce the frequency gap between the mode and the perturbation field. It will be shown that the effect of the perturbation is maximal when the frequency gap is zero, i.e. when the mode is rotating with the same frequency of the perturbation field.

The (m, n) perturbation can be seen as produced by a helical current in the coil, located at $r = r_c$, outside the plasma. In the approximation of a single helicity and in absence of plasma, the perturbation can therefore be written as $\psi_{\mathrm{vac}} = \tilde{\psi}_{\mathrm{vac}} \exp(i(m\theta + n\phi))$ with,

$$\tilde{\psi}_{\mathrm{vac}}(r, t) = \psi_c(t) \left(\frac{r}{r_{c-}} \right)^m \quad (0 < r < r_{c-}) \tag{3.47}$$

$$\tilde{\psi}_{\mathrm{vac}}(r, t) = \psi_c(t) \left(\frac{r}{r_{c+}} \right)^{-m} \quad (r_{c+} < r). \tag{3.48}$$

The amplitude $\psi_c(t)$ is the value of $\tilde{\psi}_{\mathrm{vac}}$ inside the coil and is proportional to the current applied to the coil. The ideal MHD response of the plasma to the helical current flowing in the coil is such that the perturbation field is shielded for $0 < r < r_{\mathrm{s}}^-$. Assuming that the equilibrium plasma current is mainly concentrated inside the rational surface so that $J_{0,\|} \simeq 0$ when $r > r_{s+}$ the response of the plasma is approximated as a thin layer

around the resonant surface where the shielding current is flowing. The amplitude of the corresponding flux function ψ_{sh} can be written as,

$$\tilde{\psi}_{\text{sh}}(r,t) = \psi_{\text{sh},0}(t) \left(\frac{r}{r_{s-}}\right)^m \quad (0 < r < r_{s-}) \tag{3.49}$$

$$\tilde{\psi}_{\text{sh}}(r,t) = \psi_{\text{sh},0}(t) \left(\frac{r}{r_{s+}}\right)^{-m} \quad (r_{s+} < r), \tag{3.50}$$

showing a discontinuity at the rational surface,

$$\left[r\frac{\partial \tilde{\psi}_{\text{sh}}}{\partial r}\right]_{r_s^-}^{r_s^+} = -2m\tilde{\psi}_{\text{sh}}. \tag{3.51}$$

Since in the region $r < r_s$, the sum of $\tilde{\psi}_{\text{vac}}$ and $\tilde{\psi}_{\text{sh}}$ must vanish, equating $\tilde{\psi}_{\text{vac}}(r,t)$ in equation (3.47) to $-\tilde{\psi}_{\text{sh}}(r,t)$ in equation (3.49) results in an expression for $\psi_{\text{sh},0}(t)$ in terms of $\psi_c(t)$. The amplitude of the total perturbation field $\tilde{\psi}_{\text{coil}}$, results from the superposition of the vacuum perturbation and the plasma response to the former, $\tilde{\psi}_{\text{coil}} = \tilde{\psi}_{\text{vac}}(r,t) + \tilde{\psi}_{\text{sh}}(r,t)$, as

$$\tilde{\psi}_{\text{coil}}(r,t) = 0 \qquad (0 < r < r_{s+})$$
$$= \tilde{\psi}_{\text{vac}}(r_{s+},t) \left[\left(\frac{r}{r_{s+}}\right)^m - \left(\frac{r}{r_{s+}}\right)^{-m}\right] \qquad (r_{s+} < r < r_{c-})$$
$$= \tilde{\psi}_{\text{vac}}(r_{s+},t) \left[\left(\frac{r_c}{r_{s+}}\right)^m - \left(\frac{r_c}{r_{s+}}\right)^{-m}\right] \left(\frac{r}{r_c}\right)^{-m}. \qquad (r_{c+} < r) \tag{3.52}$$

The flux function $\psi_{\text{coil}} = \tilde{\psi}_{\text{coil}} \exp(i(m\theta + n\phi - \omega t))$ has in general a time dependent component of the phase, ωt, accounting for the phase difference between the perturbation field rotation and the mode rotation. The "slip" frequency ω is assumed to be quasi-stationary. Having defined properly the perturbed flux function, the relative contribution to the modified Rutherford equation can be calculated by following the same procedure applied in section 3.4. The matching condition at the resonant surface is now modified as,

$$\int_{-\infty}^{\infty} dx \oint d\xi \, \mu_0 J_{1,\parallel}(\psi) \cos(m\xi) = \frac{\pi}{R} \left(\Delta'(w)\tilde{\psi} + \Delta'_{\text{ext}}\tilde{\psi}_{\text{coil}}\right), \tag{3.53}$$

where Δ'_{ext} is defined as,

$$\Delta'_{\text{ext}}\tilde{\psi}_{\text{coil}} = \left[\frac{\partial \psi_{\text{coil}}}{\partial r}\right]_{r_{s-}}^{r_{s+}} = \frac{2m}{r_s}\tilde{\psi}_{\text{vac}}. \tag{3.54}$$

Using the Faraday-Ohm's law in equation (3.12) and rearranging the equation as in (3.36) the following expression is obtained,

$$r_s\Delta'_{\text{ext}} = 2m\left(\frac{w_{\text{vac}}}{w}\right)^2 \cos(\Delta(m\xi)). \tag{3.55}$$

The vacuum island width $w_{\text{vac}} \propto |\psi_{\text{vac}}(r_s)|^{1/2}$ has been introduced along with $\Delta(m\xi) = (m\xi_{0,\text{plasma}} - m\xi_{0,\text{vacuum}})$, the phase difference between the O-point of the plasma and the vacuum island. As anticipated at the beginning of this subsection, Δ'_{ext} has a maximum when the island is locked in phase and rotating at the same frequency as the perturbation field, $\Delta(m\xi) = 0$.

In section 4.7, the focus will be drawn on the magnetic perturbation generated in the TEXTOR tokamak by the so called "Dynamic Ergodic Divertor" (DED) [Finken, 1997; Finken et al., 2005]. The DED consists of a set of 16 coils wound helically at the high field side of the torus. These coils are aimed to perturb the outer flux surfaces of the plasma in order to divert them to divertor plates, at the edge of the plasma. The main advantages are the distribution of the energy flux from the plasma over the divertor (target) plates and the shielding of the plasma from impurities coming from the wall. In addition the DED is found to remove efficiently helium particles from the plasma. The magnetic field produced by the DED is parallel to the field lines at $q = 3/1$ surface, with a large $2/1$ side band which becomes the dominant perturbation inside the plasma. When the amplitude of the perturbation exceeds a well defined threshold, a $2/1$ tearing mode is excited in the plasma. The $3/1$ mode is more stable and thus more difficult to excite (but is also seen to be triggered as the DED current is increased further. Since the mode is rotating with the same frequency of the perturbation field, the magnetic island is said to be "locked" [Yu and Günter, 2008] to the DED frequency, typically of the order of 1kHz. For a static perturbation, the mode can be even locked to a known, stationary position allowing a favorable setting to study the evolution of the instability.

Effect of electron cyclotron waves

The stabilizing contributions to the GRE owing to ECCD and ECRH are extensively treated in chapters 4, 5 and 6. In this subsection a brief qualitative description will be presented. As described in section 2.3, EC waves allow to deposit highly localized power inside the mode. The radial power density profile is generally well approximated with a normalized Gaussian function, $p_{\text{EC}} = P_{\text{tot}}\tilde{p}_{\text{CW}}(x)$ with,

$$\tilde{p}_{\text{CW}}(x) = \frac{1}{2\pi^{5/2}w_{\text{dep}}Rr_s}e^{-4(x-x_{\text{dep}})^2/w_{\text{dep}}^2} , \qquad (3.56)$$

where P_{tot} is the total deposited power, w_{dep} the full e^{-1} power density width and x_{dep} is the deposition location relative to the resonant radius, i.e. $r_{\text{dep}} - r_s$. By means of a significant heating power deposited at the resonant surface, a finite temperature perturbation δT_e is produced at the island O-point, with respect the temperature at the separatrix, with a consequent perturbation of the local (neoclassical) resistivity [Wesson, 2004],

$$\eta_1 \approx 2.8 \cdot 10^{-8}\frac{Z_{\text{eff}}}{\delta T_e^{3/2}}(1 - \sqrt{\epsilon})^2, \qquad (3.57)$$

where the effective ion charge Z_{eff} is assumed to be constant. The Ohm's law suggests that such a perturbation induces an inductive current density, $J_{\text{H}} = (\eta_1/\eta_0)J_{0,\parallel}$ which

can be expressed in terms of the temperature perturbation,

$$J_{\mathrm{H}} = J_{\mathrm{sep}} \frac{\delta T_{\mathrm{e}}}{T_{\mathrm{e,sep}}} \, , \tag{3.58}$$

where J_{sep} refers to the value of the inductive part of the equilibrium current density at the island separatrix. By using the current density perturbation J_{H} associated to the temperature perturbation, the contribution to the GRE owing to the local heating can be expressed as in equation (3.40),

$$\Delta'(\eta_1) = \frac{16\mu_0 L_{\mathrm{q}}}{B_{\mathrm{p}}\pi w^2} \int_{-\infty}^{\infty} \mathrm{d}x \oint \mathrm{d}\xi J_{1,\mathrm{H}} \cos(m\xi) \, . \tag{3.59}$$

Under appropriate conditions (see 2.3) EC waves have been shown to induce also a non-inductive current, a process referred to as ECCD. When the current is mostly driven within the island region, the main effect is to compensate the bootstrap current gap, which is acknowledged to be the drive for NTM growth. It is noted that it is not possible to drive a non-inductive current without also heating the plasma. On the contrary, it is possible to isolate the effect of ECRH, by injecting the power perpendicularly to the magnetic field. The amplitude and the width of the current density profile are usually calculated by means of numerical codes, but in this discussion a Gaussian profile having the same width of the power deposition profile and an amplitude j_{CD} is assumed. The total driven current is denoted I_{CD}. Following the notation used in [Sauter, 2004; Westerhof et al., 2007] and equation (3.40), one can write

$$\Delta'(J_{1,\mathrm{CD}}) = \frac{16\mu_0 L_{\mathrm{q}}}{B_{\mathrm{p}}\pi w^2} \int_{-\infty}^{\infty} \mathrm{d}x \oint \mathrm{d}\xi J_{1,\mathrm{CD}} \cos(m\xi) \, . \tag{3.60}$$

In general the integral is solved numerically, except for simplified current density profiles. More details can be found in [Hegna and Callen, 1997] or [Giruzzi et al., 1999].

A second effect of a localized non-inductive current drive concerns the change in the total equilibrium current density $J_{\parallel}$ and consequently in the linear stability index [Westerhof, 1990; Pletzer and Perkins, 1999]. Assuming the induced current to be in the same direction of the equilibrium current (co-current drive), this results in a more negative Δ', i.e. the mode is more difficult to destabilize. When the condition $I_{\mathrm{CD}} \ll I_0$ holds, I_0 being the total plasma current, the contribution to the classical stability coefficient Δ' can be derived naturally as a generalization of the perturbative model treated at the beginning of the chapter. To this purpose, the total equilibrium current density is defined as $J = J_{0,\parallel} + J_{\mathrm{CD}}$ and the perturbation of the helical flux function $\psi_{1,\mathrm{gen}} = \psi_1 + \delta\psi$ with $\delta\psi \ll \psi_1$. The classical stability index Δ' is therefore modified as,

$$
\begin{aligned}
\Delta' &= \lim_{\varepsilon \downarrow 0} \frac{[\psi_1'(r_{\mathrm{s}} + \varepsilon) + \delta\psi'(r_{\mathrm{s}} + \varepsilon)] - [\psi_1'(r_{\mathrm{s}} - \varepsilon) - \delta\psi'(r_{\mathrm{s}} - \varepsilon)]}{\psi_1(r_{\mathrm{s}}) + \delta\psi(r_{\mathrm{s}})} \\
&\approx \Delta_0' + \lim_{\varepsilon \downarrow 0} \frac{\delta\psi'(r_{\mathrm{s}} + \varepsilon) - \delta\psi'(r_{\mathrm{s}} - \varepsilon)}{\psi_1(r_{\mathrm{s}})} \\
&\approx \Delta_0' + \delta\Delta' \, ,
\end{aligned}
\tag{3.61}
$$

where in the rhs of equation (3.61) the denominator $\psi_1(r_s) + \delta\psi(r_s) \approx \psi_1(r_s)$. In analogy with equation (3.24), the radial profile of the perturbed flux function $\psi_{1,\text{gen}}(r)$ in the ideal outer region, is described as,

$$\frac{1}{r}\frac{\partial}{\partial r}r\frac{\partial(\psi_1 + \delta\psi)}{\partial r} - \left(\frac{m^2}{r^2} + \frac{\partial(J_{0,\parallel} + J_{\text{CD}})/\partial r}{\frac{B_\theta}{\mu_0}\left(1 - \frac{nq}{m}\right)}\right)(\psi_1 + \delta\psi) = 0\,, \qquad (3.62)$$

where ψ_1 is the solution for the "unperturbed" differential equation. Standard perturbation theory suggests then that perturbative terms of the same order are required to cancel each other. Neglecting the second order perturbation term, proportional to $(\partial J_{\text{CD}}/\partial r)\delta\psi \ll 1$, the equation for the first order perturbation terms appears as,

$$\frac{1}{r}\frac{\partial}{\partial r}r\frac{\partial(\delta\psi)}{\partial r} - \frac{m^2}{r^2}\delta\psi + \frac{\partial(J_{\text{CD}})/\partial r}{\frac{B_\theta}{\mu_0}\left(1 - \frac{nq}{m}\right)}\psi_1 = 0\,. \qquad (3.63)$$

In the limit of a highly localized current, $\delta\psi/r_s^2 \ll (\delta\psi)'/r_s \ll (\delta\psi)''$. For ψ_1 the constant-ψ approximation, $\psi_1 \approx \psi_1|_{r=r_s}$, is applied. With the substitution of J_{CD} in equation (3.63) and recalling the identity $x \equiv r - r_s$, the following expression,

$$\frac{1}{\psi_1(x)}\frac{\partial^2(\delta\psi(x))}{\partial x^2} \approx \frac{4L_q}{\pi^{3/2}r_s}\frac{\mu_0}{B_p}\frac{I_{\text{CD}}}{w_{\text{dep}}^2}\frac{\frac{2(x-x_{\text{dep}})}{w_{\text{dep}}}\exp\left(-\frac{4(x-x_{\text{dep}})^2}{w_{\text{dep}}^2}\right)}{x}\,, \qquad (3.64)$$

can be integrated from $x = -\infty$ to $x = -\epsilon$ and from $x = \epsilon$ to $x = +\infty$. It is reminded that the extension of the integration domain to infinity is allowed since the current is well localized. The variation of the classical stability index, $\delta\Delta'$, following [Westerhof, 1990] appears finally as

$$r_s\delta\Delta' = -\frac{4\mu_0 L_q}{B_p\pi}\frac{I_{\text{CD}}}{w_{\text{dep}}^2}\wp\int_{-\infty}^{\infty}\frac{\frac{2(x-x_{\text{dep}})}{w_{\text{dep}}}\exp\left(-\frac{4(x-x_{\text{dep}})^2}{w_{\text{dep}}^2}\right)}{x}\,, \qquad (3.65)$$

where $\wp$ indicates the principal value of the integral. The term $\delta\Delta'$ is finally found as,

$$r_s\delta\Delta' = -\frac{4\mu_0 L_q}{B_p\pi}\frac{I_{\text{CD}}}{w_{\text{dep}}^2}\left(1 + \frac{2}{w_{\text{dep}}}x_{\text{dep}}\Re\left[\mathcal{Z}\left(\frac{2}{w_{\text{dep}}}x_{\text{dep}}\right)\right]\right)\,, \qquad (3.66)$$

where $\Re[\mathcal{Z}]$ is the real part of the plasma dispersion function. This has a maximum for $x_{\text{dep}} = 0$. For a finite size island, given that only the current induced in the outer region can contribute to the stability index, the singularity at $x = 0$ is solved by splitting the integral domain in two regions, from $x = -\infty$ to $x = -w/2$ and from $x = w/2$ to $x = +\infty$. When the current density profile is centred at the resonant surface ($x_{\text{dep}} = 0$), the analytical form

$$r_s\delta\Delta' = -\frac{4\mu_0 L_q}{B_p\pi}\frac{I_{\text{CD}}}{w_{\text{dep}}^2}\left[\text{erfc}\left(\frac{w}{w_{\text{dep}}}\right)\right] \qquad (3.67)$$

is obtained.

References

Biskamp D. *Nonlinear Magnetohydrodynamics*. Cambridge Press, 1993.

de Bock MFM. *Understanding and controlling plasma rotation in tokamaks*. PhD thesis, Technische Universiteit Eindhoven, 2007.

Finken KH. Special Issue: Dynamic Ergodic Divertor. *Fusion Engineering and Design* **37**, 335 (1997).

Finken KH, Abdullaev SS, Jakubowski M, et al. The structure of magnetic field in the TEXTOR-DED. Technical report, Textor, IPP, 2005.

Fitzpatrick R. Interaction of tearing modes with external structures in cylindrical geometry (plasma). *Nucl. Fusion* **33**, 1049 (1993).

Fitzpatrick R. Helical temperature perturbations associated with tearing modes in tokamak plasmas. *Phys. Plasmas* **2**(3), 825 (1995).

Fitzpatrick R. Bifurcated states of a rotating tokamak plasma in the presence of a static error-field. *Phys. Plasmas* **5**, 3325 (1998).

Fitzpatrick R and Hender TC. The interaction of resonant magnetic perturbations with rotating plasmas. *Phys. Fluids B* **3**, 644 (1991).

Giruzzi G, Zabiego M, Ganakon TA, Garbet X, Cardinali A, and Bernabei S. Dynamical modelling of tearing mode stabilization by RF current drive. *Nucl. Fusion* **39**, 107 (1999).

Goedbloed H and Poedts S. *Principles of Magnetohydrodynamics*. Cambridge Press, 2004.

Hazeltine RD and Meiss JD. *Plasma Confinement*. Addison-Wesley, 1991.

Hegna CC and Callen JD. Stability of tearing modes in tokamak plasmas. *Phys. Plasmas* **1**, 2308 (1994).

Hegna CC and Callen JD. On the stabilization of neoclassical magnetohydrodynamic tearing modes using localized current drive or heating. *Phys. Plasmas* **4**(8), 2940 (1997).

La Haye RJ. Neoclassical tearing modes and their control. *Phys. Plasmas* **13**, 055501 (2006a).

Pletzer A and Perkins FW. Stabilization of neoclassical tearing modes using a continuous localized current drive. *Phys. Plasmas* **6**, 1589 (1999).

Sauter O. On the contribution of local current density to neoclassical tearing mode stabilization. *Phys. Plasmas* **11**(10), 4808 (2004).

Sauter O et al. Beta limits in long-pulse tokamak discharges. *Phys. Plasmas* **4**(5), 1654 (1997).

Urso L. *Modelling and experiments on NTM stabilisation at ASDEX Upgrade*. PhD thesis, Ludwig-Maximilians-Universität München, 2009.

Waelbroeck FL et al. Finite larmor-radius theory of magnetic island evolution. *Phys. Rev. Lett.* **87**, 215003 (2001).

Wesson J. *Tokamaks*. Oxford University Press, third edition, 2004.

Westerhof E. Tearing mode stabilization by local current density perturbations. *Nucl. Fusion* **30**(6), 1143 (1990).

Westerhof E et al. Tearing mode stabilization by electron cyclotron resonance heating demonstrated in the TEXTOR tokamak and the implication for ITER. *Nucl. Fusion* **47**, 85 (2007).

White RB. *The theory of toroidally confined plasmas*. Imperial College Press, 2001.

Wilson HR. Neoclassical Tearing Modes. *Fusion Sci. Tech.* **53**(2T), 152 (2008).

Wilson HR, Connor JW, Hastie RJ, and Hegna CC. Threshold for neoclassical magnetic island in a low collision frequency tokamak. *Phys. Plasmas* **3**, 248 (1996).

Yu Q and Günter S. Locking of neoclassical tearing modes by error fields and its stabilization by RF current. *Nucl. Fusion* **48**, 065004 (2008).

4 On the Merits of Heating and Current Drive for Tearing Mode Stabilization

The work presented in this chapter merges the paper published in *Nucl. Fusion* **49**, 075002 (2009) and the erratum [De Lazzari and Westerhof, 2010]. The appendix, concerning the application of the model to experimental data, refers to [De Lazzari et al., 2009; Ayten et al., 2011].

Abstract

   Neoclassical tearing modes (NTMs) are magnetohydrodynamic modes that can limit the performance of high β discharges in a tokamak, leading eventually to a plasma disruption. A NTM is sustained by the perturbation of the "bootstrap" current, which is a consequence of the pressure flattening across a magnetic island. Control and suppression of this mode can be achieved by means of electron cyclotron waves (ECW) which allow to deposit highly localized power at the island location. The ECW power replenishes the missing bootstrap current by generating a current perturbation either inductively, through a temperature perturbation (ECRH), or non-inductively by direct current drive (ECCD). Although both the methods have been applied successfully to experiments showing a predominance of ECRH for medium size limiter tokamaks (TEXTOR, T-10) and of ECCD for mid-to-large size divertor tokamaks (AUG, DIII-D, JT-60), conditions determining their relative importance are still unclear. We address to this problem with a numerical study focused on the contributions of heating and current drive to NTMs temporal evolution as described by the modified Rutherford equation. For the effects of both heating as well as current drive, simple analytical expressions have been found in terms of an efficiency forefactor times a "geometrical" term depending on the power deposition width w_{dep}, location and modulation. When the magnetic island width w equals the width of the deposition profile, $w \simeq 2w_{\mathrm{dep}}$, both geometric terms are practically identical. Whereas for current drive the geometric term approaches a constant for small island widths and is inversely proportional to $(w/w_{\mathrm{dep}})^2$ for large island widths, the heating term approaches a constant for large island widths and is proportional to (w/w_{dep}) for small island widths. For medium sized tokamaks (TEXTOR, AUG) the heating and current drive efficiencies are of the same order of magnitude, whereas in a future, large reactor like ITER the current drive efficiency is expected to be significantly larger.

4.1 Introduction

Control and stabilization of neoclassical tearing modes (NTMs) is one of the major requirements in fusion plasma physics in order to optimize performances of a tokamak discharge. For values of β well below ideal MHD limits [Sauter et al., 1997; La Haye, 2006a], these modes have been found to appear near resonant surfaces, at rational q values, giving rise to magnetic islands. The formation of an NTM leads to a flattening of the temperature and pressure profiles inside the island. The latter induces a helical perturbation of the bootstrap current which can sustain the mode and increase its amplitude. According to the so called "belt model" [Chang and Callen, 1990; Günter et al., 1999], the overall confinement is degraded up to 35% for a $3/2$ island and up to 50% for a $2/1$ island, as a consequence of the enhanced radial particle and energy flux around the island. In case of a $2/1$ island, mode locking eventually can occur; this results in further growth of the mode and leads finally to a plasma disruption.

Theoretical [Hegna and Callen, 1997; La Haye, 2006a] and experimental [Isayama et al., 2000; Gantenbein et al., 2000; Prater, 2004; La Haye et al., 2006b] publications have shown the possibility to stabilize these modes, by depositing heat and driving current through electron cyclotron waves (ECW) near the flux surface where the mode is located. Electron cyclotron resonance heating (ECRH) and electron cyclotron current drive (ECCD) affect the current density profile and the equilibrium temperature enhancing the linear and non-linear stability. ECCD inside the island can compensate the perturbation in bootstrap current reducing the size of the mode. Although both methods have been proven to be successful, a clear understanding of the conditions determining their relative importance is still missing. Experiments on magnetic island suppression in medium size limiter tokamaks like TEXTOR or T-10 [Kislov et al., 1997; Westerhof et al., 2007] revealed ECRH to be by far the dominant effect with respect to ECCD. An opposite result comes from analogous experimental campaigns performed in mid-to-large size divertor tokamaks such as JT-60, DIII-D and ASDEX-Upgrade (AUG) [Isayama et al., 2000; Gantenbein et al., 2000; La Haye et al., 2002]. In case of AUG, early theoretical work predicted ECRH to be more effective than ECCD [Yu and Günter, 1998]. A more recent theoretical paper [Yu et al., 2000] showed a dominance of ECCD, in particular towards smaller island sizes, in agreement with the experiments [Gantenbein et al., 2000]. Following the experimental results for these mid-to-large size divertor tokamaks, theoretical predictions concerning NTM stabilization in ITER do not include currently the effect of the heating.

The present paper addresses this problem with a systematic study of ECCD and ECRH contributions to the modified Rutherford equation (MRE) [Rutherford, 1973], which describes the non-linear evolution of NTMs. Section 2 presents the theoretical framework of the model. In sections 3 and 4 the efficiency of each method is calculated in the form of a fore-factor times a geometrical function depending on the properties determining the power deposition profile, namely the profile width w_{dep}, the power modulation $\mathcal{D}$ and the centre of the deposition profile with respect to the resonant radius x_{dep} [La Haye et al., 2008]. Analytical approximations to the geometrical functions have been found, describing the effect of each of these aspects. The fore-factor is proportional to

the efficiency by which the injected power generates a current perturbation either non-inductively (ECCD) or inductively trough a temperature perturbation (ECRH). In section 5 the relative importance of heating and current drive is treated, identifying the merit of each term in a relevant set of parameters for typical TEXTOR and AUG (neoclassical) tearing mode suppression scenarios. Extrapolation to ITER is also presented.

4.2   Theoretical Background

A theoretical model for the growth of a tearing mode is provided by the modified Rutherford equation (MRE) which describes the temporal evolution of the full width w of a magnetic island as a function of different driving and stabilizing mechanisms [La Haye, 2006a; Wilson, 2008], namely,

$$0.82\frac{\tau_r}{r_{\rm s}}\frac{{\rm d}w}{{\rm d}t} = r_{\rm s}\Delta'_0(w) - r_{\rm s}\sum_i \Delta'(\delta j_i)\,. \tag{4.1}$$

With the standard notation, $\tau_r = \mu_0 r_{\rm s}^2/\eta$ is the resistive time scale at the resonant radius $r_{\rm s}$ of the mode, η being the plasma resistivity and μ_0 the permeability of the free space. The classical stability index Δ'_0 is defined as the logarithmic discontinuity in the radial derivative of the perturbed magnetic flux function ψ across the island. The model assumes, for small islands, ψ to be constant across the island region. This is known also as the "constant ψ approximation". The second term on the right hand side of the equation (4.1), accounts for corrections to the classical tearing mode equation, due to either inductive or non-inductive perturbations of the parallel current density around the resonant surface,

$$r_{\rm s}\sum_i \Delta'(\delta j_i) = \frac{16\mu_0 L_{\rm q} r_{\rm s}}{B_{\rm p}\pi w^2}\int_{-\infty}^{\infty}{\rm d}x \oint {\rm d}\xi(\delta j_{\|,1} + \delta j_{\|,2} + \ldots)\cos(m\xi)\,. \tag{4.2}$$

Here the helical phase ξ is defined as $\xi = \theta - n\phi/m$ (where $\theta(\phi)$ and $m(n)$ are the poloidal (toroidal) angles and the poloidal (toroidal) mode number, respectively) and $x = r - r_{\rm s}$ is the displacement from the resonant surface; furthermore we make use of the magnetic shear length $L_{\rm q} = q/(dq/dr)$, of the poloidal component of the magnetic field $B_{\rm p}$ and of the safety factor q.

Among the contributions to $\delta j_{\|}$, the most relevant for this paper comes from the perturbed bootstrap current, which results in a driving term in the MRE given, in the notation of Ref. [La Haye, 2006a], by

$$r_{\rm s}\Delta'_{\rm BS} = -c_{\rm BS}\beta_{\rm p}\sqrt{\epsilon}\frac{L_{\rm q}}{L_{\rm p}}\frac{r_{\rm s}}{w}\frac{w^2}{w^2 + w_d^2}\,, \tag{4.3}$$

where $c_{\rm BS} \approx 1$ is a constant factor, $\beta_{\rm p}$ is the ratio between the plasma pressure and the poloidal magnetic pressure, ϵ is the inverse aspect ratio, $L_{\rm p}$ is the pressure scale length and w_d is the critical island width.

The ECW deposition inside the island can lead to the stabilization of the mode either directly through a non-inductive current $r_s\Delta'_{CD}$, or indirectly, by a perturbation of the temperature profile resulting in a perturbation of the inductive current, $r_s\Delta'_H$. Following the notation used in [Sauter, 2004; Westerhof et al., 2007], one can write

$$r_s\Delta'_{CD} = \frac{16\mu_0 L_q r_s}{B_p \pi w^2} \int_{-\infty}^{\infty} dx \oint d\xi\, j_{CD} \cos(m\xi)\,, \qquad (4.4)$$

$$r_s\Delta'_H = \frac{16\mu_0 L_q r_s}{B_p \pi w^2} \int_{-\infty}^{\infty} dx \oint d\xi\, j_H \cos(m\xi)\,, \qquad (4.5)$$

where, in equation (4.5), j_{CD} and j_H are the perturbations to the current density as a consequence of non-inductive current drive and heating, respectively. The latter is related to the temperature perturbation δT_e as $j_H \equiv \frac{j_{sep}}{T_{sep}^{3/2}}\delta(T_e^{3/2})$. The inductive part of the current density and the temperature at the island separatrix are denoted with j_{sep} and T_{sep}, respectively.

4.3 Current Drive Contribution to the modified Rutherford equation

The application of EC waves to drive off-axis current parallel to the equilibrium current is probably one of the most common and successful approaches to NTM stabilization. In the following discussion a normalized Gaussian distribution is assumed for the radial power deposition profile, $p_{EC} = P_{tot}\tilde{p}_{CW}(x)\mathcal{M}(\xi;\mathcal{D},\phi)$ with

$$\tilde{p}_{CW}(x) = \frac{1}{2\pi^{5/2} w_{dep} R r_s} e^{-4(x-x_{dep})^2/w_{dep}^2}\,, \qquad (4.6)$$

where w_{dep} is the full e^{-1} power density width, R denotes the tokamak major radius and x_{dep} is the deposition location relative to the resonant radius, i.e. $r_{dep} - r_s$. P_{tot} refers to the total injected power in case of continuous wave (CW) application, to be distinguished from the time averaged power used in reference [Sauter, 2004]. The function $\mathcal{M}$ accounts for the effect of power modulation; it is written in terms of a Heaviside function H as

$$\mathcal{M}(\xi;\mathcal{D},\phi) = H(\cos(m\xi + \phi) - \cos(\mathcal{D}\pi))\,. \qquad (4.7)$$

It depends on the helical angle ξ, the power on-time fraction $\mathcal{D}$ and the phase mismatch ϕ between the power modulation and the island rotation. In the remainder of the paper the power modulation will be assumed to be exactly centered about the island O-point, i.e. $\phi = 0$. To ease the notation, the variable ϕ will be dropped.

Under the assumption of fast transport along the field lines, the current density driven non-inductively by the absorbed EC power is a flux function $j_{CD} = j_{CD}(\psi)$ whereas the power deposition has generally a very localized profile. In order to relate these two figures, the power density can be averaged over a flux surface (see definition below) so

that $j_{CD} = 2\pi R \eta_{CD} \langle p_{EC} \rangle$. The current drive efficiency η_{CD}, defined here as $\eta_{CD} = I_{CD}/P_{tot}$, differs from a more conventional representation [Prater, 2004] by a factor $n_e R$, with n_e being the electron density. The power deposition and driven current profile widths have been assumed to be identical $w_{CD} = w_{dep}$, although the latter could be broader by the effect of the radial diffusion. As a consequence, η_{CD} is assumed constant over the deposition profile.

Here, the flux surface average of a function F is indicated as $\langle F \rangle$. Following the notation of [Hegna and Callen, 1997] and [Fitzpatrick, 1995], this flux surface average can be defined as $\langle F \rangle \equiv \{F\}/\{1\}$ with

$$\{F(\sigma, \Omega, \xi)\} \equiv m \oint \frac{d\xi}{2\pi} \frac{w}{4\sqrt{2}} \frac{F(\sigma, \Omega, \xi)}{\sqrt{\Omega + \cos(m\xi)}} \, , \tag{4.8}$$

for $\Omega > 1$ and

$$\{F(\sigma, \Omega, \xi)\} \equiv m \int_{-\hat{\xi}}^{\hat{\xi}} \frac{d\xi}{2\pi} \frac{w}{4\sqrt{2}} \frac{\frac{1}{2}[F(\sigma, \Omega, \xi) + F(-\sigma, \Omega, \xi)]}{\sqrt{\Omega + \cos(m\xi)}}, \tag{4.9}$$

for $\Omega \leq 1$. The island topology is defined here, by the normalized flux surface label Ω, which in a large aspect ratio approximation is given by $\Omega = 8x^2/w^2 - \cos(m\xi)$ [Fitzpatrick, 1995]. We denote $\sigma = \text{sgn}(x)$ and $\hat{\xi} = \arccos(-\Omega)/m$. Flux labels $-1 \leq \Omega \leq 1$ refer to the region inside the island, with $\Omega = -1$ at the O-point and $\Omega = 1$ at the separatrix.

The contribution of the current drive to the MRE can now be written as:

$$r_s \Delta'_{CD} = \frac{16\mu_0 L_q r_s}{B_p \pi w^2} \int_{-1}^{\infty} d\Omega \, \langle p_{EC} \rangle \eta_{CD} 2\pi R \oint d\xi \frac{w}{4\sqrt{2}} \frac{\cos(m\xi)}{\sqrt{\Omega + \cos(m\xi)}} \, . \tag{4.10}$$

Substituting the modulated power density $\langle p_{EC} \rangle$ in 4.10 and following the formulation of [Sauter, 2004], the term $r_s \Delta'_{CD}$ is given by,

$$r_s \Delta'_{CD} = \frac{16\mu_0 L_q}{B_p \pi} \frac{\eta_{CD} P_{tot}}{w_{dep}^2} F_{CD}(w^*, x_{dep}, \mathcal{D}) \, , \tag{4.11}$$

$$F_{CD}(w^*, x_{dep}, \mathcal{D}) = \frac{w_{dep}^2}{w^2} \frac{\int_{-1}^{\infty} d\Omega \, \langle \tilde{p}_{CW} \mathcal{M} \rangle \{\cos(m\xi)\}}{\int_{-1}^{\infty} d\Omega \, \langle \tilde{p}_{CW} \rangle \{1\}} \, , \tag{4.12}$$

where $w^* = w/w_{dep}$ is the normalized island width. In this way the contribution $r_s \Delta'_{CD}$ from non-inductive current to the MRE, according to 4.11, is split into a fore-factor times a dimensionless effectivity. F_{CD} depends only on geometrical parameters like the normalized island width, the displacement of the power deposition from the resonant surface and the modulation. The fore-factor is seen to be proportional to the total injected power and the current drive efficiency η_{CD}.
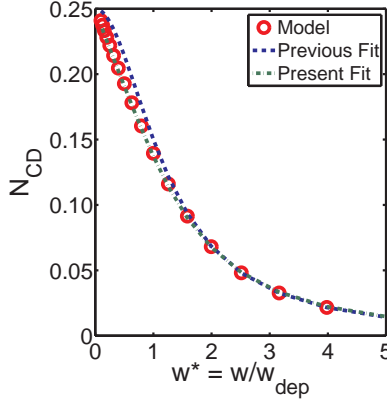
Figure 4.1: The ECCD geometrical function F_{CD} (red circles), obtained from a numerical evaluation of equation (4.12) in the case of no misalignment and continuous power deposition, i.e. $F_{CD} = N_{CD}$. The green dash-dotted curve displays the fit to N_{CD} given in equation (4.14). The blue dotted curve represents the fit given in [Perkins and Harvey, 2003; Sauter, 2004].

Evaluation of the geometrical function, F_{CD}

Equation (4.12), although rather simple, is time consuming to evaluate numerically. In order to achieve a fast calculation of Rutherford equation including the effect of current drive, an analytical approximation for F_{CD} is needed. At first let us suppose the effect of relative misalignment with respect to the rational surface to depend weakly on w^*; secondly the dependence on the on-time fraction, within a good approximation ($\approx 10\%$), not to change for different values of x_{dep}. Under these assumptions the geometrical function can be factorized into three figures of merit:

$$F_{CD}(w^*, x_{norm}, \mathcal{D}) = N_{CD}(w^*)G_{CD}(w^*, x_{norm})M_{CD}(w^*, \mathcal{D}) , \qquad (4.13)$$

where $N_{CD}(w^*)$ provides the normalization to the geometrical function depending on the normalized island width, G_{CD} accounts for the misalignment and M_{CD} for the modulation. The parameter $x_{norm} = x_{dep}/\max(w, w_{dep})$ denotes the normalized radial excursion from the O-point. Note that $G_{CD}(w^*, x_{norm} = 0) = 1$, $M_{CD}(w^*, \mathcal{D} = 1) = 1$.

The simplest case in exam presumes a continuous power deposition on the island ($\mathcal{D} = 1$), centered at the O-point ($x_{norm} = 0$), with a constant width. Figure 4.1 compares the present calculations for $F_{CD}(w^*, x_{norm} = 0, \mathcal{D} = 1) = N_{CD}(w^*)$ (red circles) with a previous fit (blue dotted line) proposed in [Perkins and Harvey, 2003; Sauter, 2004] showing a quite good agreement. The discrepancy in the range $0 < w^* < 1.5$ appears also in the cited papers. A more precise approximation to the present numerical calcula-

tion is proposed here,

$$N_{\mathrm{CD}}(w^*) = \frac{0.25 + 0.24w^*}{1 + 0.64w^{*3} + 0.43w^{*2} + 1.5w^*} \ , \tag{4.14}$$

converging to the previous one for $w^* \ll 1$ and for $w^* \gg 1$, but giving a significantly better fit in the range of $0 < w^* < 1.5$ as it is shown in figure 4.1 (green dash-dotted curve).

The loss in efficiency due to deposition misalignment is represented in figure 4.2, as function of the normalized radial excursion from the O-point. The curve shows a steep decrease of G_{CD}, such that it is reduced by 50% for $|x_{\mathrm{norm}}| \approx 0.3$. For $|x_{\mathrm{norm}}| \gtrsim 0.5$ (deposition around the separatrix) the function assumes even negative values, i.e. current drive destabilizes the mode. These results implicate a strong constraint on ECCD localization accuracy in order to achieve island stabilization, as recently reported in [La Haye et al., 2008]. Figure 4.3 shows the function M_{CD} accounting for the effect of
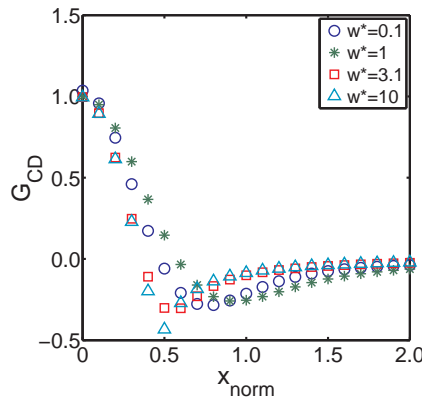
Figure 4.2: Detrimental effect of deposition misalignment on the CD normalized geo-metrical function $G_{\mathrm{CD}}(w^*, x_{\mathrm{norm}})$, varying the island size $w^* = w/w_{\mathrm{dep}}$. The displacement is normalized as $x_{\mathrm{norm}} = x_{\mathrm{dep}}/\max(w, w_{\mathrm{dep}})$. This nor-malization results in the non-monotonic dependence of the minimum effi-ciency with w^*.

modulation as a function of the on-time fraction assuming perfect phasing of the modu-lation centered around the island O-point, i.e. $\phi = 0$. Also calculations for finite phase mismatch have been performed. These showed that the stabilization efficiency drops by less than 10% provided the phase mismatch does not exceed $|\phi| = 20°$. For small values of w^* (in ITER $w^* \approx 0.5$ is expected) efficiency is optimized modulating the power with 50% on-time fraction. For larger islands this estimate rises to an on-time fraction of 70%. A set of fitting functions has been obtained for both terms, G_{CD} and M_{CD} with a discrepancy $\leq 15\%$ with respect to the numerical evaluation of equation (4.11). The
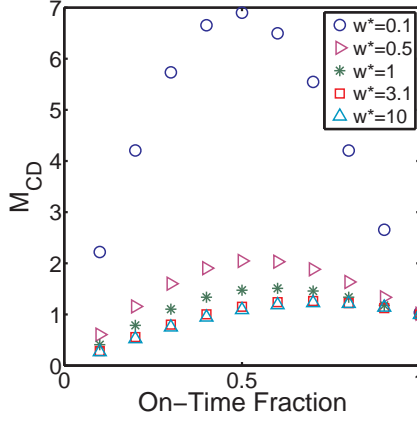
Figure 4.3: Enhancement of the CD normalized geometrical function $M_{\mathrm{CD}}(w^*, \mathcal{D})$, with on-time fraction $\mathcal{D}$, varying the island size $w^* = w/w_{\mathrm{dep}}$. Modulating the power with 50% on-time fraction, the efficiency is found to be, for $w^* = 0.1$, up to 7 times larger (blue circles) than the case of continuous wave application.

effect of the misalignment can be fitted reasonably well with the help of the real part of the plasma dispersion function as,

$$G_{\mathrm{CD}}(w^*, x_{\mathrm{norm}}) = 1 - 2\frac{x_{\mathrm{norm}}}{g(w^*)} \int_0^{x_{\mathrm{norm}}/g(w^*)} \mathrm{d}t e^{(t^2 - (x_{\mathrm{norm}}/g(w^*))^2)} , \qquad (4.15)$$

with

$$g(w^*) = \frac{0.38w^{*2} + 0.26w^* + 0.5}{w^* + 1} ,$$

where $g(w^*)$ accounts for the changing scale of the effect as the island width is varied. In the limit of small islands $g = 1/2$. The real part of the plasma dispersion function appears to fit accurately G_{CD} for $0.1 < w^* < 1$. For $w^* \geq 1$ the plasma dispersion function provides a far less accurate fit in particular of the regions with negative efficiency.

Concerning the modulation, a fit in terms of an algebraic function has been found, which can be written as

$$M_{\mathrm{CD}}(w^*, \mathcal{D}) = \frac{1}{w^{*3}}(m_1(\mathcal{D})w^{*2} + m_2(\mathcal{D})) + m_3(\mathcal{D}) , \qquad (4.16)$$

where

$$m_1(\mathcal{D}) = 2.26\mathcal{D}^4 - 3.44\mathcal{D}^3 - 0.99\mathcal{D}^2 + 2.2\mathcal{D} - 0.02 ,$$
$$m_2(\mathcal{D}) = 10^{-2}(0.34\mathcal{D}^5 - 1.02\mathcal{D}^4 + 0.87\mathcal{D}^3 - 0.28\mathcal{D}^2 + 0.1\mathcal{D}) ,$$
$$m_3(\mathcal{D}) = (1.34\mathcal{D}^4 - 3.54\mathcal{D}^3 + 1.1\mathcal{D}^2 + 2.09\mathcal{D} + 0.01) .$$

The fit is valid in the domain $0.1 \leq w^* \leq 10$, $0 \leq x_{\mathrm{norm}} \leq 2$ and $0.1 \leq \mathcal{D} \leq 1$.

4.4 Local Heating Contribution to the modified Rutherford equation

The effect of local heating on a neoclassical tearing mode is a perturbation of the inductive current density inside the magnetic island due to a perturbation of the electron temperature T_e. In order to calculate the latter, we assume that, on the time scales of interest, T_e equilibrates along the perturbed field lines, so that $T_e = T_e(\Omega)$. Introducing the heat flux $\mathbf{\Gamma}$ through the magnetic surface, the heat diffusion equation appears as,

$$\langle p_{\mathrm{EC}} \rangle = \nabla \cdot \mathbf{\Gamma} + \frac{3}{2} \frac{\partial n_e k_{\mathrm{B}} T_e}{\partial t} \ . \tag{4.17}$$

Assuming steady state conditions (for $\tau_r \gg \tau_{\mathrm{diff}}$ with $\tau_{\mathrm{diff}} = w^2/\chi_\perp$) and neglecting the convective contribution to the heat flux one obtains,

$$\langle p_{\mathrm{EC}} \rangle + \frac{\partial \Omega}{\partial V} \frac{\partial}{\partial \Omega} \left(\frac{\partial V}{\partial \Omega} \langle (\nabla \Omega)^2 \rangle n_e \chi_\perp k_{\mathrm{B}} \frac{\partial T_e}{\partial \Omega} \right) = 0 \ , \tag{4.18}$$

where the gradient is written in terms of the normalized flux surface label Ω and $V(\Omega)$ denotes the total volume enclosed within a given flux surface. The perpendicular heat conductivity $\chi_\perp$ is assumed to be a constant; n_e is the electron density, and k_{B} is the Boltzmann constant (in units of J/keV). Calculating the volume of the flux shell as $\partial V / \partial \Omega = 8\pi^2 R r_{\mathrm{s}} \{1\}$, the previous equation reduces to

$$\langle p_{\mathrm{EC}} \rangle \partial V = -\partial \left(8\pi^2 R r_{\mathrm{s}} \{|\nabla \Omega|^2\} n_e \chi_\perp k_{\mathrm{B}} \frac{\partial T_e}{\partial \Omega} \right) \ . \tag{4.19}$$

Integrating twice 4.19 over Ω and denoting with $P(\Omega)$ the total power injected inside the flux tube between the O-point and the flux surface labeled Ω, an expression for $T_e = T_{\mathrm{sep}} + \delta T_e$ is obtained, where

$$\delta T_e = \frac{P_{\mathrm{tot}} w}{8\pi^2 R r_{\mathrm{s}} \chi_\perp n_e k_{\mathrm{B}}} \delta \tilde{T}_e \ , \tag{4.20}$$

and[1]

$$\delta \tilde{T}_e \equiv \int_\Omega^1 d\Omega \frac{\tilde{P}}{\{|\nabla \Omega|^2\}} \frac{1}{w} \ ; \quad \tilde{P} = \frac{P(\Omega)}{P_{\mathrm{tot}}} \ . \tag{4.21}$$

The integral fore-factor in equation (4.20) is dimensionally a temperature while $\delta \tilde{T}_e$ is dimensionless. Let us introduce an approximation for the current perturbation $j_{\mathrm{H}} \propto \delta(T_e^{3/2})$,

$$\delta(T_e^{3/2}) = (T_{\mathrm{sep}} + \delta T_e)^{3/2} - T_{\mathrm{sep}}^{3/2} \approx T_{\mathrm{sep}}^{1/2} \frac{3}{2} \delta T_e \ , \tag{4.22}$$

such that j_{H} can be approximated as,

$$j_{\mathrm{H}} \approx \frac{j_{\mathrm{sep}}}{T_{\mathrm{sep}}} \frac{3}{2} \delta T_e \ . \tag{4.23}$$

---

[1]Equation (4.21) differs from equation (21) in the original paper by a factor $8\pi^2 R r_{\mathrm{s}}$.

Substituting equations (4.20) and 4.23 in equation (4.5) a new expression for $r_s\Delta'_H$ is obtained,

$$r_s\Delta'_H \approx \frac{16\mu_0 L_q}{B_p\pi}\frac{\eta_H P_{tot}}{w_{dep}^2}F_H(w^*, x_{dep}, \mathcal{D}) \tag{4.24}$$

where

$$F_H(w^*, x_{dep}, \mathcal{D}) = \frac{1}{2\pi w}\int_{-1}^{1}d\Omega\,\delta\tilde{T}_e\oint d\xi\frac{w}{4\sqrt{2}}\frac{\cos(m\xi)}{\sqrt{\Omega + \cos(m\xi)}} \tag{4.25}$$

The factor η_H has been defined as the efficiency with which the power is converted into a perturbative inductive current. It can be shown [de Baar et al., 2008] that

$$\eta_H = \frac{3w_{dep}^2}{8\pi Rn_e\chi_\perp k_B}\frac{j_{sep}}{T_{sep}} . \tag{4.26}$$

The expression obtained for η_H is such that it is independent of the island size; it contains only plasma parameters, the power deposition width and an estimate of the anomalous heat diffusivity inside the island. The reader is reminded that j_{sep} refers to the inductive part of the current density at the separatrix only. In cases where a significant fraction of the equilibrium current density is non-inductively driven, for example in the presence of a large bootstrap current fraction, this can result in a significant reduction of η_H. All the geometrical properties describing $r_s\Delta'_H$ are enclosed in the dimensionless function F_H.

Evaluation of the geometrical function, F_H

In analogy with the previous section the last dimensionless integral can be modeled with an analytical function F_H,

$$F_H(w^*, x_{norm}, \mathcal{D}) = N_H(w^*)G_H(w^*, x_{norm})M_H(w^*, \mathcal{D}) . \tag{4.27}$$

As in the case of current drive the functions G_H and M_H are defined as $G_H(w^*, x_{norm} = 0) = 1$, $M_H(w^*, \mathcal{D} = 1) = 1$. The normalization function N_H is shown in figure 4.4. The trend is approximately linear for small values of w^* converging to a constant for $w^* \gg 1$. Figures 4.5 and 4.6 show the dependencies on the radial mismatch and the power modulation. The trend of G_H in figure 4.5 presents a peak at $x_{norm} = 0$ which rapidly decreases to zero for a displacement $0.5 < x_{norm} < 1$. The curve does not assume negative values around the separatrix region. In figure 4.6 the effect of power modulation on the normalized geometrical factor appears essentially independent from the island width. In contrast with the case of $M_{CD}(w^*, \mathcal{D})$, modulation never results in a improved efficiency. A strongly reduced efficiency is found for on time fractions below $\mathcal{D} < 50\%$. Following the same procedure as shown in paragraph 3.1, a set of fitting functions has been obtained[2], with a discrepancy $< 10\%$ with respect to the numerical evaluation of 4.25:

$$N_H(w^*) = \frac{0.077w^{*2} + 0.088w^*}{w^{*2} + 0.8w^* + 2.17} , \tag{4.28}$$

[2]Equation (4.28) differs from equation (28) in the original paper approximately by a constant factor 0.26.
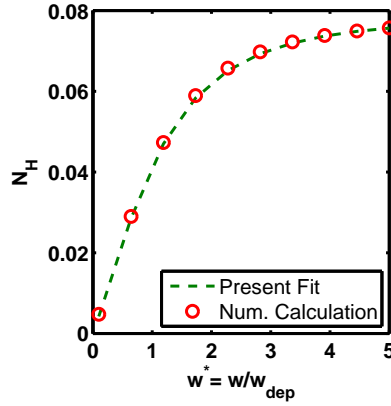
Figure 4.4: The ECRH geometrical function F_{H} (red circles), obtained from a numerical evaluation of equation (4.25) in the case of no misalignment and continuous power deposition, i.e. $F_{\mathrm{H}} = N_{\mathrm{H}}$. The green dash-dotted curve displays the fit to N_{H} given in equation (4.28). This picture has been corrected according to [De Lazzari and Westerhof, 2010].
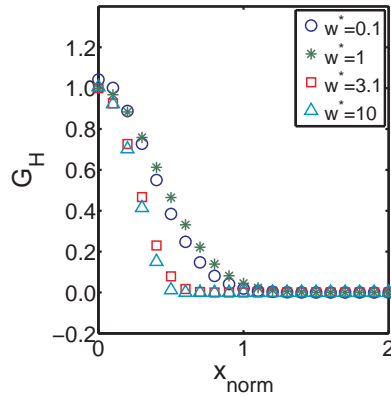
Figure 4.5: Detrimental effect of deposition misalignment on the heating normalized geometrical function $G_{\mathrm{H}}(w^*, x_{\mathrm{norm}})$, varying the island size $w^* = w/w_{\mathrm{dep}}$. The displacement is normalized as $x_{\mathrm{norm}} = x_{\mathrm{dep}}/\max(w, w_{\mathrm{dep}})$. Note that, differently from figure 4.2, the function does not assume negative values around the separatrix.
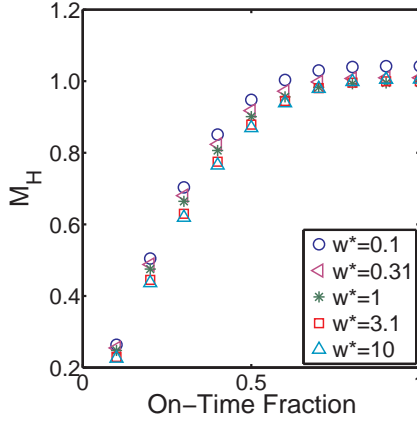
Figure 4.6: Effect of power modulation on the heating normalized geometrical function $M_H(w^*, \mathcal{D})$ with on-time fraction $\mathcal{D}$. No improvement of the efficiency appears from the picture. The dependence on the island size in this case is negligible.

$$G_H(w^*, x_{norm}) = \exp\left(-\left(\frac{x_{norm}}{g(w^*)}\right)^2\right), \tag{4.29}$$

with

$$g(w^*) = 0.00035w^{*4} - 0.008w^{*3} + 0.07w^{*2} + 0.02w^* + 0.5,$$

$$M_H(\mathcal{D}) = 1.2\mathcal{D}^3 - 3.5\mathcal{D}^2 + 3.3\mathcal{D} - 0.06. \tag{4.30}$$

4.5 About the relative merits of Heating and Current Drive

In the previous sections $r_s\Delta'_{CD}$ and $r_s\Delta'_H$ have been treated separately in terms of their geometrical properties. At first glance (figures 4.2 and 4.5) the most striking difference appears in the misalignment dependence where G_{CD} is assuming negative values near the X-point. In this region current drive is destabilizing the island, while the heating contribution is still positive. This affects the requirements for power deposition accuracy: at $x_{norm} \approx 0.4$, G_{CD} decreases by 83%, while G_H is reduced by 45%.

To derive the relative impact on the Rutherford equation, the full expressions for $r_s\Delta'_{CD,H}$ (i.e. equations (4.11) and (4.24), respectively) must be compared. It is noted that the expressions for $r_s\Delta'_{CD}$ and $r_s\Delta'_H$ differ only in the appearance of the current generation efficiency $\eta_{CD,H}$ and the geometrical function $F_{CD,H}$,

$$r_s\Delta'_{CD,H} \propto \eta_{CD,H}F_{CD,H}(w^*, x_{norm}, \mathcal{D}). \tag{4.31}$$

Values for $\eta_{CD,H}$ shown in the table 4.1 indicate that the relative merits of heating and current drive in TEXTOR are directly related to their geometrical factors. This suggests a direct comparison for the case of continuous power deposition at the O-point $x_{norm} = 0$ and $\mathcal{D} = 1$, shown in figure 4.7. The plot shows the trend of $N_{CD,H}$ (marked with green stars and blue circles, respectively), which are found to take the same value at $w^* = 2$. In the region $w^* \ll 2$ current drive appears almost two orders of magnitude more effective than the heating. The efficiency of the former scales as a constant, while for the latter, it grows linearly.

In the region where $w^* \gg 2$ this trend is opposite: N_H approaches a constant and N_{CD} is decreasing quadratically as $1/w^{*2}$. Observing the typical range of the island width, during its evolution, in a particular tokamak, it is possible to determine whether the mode will be affected by either ECCD or ECRH. For a medium-size tokamak like TEXTOR, experiments on the suppression of resonant magnetic perturbations (RMP) induced tearing modes confirmed the island suppression is highly independent on the current drive. These measurements are compatible with the theoretical predictions (see red arrows in figure 4.7), since the typical 2/1 island detected is larger than the deposition width. In this region the ratio $N_H/N_{CD} \gg 1$.

In the ASDEX Upgrade experiments electron cyclotron current drive is predicted to play a dominant role over most of the relevant parameter regime with still a significant contribution from heating. This is consistent with the experiments and the theoretical analyses of these experiments[Yu et al., 2000; Gantenbein et al., 2000]. The previous picture, together with figure 4.3, are helpful also to discuss the merits of the modulation in the island suppression. The method seems to enhance the stabilization primarily in the case of small islands, whereas it appears pointless in the region where the heating contribution is dominant, for $w^* \gg 2$.

Observing the values of $\eta_{CD,H}$ reported in table 1 for a large tokamak such as ITER "scenario 2", ECCD appears one order of magnitude more efficient than ECRH. This is

Table 4.1: Typical values of $\eta_{CD,H}$ (in units of $[kA]/[MW]$) estimated for different tokamaks. These should be considered as a rough estimation, provided the uncertainty on the perpendicular heat diffusivity $\chi_\perp$. Parameters used to determine $\eta_{CD,H}$ refer to datasets reported in [Westerhof et al., 2007] for TEXTOR and in [Leuterer et al., 2001; Urso et al., 2005] for AUG. In the case of ITER, our calculations refer to the so called "scenario 2" [Prater et al., 2008].

	η_{CD}	η_H
TEXTOR	2.5	2.8
AUG	$4 - 6$	$5 - 9$
ITER	5.7	0.4
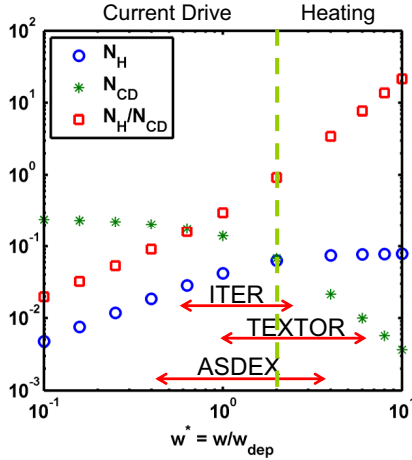
Figure 4.7: Geometrical efficiency for ECCD and ECRH (green stars and blue circles, respectively), calculated at $x_{\mathrm{norm}} = 0$ with continuous power deposition. Note that the ratio $N_{\mathrm{H}}/N_{\mathrm{CD}}$ (red squares) is ranging from 10^{-1} for $w^* \simeq 0.1$ to 10^2 for $w^* \simeq 10$. Red arrows refer to the typical range of a $3/2$ island in AUG and ITER, and of a $2/1$ island in TEXTOR. This picture has been corrected according to [De Lazzari and Westerhof, 2010].

in agreement with the results of [Yu and Günter, 1998]. The contour plot in figure 4.8 represents the $\log(\eta_{\mathrm{CD}} F_{\mathrm{CD}}/\eta_{\mathrm{H}} F_{\mathrm{H}})$ depending on the island width and the power modulation. Positive values of the logarithmic ratio correspond to the region where current drive is predominant. This one is found for $w^* \lesssim 8$. The figure 4.8 permits to draw some conclusions concerning the possible improvement of the island stabilization due to ECRH in ITER. For a saturated $3/2$ island with an estimated width of 12.5 cm, ECCD appears about 4.5 times more efficient than ECRH. This implies that in the early phase of NTM evolution, ECRH adds a $\approx 6 - 7\%$ contribution to the stabilization of the mode. This contribution rapidly decreases along with the island shrinkage.

4.6   Conclusion

The successful application of EC waves to the stabilization of magnetic islands has motivated a further theoretical effort in order to assess which conditions are determining the relative importance of ECCD and ECRH. These conditions are important for a correct prediction of the power required for mode suppression.

The paper has shown the possibility to compare ECCD and ECRH by describing their
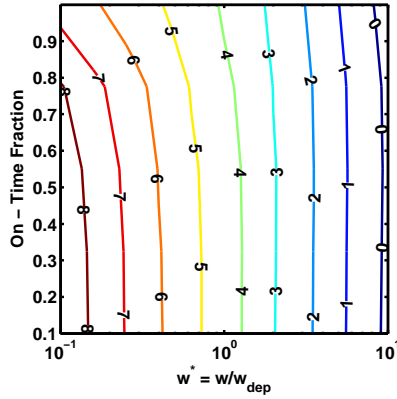
Figure 4.8: Contour plot of $\log(\eta_{\mathrm{CD}} F_{\mathrm{CD}}/\eta_{\mathrm{H}} F_{\mathrm{H}})$ representing the relative merits of heating and current drive for ITER scenario 2, with front steering deposition. Typical parameters are: $P_{\mathrm{tot}} = 13.3\mathrm{MW}$, $I_{\mathrm{CD}} = 0.076\mathrm{MA}$, $w_{\mathrm{dep}} = 4.9\mathrm{cm}$. The curve labeled with 0 represents the locus of points where $\eta_{\mathrm{CD}} F_{\mathrm{CD}} = \eta_{\mathrm{H}} F_{\mathrm{H}}$. This picture has been corrected according to [De Lazzari and Westerhof, 2010].

contribution to the Rutherford equation with a parallel structure as represented by equations (4.11) and 4.24, respectively. This formulation allows to separate the machine-related parameters from the geometrical properties of the deposition, namely deposition width, location and modulation.

For each of these parameters a systematic study has been performed, delineating two main regimes. Current drive is shown to be the dominant effect for $w^* \ll 2$, where w^* is equal to the full width w of the island normalized to the full Gaussian width w_{dep} of the power deposition profile. In this scenario deposition location and modulation are playing a crucial role; the former causes a strong reduction of the efficiency as it moves away from the island O-point, the latter avoids power from being deposited around the separatrix (assuming no phase mismatch) with the consequent destabilization of the mode. In the region where $w^* \gg 2$, ECRH becomes the main reason for island stabilization. In this case a radial misalignment does not cause mode destabilization. As the temperature perturbation is a solution of a diffusion equation, it will always be peaked at the island O-point. Accordingly, also power modulation does not enhance the geometrical efficiency.

Results of the calculations have been compared to different experiments, such as TEXTOR, AUG and ITER scenario 2. It is worthwhile to mention that, for significant fraction of bootstrap current, the perturbative model used for the modified Rutherford equation might not be entirely valid. For TEXTOR theoretical predictions are in qualitative agreement with experiments, showing that heating is the dominant cause of the achieved stabilization. In AUG, on the contrary, heating is expected to play a marginal

role, in agreement with the experimental results. Extrapolations to ITER predict a strong predominance of current drive with respect to ECRH.

4.7   Appendix: Application to TEXTOR experiments

In this appendix the theoretical predictions developed so far are benchmarked with a number of experiments [Westerhof et al., 2007; Classen et al., 2007] addressing the suppression of $m/n = 2/1$ tearing mode by ECRH and ECCD. The results presented here are part of a more extensive analysis, acknowledged to [Ayten et al., 2011], performed on experimental measurements obtained from a medium-size limiter tokamak, TEXTOR [Samm, 2005]. A brief description of the machine parameters is given in the table below.

Table 4.2: TEXTOR machine and plasma parameters

Major radius (R)	1.75 m
Plasma radius (a)	0.47 m
Plasma volume	7.0 m^3
Magnetic field (B)	$1.1 - 2.9$ T
Plasma current (I_p)	200-800 kA
Pulse length	<10 s
Ohmic power	$0.3 - 0.5$ MW
Electron temperature (T_i)	1 keV
Ion temperature (T_i)	1 keV
Electron density (n_e)	3×10^{19} m^{-3}

In these experiments magnetic islands are driven by the dynamic ergodic divertor (DED), introduced in 3.5, located on the high field side of the tokamak and operating at a frequency of 1 kHz. The resulting tearing mode, the saturated width being denoted with w_DED, is therefore locked to the rotating perturbation field, at $r_\mathrm{s} = 0.25 - 0.28$ m. Tearing mode control is achieved by means of a 800 kW, 140 GHz, long pulse gyrotron injecting microwave radiation into the plasma. This causes the heating of electrons by the resonant absorption of the waves at the 2$^\mathrm{nd}$ harmonic of the electron cyclotron resonance (from which the name ECRH). The gyrotron can be operated either continuously (CW) or modulated. The radial position of the ECRH deposition is tuned by rotating the front mirror of a steerable launcher. An appropriate choice of the toroidal injection angle allows to drive non-inductive current, ECCD. The two main diagnostics in use to determine the size of magnetic islands are the electron cyclotron emission (ECE) receiver and the soft x-ray camera (sxr). Both can measure the temperature oscillations of the plasma at the resonant surface, from which the island width can be estimated. In particular the 141 GHz ECE channel measures the radiation temperature on the high-field side coming from a region several cm inside the q = 2 surface. The measurement of the island width

has been realized by measuring the amplitude of the temperature oscillations, having the same frequency as the DED. A detailed description of these instruments is beyond the scope of the thesis; further informations concerning TEXTOR diagnostics can be found in [Donné et al., 2005]. All the experiments reported in the following discussion, have been set up with a toroidal magnetic field $B_\phi = 2.25$ T, a toroidal plasma current $I_p = 300$ kA, and a line averaged density of $2 \times 10^{19} \mathrm{m}^{-3}$. The current in the DED coils was ramped up to reach a value of 2 kA. It should be noted that in TEXTOR the bootstrap current is usually negligible and consequently insufficient to drive an NTM. This implies that the benchmark addresses only classical tearing modes. The benchmark of the GRE is performed by comparing the simulated reduction in saturated island width, according to equation (4.11), for ECRH and ECCD with the experimental data. In order to calculate the effectivity of the heating η_H, the heat conductivity and the plasma parameters as obtained in [Classen et al., 2007; Westerhof et al., 2007] are used, while the current drive efficiency η_{CD} is obtained from beam tracing calculations.

In the first dataset, two radial deposition scans at 750 kW with $w_{dep} = 1.2$cm and $w_{dep} = 4.6$ cm respectively, are performed (see figures 4.9). Each scan shows the trend of the island width (normalized to w_{DED}) as function of the power deposition location. In the first case the vertical injection angle has been varied from $0°$ to $12°$, resulting in a deposition radius ranging from $r_{dep} = 0.23$ m to 0.31 m. In the second scan, the vertical injection angle was scanned from $1°$ to $13°$ and accordingly, the deposition radius from 0.21 m to 0.34 m. The model, although qualitatively compatible with experimental data, results in a symmetric suppression around the resonant radius $r_s \approx 28$ cm which does not match the asymmetric trend of the data (see black solid lines). This could be due to a modification in the magnetic equilibrium in response to the heating well outside the island resulting in a further destabilization for $r_{dep} < r_s$ and a further stabilization for $r_{dep} > r_s$. In the wide deposition scan 4.9-b a finite local current drive has been induced, although the effect on the saturated island width appears negligible. These observations are compatible with the theoretical predictions (see red arrows in figure 4.7), since the typical 2/1 island detected is larger than the deposition width. A second dataset has been used to benchmark the dependence of the (normalized) saturated island width on the modulation (see equation (4.11)) as shown in figure 4.10. The modulated power varies between 70 kW and 400 kW, while the duty-cycle has been varied from 0% to 100%. The power is deposited in phase with the O-point, at the resonant radius. This is assumed to coincide with the deposition radius $r_{dep} = 0.262$ m. In addition the efficiency of 200 kW CW power is compared with that of the modulated power with 40% duty-cycle for the 400 kW, which corresponds to the same average power. In the case of modulated ECRH and varying the duty-cycle, a reasonable agreement with the experimental data appears when the on-time fraction is larger than 50%. At lower duty-cycle, the discrepancy might be due to a radial misalignment: in the experiments the power deposition was optimized to coincide with r_s for the high power, high duty cycle cases; as a consequence of small, global profile changes at lower powers r_s may be slightly shifted for those cases. As the duty-cycle is increased, the suppression efficiency increases as well but no further improvement is observed beyond a duty-cycle of about 60%. Modulated ECRH power with 40% duty-cycle provides a stronger suppression than CW ECRH at the same average
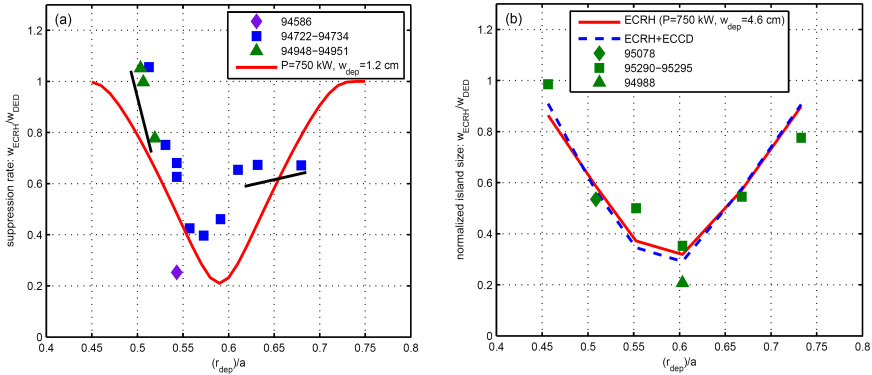
Figure 4.9: Suppression of the 2/1 magnetic island as a function of the radial deposition displacement (normalized to the minor radius, $a = 47$cm) for different toroidal injection angles ϕ and deposition width at full power $P = 750$kW: (a) $\phi = +0.5°$ and $w_{\mathrm{dep}} = 1.2$ cm; (b) $\phi = -16°$ and $w_{\mathrm{dep}} = 4.6$ cm. The red solid curve in (a) represents the numerical calculation of pure ECRH stabilization. In (b) green markers refer to experimental points, while the red solid line refer to the effect of pure ECRH. Note that the contribution of ECCD (blue dashed line) is clearly negligible. Different symbols refer to data taken on different days which may imply slight variations in the position of the $q = 2$ surface.
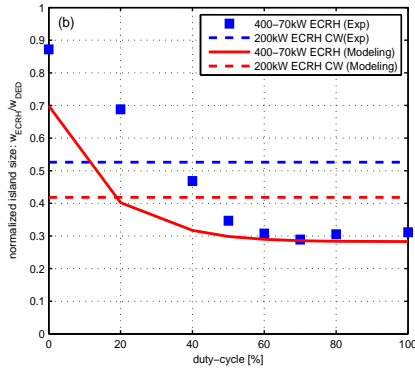
Figure 4.10: Suppression of a 2/1 mode by modulated ECRH centered around the O-point as a function of the duty cycle of the ECRH high-power phase. Red solid lines refer to the numerical simulations while blue markers to experimental data. Horizontal lines refer to the 200 kW continuous power deposition case.

power of 200 kW.

Acknowledgments

References

Ayten B, De Lazzari D, De Baar MR, Hennen B, Westerhof E, and the TEXTOR Teamg. Modeling of tearing mode suppression experiments in TEXTOR based on the generalized Rutherford equation. *Nucl. Fusion* **51**, 43007 (2011).

Chang Z and Callen J. Global energy confinement degradation due to macroscopic phenomena in tokamaks. *Nucl. Fusion* **30**(2), 219 (1990).

Classen IGJ et al. Effect of heating on the suppression of tearing modes in tokamaks. *Phys. Rev. Lett.* **98**, 035001 (2007).

de Baar MR et al. Physics and real time control of tearing modes in TEXTOR. In *22nd IAEA Fusion Energy Conference*, 2008.

De Lazzari D and Westerhof E. Erratum: On the merits of heating and current drive for tearing mode stabilization. *Nucl. Fusion* **50**, 79801 (2010).

De Lazzari D, Westerhof E, Ayten B, and the TEXTOR team. On the merits of heating and current drive for tearing modes stabilization. In *36th EPS Conference on Plasma Physics*, volume 33E, pages P–1.124, 2009.

Donné AJH et al. Overview of core diagnostics for TEXTOR. *Fusion Sci. Tech.* **47**, 220 (2005).

Fitzpatrick R. Helical temperature perturbations associated with tearing modes in tokamak plasmas. *Phys. Plasmas* **2**(3), 825 (1995).

Gantenbein G, Zohm H, Giruzzi G, Günter S, Leuterer F, Maraschek M, Meskat J, Yu Q, ASDEX Upgrade Team, and ECRH-Group (AUG)l. Complete suppression of neoclassical tearing modes with current drive at the electron-cyclotron-resonance frequency in ASDEX Upgrade Tokamak. *Phys. Rev. Lett.* **85**(6), 1242 (2000).

Günter S, Gude A, Maraschek M, Yu Q, and the ASDEX Upgrade Team. Influence of neoclassical tearing modes on energy confinement. *Plasma Phys. Control. Fusion* **41** (6), 767 (1999).

Hegna CC and Callen JD. On the stabilization of neoclassical magnetohydrodynamic tearing modes using localized current drive or heating. *Phys. Plasmas* **4**(8), 2940 (1997).

Isayama A et al. Complete stabilization of a tearing mode in steady state high-β_p H-mode discharges by the first harmonic electron cyclotron heating/current drive on JT-60U. *Plasma Phys. Control. Fusion* **42**(12), L37 (2000).

Kislov DA, Alikaev VV, Esipchuk Yu V, Kakurtn AM, Kislov A Ya, Martynov DA, Notkin GE, Razumova KA, Sushkov AV, and Volkov VV. The m=2, n=1 mode suppression by ECRH on the T-10 tokamak. *Nucl. Fusion* **37**(3), 339 (1997).

La Haye RJ. Neoclassical tearing modes and their control. *Phys. Plasmas* **13**, 055501 (2006a).

La Haye RJ, Günter S, Humphreys DA, Lohr J, Luce TC, Maraschek ME, Petty CC, Prater R, Scoville JT, and Strait EJ. Control of neoclassical tearing modes in DIII–D. *Phys. Plasmas* **9**(5), 2051 (2002).

La Haye RJ, Prater R, Buttery RJ, Hayashi N, Isayama A, Maraschek ME, Urso L, and Zohm H. Cross-machine benchmarking for ITER of neoclassical tearing mode stabilization by electron cyclotron current drive. *Nucl. Fusion* **46**, 451 (2006b).

La Haye RJ, Ferron JR, Humphreys DA, Luce TC, Petty CC, Prater R, Strait EJ, and Welander AS. Requirements for alignment of electron cyclotron current drive for neoclassical tearing mode stabilization in ITER. *Nucl. Fusion* **48**, 054004 (2008).

Leuterer F, Günter S, Maraschek M, Ryter F, Suttrop W, Wolf R, the ASDEX Upgrade Team, Gantenbein G, and Zohm H. ECRH experiments in ASDEX upgrade. *Fusion Eng. Des.* **53**(1-4), 277 (2001).

Perkins FW and Harvey RW. On Neoclassical Tearing Modes. *Bull. Am. Phys. Soc.* **48** (2003).

Prater R. Heating and current drive by electron cyclotron waves. *Phys. Plasmas* **11**(5), 2349 (2004).

Prater R et al. Benchmarking of codes for electron cyclotron heating and electron cyclotron current drive under ITER conditions. *Nucl. Fusion* **48**, 035006 (2008).

Rutherford PH. Nonlinear growth of tearing mode. *Phys. Fluids* **16**(11), 1903 (1973).

Samm U. TEXTOR: a pioneering device for new concepts in plasma-wall interaction, exhaust and confinement. *Fusion Sci. Tech.* **47**, 76 (2005).

Sauter O. On the contribution of local current density to neoclassical tearing mode stabilization. *Phys. Plasmas* **11**(10), 4808 (2004).

Sauter O et al. Beta limits in long-pulse tokamak discharges. *Phys. Plasmas* **4**(5), 1654 (1997).

Urso U, Maraschek M, Zohm H, and the ASDEX Upgrade Team. Fitting of the Rutherford equation for neoclassical tearing mode stabilization in ASDEX Upgrade. *J. Phys.: Conf. Ser.* **25**, 266 (2005).

Westerhof E et al. Tearing mode stabilization by electron cyclotron resonance heating demonstrated in the TEXTOR tokamak and the implication for ITER. *Nucl. Fusion* **47**, 85 (2007).

Wilson HR. Neoclassical Tearing Modes. *Fusion Sci. Tech.* **53**(2T), 152 (2008).

Yu Q and Günter S. On the stabilization of neoclassical tearing modes by phased electron cyclotron waves. *Plasma Phys. Control. Fusion* **40**, 1977 (1998).

Yu Q, Günter S, Giruzzi G, Lackner K, and Zabiego M. Modeling of the stabilization of neoclassical tearing modes by localized radio frequency current drive. *Phys. Plasmas* **7**(1), 312 (2000).

5 The role of asymmetries in the growth and suppression of neoclassical tearing modes

Abstract

The evolution of neoclassical tearing modes (NTMs) is usually described by the generalized Rutherford equation (GRE) for a symmetric magnetic island. Despite the success of this representation, various experiments have found the evidence of asymmetries in the island geometry. A generalization of the model suggests that a number of effects, such as a quasi-linear correction of the constant-ψ approximation, a shear flow or a temperature gradient across the island, might be responsible for the deformation of the island geometry. In addition, it is noticed that the symmetry is broken in the radial direction also by approximating the equilibrium helical flux function by a Taylor expansion up to the third order derivative. The present paper addresses the role of these asymmetries in the growth and suppression of neoclassical tearing modes in a slab geometry, with particular attention to the implications for the local current drive (ECCD) and resonant heating (ECRH) terms. The stabilizing contributions provided by electron cyclotron waves to neoclassical tearing modes are found to be largely unaffected by these perturbations. These results correct and extend some of the conclusions presented in Lazzaro and Nowak (2009 Plasma Phys. Control. Fusion **51**, 035005).

5.1   Introduction

Neoclassical tearing modes (NTMs) are acknowledged to severely limit the tokamak performance well below the ideal β_N limit [Chang et al., 1995], [Sauter et al., 1997; La Haye et al., 1997; Zohm et al., 1997; Gates et al., 1997], [Isayama et al., 1999; JET, 1999] and [La Haye, 2006a]. Localized heating and current drive at the location of the magnetic island created by an NTM have been demonstrated both experimentally and theoretically to provide efficient suppression of these modes [Hegna and Callen, 1997; Gantenbein et al., 2000; Isayama et al., 2000; La Haye et al., 2002; Westerhof et al., 2007; De Lazzari et al., 2009]. The main mechanism for the suppression is the replacement inside the island of the missing bootstrap current (i.e. the reason for the growth of the mode) with an inductive or non-inductive current perturbation, respectively. The framework for the description of the mode growth and suppression is formed by a generalization of the Rutherford equation [Rutherford, 1973] to take into account localized perturbations to Ohm's law inside and around the magnetic island [Sauter et al., 1997; La Haye, 2006a].

The Rutherford equation and its generalization have been derived originally for symmetric islands in the so-called constant-ψ approximation only. Despite the success of this representation, various experiments performed in ASDEX Upgrade, in DIII-D, in JT-60 and in TEXTOR have found the evidence of asymmetric islands [Meskat et al., 2001; Udintsev et al., 2003; La Haye et al., 2010; Urso et al., 2010]. Also from a theoretical point of view, several effects have been identified that introduce asymmetries in the magnetic islands. For example, an in-out asymmetry can be generated both by a finite third order derivative in the equilibrium helical flux function as well as by a quasi-linear correction to the constant-ψ approximation. Furthermore, a finite flow shear across the magnetic island can result in a poloidal deformation of the island [Ren et al., 1999; Smolyakov et al., 2001]. A priori, such changes to the geometry of the flux surfaces can be expected to affect the two dimensional integrals over the island region appearing in the generalized Rutherford equation. In particular, changes can be expected to the stabilizing terms coming from localized heating or localized current drive as affected, for example, by electron cyclotron resonance heating (ECRH) or current drive (ECCD), as these terms involve in addition the flux surface average of the EC power deposition profile which is highly localized in minor radius as well as in toroidal and poloidal angles.

A first study of the effects of these asymmetries on the efficiency of localized current drive for mode stabilization has appeared in [Lazzaro and Nowak, 2009]. The present paper extends these results to the case of localized heating, and corrects the generalized Rutherford equation as proposed in [Lazzaro and Nowak, 2009] to take into account the consequences of the asymmetries in the magnetic island more properly. The theoretical background, both of the origin of the asymmetries and of the resulting modifications to the generalized Rutherford equation are presented in section 5.2. In section 5.3 the consequences of the asymmetries for the drive of the NTM by the perturbation of the bootstrap current and for the mode suppression by localized heating and current drive are presented, while in section 5.4 the validity of the model is discussed with respect to the previous literature. The final section provides a summary of the main conclusions of this work.

5.2 Asymmetric islands and the generalized Rutherford equation

Island geometry

Considering a single helicity perturbation, the geometry of a magnetic island is determined by the surfaces of constant helical flux ψ, i.e.

$$\psi \equiv \psi_0 + \psi_1, \tag{5.1}$$

where $\psi_0(r)$ is the axisymmetric equilibrium helical flux, which is defined up to an arbitrary constant, and ψ_1 is the perturbation to the helical flux. A Taylor expansion of the equilibrium flux around the rational surface r_s, where the first derivative of ψ_0 vanishes, reads

$$\psi_0(r) = \frac{1}{2}\psi_0'' x^2 + \frac{1}{6}\psi_0''' x^3 + \mathcal{O}(x^4) \tag{5.2}$$

with $x = r - r_s$ and a prime indicating derivation with respect to r at $r = r_s$. A quite general form of the helical flux function perturbation in the region of the magnetic island itself can be written as [Smolyakov et al., 2001; van der Plas and de Blank, 2007; Lazzaro and Nowak, 2009]

$$\psi_1 = \tilde{\psi}(1 + \tfrac{1}{2}\Delta_c' x)\cos(\xi - \tfrac{1}{2}\Delta_s' x - \tfrac{1}{2}\Delta_T'|x|), \tag{5.3}$$

where $\tilde{\psi} = \psi_1(r_s)$ is a constant giving the amplitude of the helical flux perturbation at the resonant surface and $\xi = m\theta - n\phi$ is the helical angle. The third order derivative of the equilibrium helical flux and the constant Δ_c' are both seen to break the up-down symmetry in the radial shape of the island. The constants Δ_s' and Δ_T' are responsible for the generation of different types of asymmetries in the phase of the magnetic island. In principle all these symmetry breaking terms should remain small over the full island width, w. Possible physical origins for these terms will be discussed below. As a slab approximation will be used for the region covering both the island and the EC deposition, both w and x are required to remain much smaller than the minor radius a.

Outside the magnetic island the shape of the perturbed flux function is determined by the linearized ideal MHD equations. Matching across a small island in the approximation of constant-$\psi_1(x)$, i.e. $\Delta_c' = 0$, results in the well known tearing mode stability parameter Δ' which is defined by the jump of the logarithmic derivative (in the limit of vanishing island width) of the perturbed helical flux function,

$$\Delta' \equiv \lim_{\epsilon \downarrow 0} \frac{\psi_1'(r_s + \epsilon) - \psi_1'(r_s - \epsilon)}{\psi_1(r_s)}. \tag{5.4}$$

For large islands, an instability index $\Delta'(w)$ can be introduced by substituting $\epsilon \downarrow 0$ with $w/2$. In addition, the constant-$\psi_1(x)$ approximation will be broken due to the non-zero average gradient in the perturbed flux function across the island. The latter effect is

accounted for by a quasi-linear correction introducing the parameter Δ'_c which through matching to the exterior solution is given by

$$\Delta'_c \equiv \frac{\psi'_1(r_s + w/2) + \psi'_1(r_s - w/2)}{\psi_1(r_s)}. \tag{5.5}$$

This parameter Δ'_c is responsible for the breaking of the up-down symmetry of the magnetic island (as shown in figure 5.1(a)). To estimate the size of this symmetry breaking the dimensionless smallness parameter ε is introduced as

$$\varepsilon \equiv \frac{w}{2}\Delta'_c \quad \text{with} \quad |\varepsilon| = \mathcal{O}\left(\frac{w}{a}\right) \ll 1\,, \tag{5.6}$$

which is seen to be smaller than unity in general. A second cause for breaking of the up-down symmetry in case of large islands is the third order term in the equilibrium flux. To estimate the relative size of this effect, the third order equilibrium term can be compared with the amplitude of the perturbation. This defines the dimensionless smallness parameter γ

$$\gamma \equiv \frac{w^3}{6}\frac{\psi'''_0|\psi''_0|}{\psi''_0\tilde{\psi}} = \frac{16}{6}\frac{\psi'''_0}{\psi''_0}w = \mathcal{O}\left(\frac{w}{a}\right) \ll 1, \tag{5.7}$$

which is also seen generally to be a small number. For typical tokamak conditions both the third order term in the equilibrium flux and the quasi-linear correction to $\psi_1(x)$, result in a larger island width inside r_s and a smaller width outside. Up-down asymmetries due to cylindrical and toroidal effects have not been taken into account in this paper. It is noticed though that these might be described in a slab model with a similar coefficient ε as introduced above.

The symmetry of the island can also be broken by a radial dependence of the phase. For example, a sheared flow has been shown to result in a small, yet finite $\sin(\xi)$ contribution to the perturbed flux function, which depends linearly on x. This can be seen as a finite phase shift, $\frac{1}{2}\Delta'_s x$, in equation (5.3) [Smolyakov et al., 2001] and results in a shearing of the shape of the island (see figure 5.1(b)). An expression for the phase shift can be obtained which, in the notation of [Smolyakov et al., 2001], is given by

$$\Delta'_s = -64\frac{\nu V'_0 L_q^2}{k_\theta v_{Ap}^2 w^4}\,. \tag{5.8}$$

Here, ν is the viscosity, V'_0 is the local velocity shear, $L_q = q/q'$ the shear length, $k_\theta = m/r_s$, and $v_{Ap} = \sqrt{B_p^2/\mu_0\rho}$ the poloidal Alfvén velocity. In addition the following parameters are used, q the safety factor, m the poloidal mode number, B_p the poloidal magnetic field, μ_0 the permeability of free space and ρ the plasma mass density. Note that this effect is largest for small islands. This suggests that the phase shift and the up-down asymmetry of the island width will not simultaneously be large, and that their consequences can be studied separately. A dimensionless smallness parameter is again introduced as $\delta \equiv \Delta'_s w/2$.

Finally, a phase shift across the island can be generated which is up-down symmetric as represented by the term with Δ'_T. This results in a droplet shaped island (see figure 5.1(b)). Such a phase shift is introduced, for example, by the presence of finite temperature gradients across the magnetic island as discussed in [van der Plas and de Blank, 2007]. In the relevant parameter regime it may be written as

$$\Delta'_T = 2c_T\omega_* \frac{qR}{v_t r_\mathrm{s}} , \tag{5.9}$$

where c_T is a constant of order 1, $\omega_* = mT'_e/eBr_\mathrm{s}$ the electron diamagnetic frequency, R the major radius and v_t the electron thermal velocity. In the expression for ω_*, T'_e is the equilibrium temperature gradient, B the magnetic field and e the elementary charge. Also for this case a dimensionless parameter $\tau \equiv \Delta'_T w/2$ is introduced, which under normal conditions will be very small, but may become significant within a transport barrier.

When we normalize the distances from the rational surface by the island width as $\bar{x} \equiv x/w$ and normalize the helical flux function as $\Omega \equiv \psi/\mathrm{sign}(\psi''_0)\tilde{\psi}$, the normalized perturbed flux takes the general form

$$\Omega = 8\bar{x}^2 + \gamma\bar{x}^3 + \mathrm{sign}(\psi''_0)(1 + \varepsilon\bar{x})\cos(\Phi(\xi, \bar{x})), \tag{5.10}$$

where the spatially varying phase $\Phi(\xi, \bar{x}) \equiv \xi - \delta\bar{x} - \tau|\bar{x}|$ is introduced. It is noted again, that in the notation of this paper the parameters γ, ε, δ, and τ are dimensionless. In a comparison with [Lazzaro and Nowak, 2009] for, in particular, ε and δ, these dimensionless parameters need to be divided by w to obtain the corresponding parameters in the notation of [Lazzaro and Nowak, 2009]. When the parameters γ, ε, δ, and τ responsible for the different types of asymmetry all are vanishingly small, the usual equation for a symmetric island is obtained. Taking into account that under normal shear conditions in a tokamak ψ''_0 is negative, the symmetric case is written

$$\Omega = 8\bar{x}^2 - \cos(\xi), \tag{5.11}$$

where the island interior is given by $-1 \le \Omega < +1$ with $\Omega = -1$ corresponding to the O-point and $\Omega = +1$ to the separatrix.

The condition determining the radial position of the O(X)-point, the phase and the corresponding value for Ω can be formulated as

$$\begin{cases} \frac{\partial\Omega}{\partial\bar{x}}(\bar{x} = \bar{x}_{\mathrm{O-point}}, \ \Phi(\xi, \bar{x}_{\mathrm{O-point}}) = 0) & = 0 \\ \frac{\partial\Omega}{\partial\bar{x}}(\bar{x} = \bar{x}_{\mathrm{X-point}}, \ \Phi(\xi, \bar{x}_{\mathrm{X-point}}) = \pm\pi) & = 0 \end{cases} \tag{5.12}$$

where $\bar{x}_{\mathrm{O-point}}$ and $\bar{x}_{\mathrm{X-point}}$ indicate the radial position of the O-point and of the X-point, respectively. These two do not coincide as a consequence of the up-down symmetry breaking, $\varepsilon \ne 0$. The O-point is located at

$$\begin{aligned} \bar{x}_{\mathrm{O-point}} &= -\frac{8}{3\gamma} + \left(\left(\frac{8}{3\gamma}\right)^2 + \frac{\varepsilon}{3\gamma}\right)^{1/2} \\ \xi_{\mathrm{O-point}} &= \delta\bar{x}_{\mathrm{O-point}} + \tau|\bar{x}_{\mathrm{O-point}}| \\ \Omega_{\mathrm{O-point}} &= \gamma\bar{x}^3_{\mathrm{O-point}} + 8\bar{x}^2_{\mathrm{O-point}} - \varepsilon\bar{x}_{\mathrm{O-point}} - 1 , \end{aligned} \tag{5.13}$$

while the X-point is located at

$$
\begin{aligned}
\bar{x}_{\text{X-point}} &= -\tfrac{8}{3\gamma} + \left(\left(\tfrac{8}{3\gamma}\right)^2 - \tfrac{\varepsilon}{3\gamma} \right)^{1/2} \\
\xi_{\text{X-point}} &= \pm\pi + \delta\bar{x}_{\text{X-point}} + \tau|\bar{x}_{\text{X-point}}| \\
\Omega_{\text{X-point}} &= \gamma\bar{x}_{\text{X-point}}^3 + 8\bar{x}_{\text{X-point}}^2 + \varepsilon\bar{x}_{\text{X-point}} + 1 \, .
\end{aligned}
\tag{5.14}
$$

It is noticed here that for $\gamma \neq 0$ each equation in 5.12 has two solutions. In the following discussion we will consider only the solution, consistent with the condition $\bar{x}_{\text{O-point}} = \bar{x}_{\text{X-point}} = 0$ for $\varepsilon = 0$. A finite γ introduces a second solution which represents a non-physical island chain, the O-point and the X-point being located at $-\tfrac{8}{3\gamma} - \sqrt{\left(\tfrac{8}{3\gamma}\right)^2 \pm \tfrac{\varepsilon}{3\gamma}}$ far from the original resonant surface. This reflects the breakdown of the Taylor expansion of the equilibrium flux function far from the resonant flux surface. This could be resolved using the exact ψ_0 instead of its Taylor expansion. For a general case with a monotonic q-profile, then only the first solution is found. The "extra" island chain limits the validity of the approach to the region of parameters where it does not affect the field lines. For $\gamma = 0$, equation 5.10 reduces to a second order equation and consequently $\bar{x}_{\text{O-point}} = \varepsilon/16$, $\bar{x}_{\text{X-point}} = -\varepsilon/16$. Further details can be found in [Lazzaro and Nowak, 2009].

In the remainder of the paper the dimensionless parameters ε, γ, δ and τ will all be treated as arbitrary numbers which will mostly be held fixed as both the island width and the width of the EC deposition profile are varied. This in fact corresponds to the presentation of the results in [Lazzaro and Nowak, 2009], where generally $w\Delta_s$, and $w\Delta_t$ are held constant. Both amount to keeping the shape of the island constant as its size is varied.

Generalized Rutherford equation

Here, we analyze the consequences of the island asymmetries for the generalized Rutherford equation [Rutherford, 1973; Sauter et al., 1997; La Haye, 2006a]. In our analysis we closely follow the derivation of the Rutherford equation as presented, for example, in [Biskamp, 1993] with appropriate generalizations for the case of asymmetric islands and in the presence of both inductive and non-inductively driven current density perturbations. Starting points are Ampère's law relating the perturbation of the helical flux to the parallel current density perturbation $J_{1,\parallel}(\psi)$,

$$
\frac{1}{R}\nabla^2\psi_1 = \mu_0 J_{1,\parallel}(\psi),
\tag{5.15}
$$

and the flux surface averaged Ohm's law relating the time rate of change of the helical flux perturbation, i.e. the helical electric field, to the parallel current density perturbation with the same helicity,

$$
\frac{1}{R}\left\langle \frac{\partial\psi_1}{\partial t} \right\rangle = \eta_1(\psi)(J_0 - J_{0,\text{BS}} - J_{0,\text{CD}}) + \eta_0\left(J_{1,\parallel}(\psi) - J_{1,\text{BS}}(\psi) - J_{1,\text{CD}}(\psi)\right).
\tag{5.16}
$$
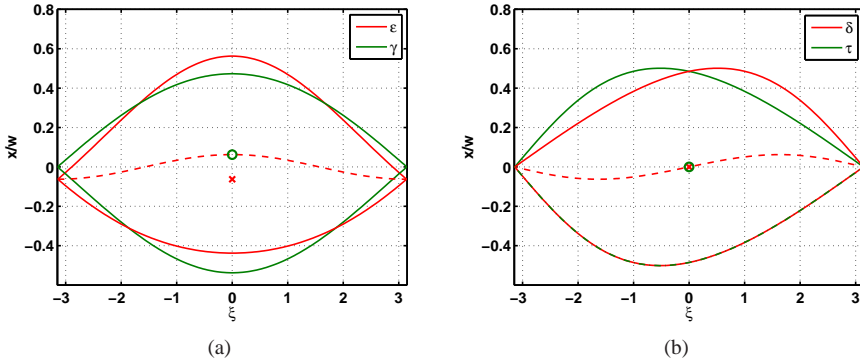
Figure 5.1: Geometry of an asymmetric island with $w = 1$. Figure (a) shows the deformation in amplitude due to the effect of either the quasi-linear correction to the constant-$\psi_1(r)$ approximation, $\varepsilon = 1$, or the third order term in the equilibrium flux, $\gamma = 1$. The circle and the x markers represent the radial position of the O-point and of the X-point, respectively. These are not coincident owing to the ε-asymmetry. In the plot the perturbations are shown to deform the island in the opposite directions; it is noticed that in a tokamak both are directed towards the magnetic axis. Figure (b) shows the deformation in phase due to the shear flow, $\delta = 1$, or to a finite temperature gradient across the magnetic island, $\tau = 1$. The dashed lines represent the locus of the inversion points for the "ε-asymmetry" (a) and for the "δ-asymmetry" (b).

In equation 5.16, $\eta_1(\psi)$ represents a possible helical perturbation to the resistivity as a consequence of heating (or cooling) inside the island, J_0, $J_{0,\mathrm{BS}}$ and $J_{0,\mathrm{CD}}$ are the total equilibrium current density, the non-inductive contribution to the latter of the bootstrap current and the non-inductive contribution of a possible current drive, respectively. The helical perturbations of the non-inductive bootstrap current density and of the non-inductively driven current density are indicated with $J_{1,\mathrm{BS}}$ and $J_{1,\mathrm{CD}}$, respectively. Note that in the island region, for $-1 \leq \Omega \leq 1$, the relation $J_{1,\mathrm{BS}}(\Omega) = -J_{0,\mathrm{BS}}|_{r_{\mathrm{s}}}$ is valid. It is also remarked that the helical current density perturbation is a flux function since the tearing mode evolves on a slow time scale such that the equation of motion is degenerated to the equilibrium condition $\mathbf{B} \cdot \nabla J = 0$ [Biskamp, 1993]. The operation of flux surface averaging, as indicated by the brackets, is defined as

$$\langle A \rangle \equiv \frac{\oint A(\mathrm{d}l/|\nabla \psi|)}{\oint (\mathrm{d}l/|\nabla \psi|)},$$

where the integral is along the closed line segment with constant helical flux ψ.

In the next step, Ampère's law (5.15) is multiplied by the phase factor $\cos(\Phi(\xi, \bar{x}))$, with the spatially varying phase $\Phi(\xi, \bar{x})$ and integrated over the interior region. At the

same time using the approximation $\nabla^2 \psi_1 \approx \partial^2 \psi_1 / \partial \bar{x}^2$, one obtains

$$\int_{-\infty}^{\infty} \mathrm{d}\bar{x} \oint \mathrm{d}\xi \, \frac{\partial^2 \psi_1}{R \partial \bar{x}^2} \cos(\Phi(\xi, \bar{x})) = \int_{-\infty}^{\infty} \mathrm{d}\bar{x} \oint \mathrm{d}\xi \, \mu_0 J_{1,\parallel}(\psi) \cos(\Phi(\xi, \bar{x})).$$

Now the left hand side can be integrated and matched to the linear exterior solution with the usual result of

$$\int_{-\infty}^{\infty} \mathrm{d}\bar{x} \oint \mathrm{d}\xi \, \frac{\partial^2 \tilde{\psi}(1 + \frac{1}{2}\Delta_c' \bar{x})}{R \partial \bar{x}^2} \cos^2(\Phi(\xi, \bar{x})) = \frac{\pi}{R} \Delta'(w) \tilde{\psi}.$$

The right hand side of equation (5.17) is rewritten by substitution from Ohm's law (5.16) as (see also section 5.4):

$$\int_{-\infty}^{\infty} \mathrm{d}\bar{x} \oint \mathrm{d}\xi \, \mu_0 J_{1,\parallel}(\psi) \cos(\Phi(\xi, \bar{x})) =$$

$$\int_{-\infty}^{\infty} \mathrm{d}\bar{x} \oint \mathrm{d}\xi \, \mu_0 \left[\frac{1}{\eta_0 R} \left\langle \frac{\partial \psi_1}{\partial t} \right\rangle - \frac{\eta_1(\psi)}{\eta_0} (J_0 - J_{0,\mathrm{BS}} - J_{0,\mathrm{CD}}) \right.$$

$$\left. + J_{1,\mathrm{BS}}(\psi) + J_{1,\mathrm{CD}}(\psi) \right] \cos(\Phi(\xi, \bar{x})) = \qquad (5.17)$$

$$\int_{-\infty}^{\infty} \mathrm{d}\bar{x} \oint \mathrm{d}\xi \, \mu_0 \left[\frac{1}{\eta_0 R} \frac{\partial \tilde{\psi}}{\partial t} \left\langle (1 + \tfrac{1}{2}\Delta_c' \bar{x}) \cos(\Phi(\xi, \bar{x})) \right\rangle \right.$$

$$\left. - \frac{\eta_1(\psi)}{\eta_0} (J_0 - J_{0,\mathrm{CD}}) + J_{1,\mathrm{BS}}(\psi) + J_{1,\mathrm{CD}}(\psi) \right] \cos(\Phi(\xi, \bar{x})).$$

It is stressed here, that the multiplication with the full, space dependent phase factor is essential. Multiplication instead with $\cos(\xi)$ as is done in [Lazzaro and Nowak, 2009] adds additional terms both on the left (neglected in [Lazzaro and Nowak, 2009]) and right hand sides of equation (5.17). Such terms will be important, in particular, for the stabilizing contribution of non-inductive current drive in the case of a power deposition or driven current density profile much broader than the island width. The integration domain then covers the full width of this deposition profile and, consequently, extends well beyond the island width into regions where the phase shift in $\Phi(\xi, x)$ becomes large.

The combination of these equations results in an equation for the evolution of the amplitude $\tilde{\psi}$ of the perturbed flux function which can be transformed into an equation for the evolution of the "full island width" w by means of the relation $w \equiv 4\sqrt{\tilde{\psi}/\psi_0''}$. It must be noted that, in the presence of finite ε or γ asymmetries, the value of w defined here is not identical to but a good approximation of the full island width as defined by the radial distance between the maximal radial excursion of the separatrix. The result is known as the generalized Rutherford equation, which we write as

$$g_1(\gamma, \varepsilon, \delta, \tau) \frac{\tau_r}{r_\mathrm{s}} \frac{dw}{dt} = r_\mathrm{s} \Delta'(w) + r_\mathrm{s} \Delta_\mathrm{BS}' + r_\mathrm{s} \Delta_\mathrm{H}' + r_\mathrm{s} \Delta_\mathrm{CD}' \qquad (5.18)$$

where $g_1(\gamma, \varepsilon, \delta, \tau)$ is a quantity of order unity defined by

$$g_1(\gamma, \varepsilon, \delta, \tau) = \frac{2}{\pi} \int_{\Omega_{\text{O-point}}}^{\infty} \mathrm{d}\Omega \frac{\oint \mathrm{d}\xi \frac{(1+\varepsilon\bar{x})\cos(\Phi(\xi,\bar{x}))}{\partial\Omega/\partial\bar{x}} \oint \mathrm{d}\xi \frac{\cos(\Phi(\xi,\bar{x}))}{\partial\Omega/\partial\bar{x}}}{\oint \mathrm{d}\xi \frac{1}{\partial\Omega/\partial\bar{x}}}, \qquad (5.19)$$

with Ω given by equation (5.10). The parameter $\tau_r \equiv \mu_0 r_{\mathrm{s}}^2/\eta$ is the local resistive time scale for the resistivity η at the rational surface r_{s} of the mode (μ_0 is the permeability of the free space). A transition from a representation in $\{\bar{x}, \xi\}$ coordinates to one in flux coordinates $\{\Omega, \xi\}$ has been made here for consistency of notation with most existing literature. In this notation, the effect of the asymmetric deformations of the island appears, apart from the flux surface averages, also in the Jacobian $\partial\Omega/\partial\bar{x}$. Outside the island, i.e. for $\Omega > \Omega_{\text{X-point}}$, the Ω integral implicitly contains a sum over the contributions at the two surfaces at positive and negative $\bar{x}$, which in the case of asymmetric islands will generally not be identical. Note, that g_1 is no longer a simple constant but depends implicitly on w through its dependence on the normalized asymmetry parameters γ, ε, δ, and τ. In case of symmetric islands, g_1 becomes a constant which can be evaluated analytically resulting in the well known value of 0.82 [Biskamp, 1993].

The contribution to the Rutherford equation owing to the "missing" bootstrap current [Hegna and Callen, 1997] within the island separatrix, can be written as,

$$r_{\mathrm{s}}\Delta'_{\text{BS}} = \frac{16Rr_{\mathrm{s}}\mu_0}{\pi|\psi_0''|w} J_{\text{BS}} \int_{\Omega_{\text{O-point}}}^{\Omega_{\text{X-point}}} \mathrm{d}\Omega \oint \mathrm{d}\xi \frac{\cos(\Phi(\xi,\bar{x}))}{\partial\Omega/\partial\bar{x}} \, . \qquad (5.20)$$

The shear factor is written here as $|\psi_0''| = RB_{\mathrm{p}}/L_{\mathrm{q}}$. Reminding that, in the limit of small inverse aspect ratio ϵ and negligible temperature gradient, the bootstrap current can be approximated [La Haye, 2006a] as $J_{\text{BS}} \approx -\frac{\sqrt{\epsilon}}{B_{\mathrm{p}}}\frac{\partial p}{\partial r}$, equation 5.20 can be rearranged as

$$r_{\mathrm{s}}\Delta'_{\text{BS}} = \frac{L_{\mathrm{q}}}{L_{\mathrm{p}}} \frac{r_{\mathrm{s}}}{w} \beta_{\mathrm{p}} \sqrt{\epsilon} c_{\text{neo}} \, , \qquad (5.21)$$

where $L_{\mathrm{p}} = -p/p'$ is the pressure scale length and $\beta_{\mathrm{p}} = \frac{2\mu_0 p}{B_{\mathrm{p}}^2}$ is the ratio between the plasma pressure and the poloidal magnetic pressure. The last term accounts for the perturbations of the island geometry,

$$c_{\text{neo}}(\gamma, \varepsilon, \delta, \tau) = \frac{8}{\pi} \int_{\Omega_{\text{O-point}}}^{\Omega_{\text{X-point}}} \mathrm{d}\Omega \oint \mathrm{d}\xi \frac{\cos(\Phi(\xi,\bar{x}))}{\partial\Omega/\partial\bar{x}} \, . \qquad (5.22)$$

For the symmetric case, this integral is evaluated analytically to yield $32/3\pi \simeq 3.4$. Effects due to a finite perpendicular transport limiting the bootstrap current perturbation for small islands, are neglected.

The contributions from either a perturbation to the inductive current or the non-inductively driven current density are represented by Δ'_{CD} and Δ'_{H}, respectively. An explicit equation for the term coming from a non-inductively driven current is

$$r_{\mathrm{s}}\Delta'_{\text{CD}} = -\frac{16Rr_{\mathrm{s}}\mu_0}{\pi|\psi_0''|w} \int_{\Omega_{\text{O-point}}}^{\infty} \mathrm{d}\Omega \left(J_{1,\text{CD}}(\psi) \oint \mathrm{d}\xi \frac{\cos(\Phi(\xi,\bar{x}))}{\partial\Omega/\partial\bar{x}} \right), \qquad (5.23)$$

which can be brought into a form similar to the expressions obtained in [Sauter, 2004; De Lazzari et al., 2009]. The power deposition, as for example in the case of ECRH and ECCD, is assumed to be highly localized in radius as well as in poloidal and toroidal angle with a possible periodic on-off modulation in time synchronous to the island rotation. As is commonly done, a fast rotating island is assumed and the power deposition is averaged over a single rotation period. The resulting power source is symbolically written as $p_{\text{CW}}\mathcal{M}$. Here, the CW radial power deposition profile is a function of radius only, which is taken to be a Gaussian $p_{\text{CW}} \propto \exp(-4(x-x_{\text{dep}})^2/w_{\text{dep}}^2)$ localized at $x_{\text{dep}} = r_{\text{dep}}-r_{\text{s}}$ and with full Gaussian width w_{dep}, and the modulation $\mathcal{M}$ becomes a function only of ξ, approximated as $\mathcal{M}(\xi; \mathcal{D}, \phi) = \text{H}(\cos(\xi + \phi) - \cos(\mathcal{D}\pi))$. In this formulation the $\mathcal{M}$ depends on the power on-time fraction $\mathcal{D}$ and the phase mismatch ϕ between the power modulation and the island rotation. The symbol H denotes the Heaviside function.

A current drive efficiency, $\eta_{\text{CD}} \equiv I_{\text{CD}}/P_{\text{tot}}$, is introduced as the ratio of the total driven current I_{CD} and the total unmodulated power P_{tot}, which is assumed to be a simple constant. The current density driven non-inductively by the absorbed EC power is a flux function $J_{1,\text{CD}} = J_{1,\text{CD}}(\psi)$ whereas the power deposition now is a localized function in radius and ξ. In order to relate these two, the power density is averaged over a flux surface so that $J_{1,\text{CD}}(\psi) = 2\pi R\eta_{\text{CD}}\langle p_{\text{CW}}\mathcal{M}\rangle$. A deformation of the flux surfaces will change the flux surface average of the deposited power and, consequently, the driven current density $J_{1,\text{CD}}$. Finally, noting that the total unmodulated power is

$$P_{\text{tot}} = 2\pi Rr_{\text{s}}w \int_{\Omega_{\text{O-point}}}^{\infty} \text{d}\Omega \oint \text{d}\xi \frac{\langle p_{\text{CW}}\rangle}{\partial\Omega/\partial\bar{x}},$$

one obtains [De Lazzari et al., 2009]

$$r_{\text{s}}\Delta'_{\text{CD}} = -\frac{16\mu_0 L_{\text{q}}}{B_{\text{p}}\pi}\frac{\eta_{\text{CD}}P_{\text{tot}}}{w_{\text{dep}}^2}F_{\text{CD}}(w/w_{\text{dep}}, x_{\text{dep}}, \mathcal{M}; \gamma, \varepsilon, \delta, \tau). \tag{5.24}$$

F_{CD} is a dimensionless function which depends on the geometrical properties of the power deposition profile (its width in relation to the island width, its radial location, and its modulation) and now also on the parameters defining the particular shape of the magnetic island:

$$F_{\text{CD}} \equiv \frac{w_{\text{dep}}^2}{w^2}\frac{\int_{\Omega_{\text{O-point}}}^{\infty} \text{d}\Omega\,\langle p_{\text{CW}}\mathcal{M}\rangle \oint \text{d}\xi \frac{\cos(\Phi(\xi,\bar{x}))}{\partial\Omega/\partial\bar{x}}}{\int_{\Omega_{\text{O-point}}}^{\infty} \text{d}\Omega\,\langle p_{\text{CW}}\rangle \oint \text{d}\xi \frac{1}{\partial\Omega/\partial\bar{x}}} \tag{5.25}$$

It is assumed that the dependencies on deposition width, location and modulation are such that F_{CD} can be factorized as

$$F_{\text{CD}}(w^*, x_{\text{dep}}, \mathcal{M}; \gamma, \varepsilon, \delta, \tau) = N_{\text{CD}}(w^*)G_{\text{CD}}(w^*, x_{\text{dep}})M_{\text{CD}}(w^*, \mathcal{M}), \tag{5.26}$$

where $w^* \equiv w/w_{\text{dep}}$. The function $N_{\text{CD}}(w^*)$ represents the geometrical function in case of a power source which is exactly positioned at $r_{\text{dep}} = r_{\text{s}}$, and unmodulated. This means that functions $G_{\text{CD}}(w^*, x_{\text{dep}})$ and $M_{\text{CD}}(w^*, \mathcal{M})$ are normalized such that,

for $r_{\mathrm{dep}} = r_{\mathrm{s}}$, $G_{\mathrm{CD}}(w^*, x_{\mathrm{dep}} = 0) = 1$, and that for the unmodulated power case, $M_{\mathrm{CD}}(w^*, \mathrm{CW}) = 1$. $G_{\mathrm{CD}}(w^*, x_{\mathrm{dep}})$ describes the effect of misalignment of the power, and $M_{\mathrm{CD}}(w^*, \mathcal{M})$ accounts for the effect of power modulation.

For the effect of heating inside the magnetic island one obtains the expression

$$r_{\mathrm{s}}\Delta'_{\mathrm{H}} = \frac{16Rr_{\mathrm{s}}\mu_0}{\pi|\psi''_0|w} \int_{\Omega_{\mathrm{O-point}}}^{\infty} \mathrm{d}\Omega \left(\frac{\eta_1(\psi)}{\eta_0}(J_0 - J_{0,\mathrm{CD}}) \oint \mathrm{d}\xi \frac{\cos(\Phi(\xi,\bar{x}))}{\partial\Omega/\partial\bar{x}} \right). \quad (5.27)$$

The helical perturbation to the resistivity is now associated with the perturbation of the electron temperature due to net power deposition inside the magnetic island,

$$\eta_1(\psi) \approx -\frac{3\delta T(\psi)}{2T_{\mathrm{sep}}}\eta_0 \quad (5.28)$$

where η_0 and T_{sep} are the resistivity and electron temperature at the separatrix. The electron temperature perturbation inside the island $\delta T(\psi)$ is obtained from the solution of the power balance equation inside the island. Following the discussion in [De Lazzari et al., 2009], it is assumed that the power balance is given by the localized electron heating represented by the power source $p_{\mathrm{CW}}\mathcal{M}$ as above, balanced by cross field anomalous transport characterized by a heat diffusivity $\chi_\perp$ which is assumed to be constant over the entire magnetic island. Thus, the electron temperature perturbation is obtained through solution of [De Lazzari et al., 2009],

$$\delta T(\Omega) = \int_{\Omega}^{\Omega_{\mathrm{X-point}}} \mathrm{d}\Omega \frac{P(\Omega)}{n_e\chi_\perp k_B 4\pi^2 R r_{\mathrm{s}} \oint \mathrm{d}\xi |\nabla\Omega|^2/(\partial\Omega/\partial\bar{x})}, \quad (5.29)$$

where $P(\Omega)$ represents the total power absorbed inside the volume enclosed by the flux surface labeled Ω, n_e the electron density and k_B is the Boltzmann constant. As in the case of non-inductive current drive, the temperature perturbation is affected by the island asymmetries trough both the flux surface averaged power deposition profile and the term $|\nabla\Omega|^2/(\partial\Omega/\partial\bar{x})$.

Next, the normalized, dimensionless temperature perturbation $\delta\tilde{T}$ is introduced as

$$\delta\tilde{T} \equiv \frac{8\pi^2 R r_{\mathrm{s}} n_e \chi_\perp k_B}{P_{\mathrm{tot}} w} \delta T , \quad (5.30)$$

and an "efficiency of current generation" through heating in a plasma slab of width w_{dep} is defined as

$$\eta_{\mathrm{H}} \equiv \frac{3w_{\mathrm{dep}}^2}{8\pi^2 R r_{\mathrm{s}} n_e \chi_\perp k_B} \frac{J_0 - J_{0,BS} - J_{0,\mathrm{CD}}}{T_{\mathrm{sep}}}. \quad (5.31)$$

With these definitions, the heating term can now also be written is accordance with [De Lazzari et al., 2009] as

$$r_{\mathrm{s}}\Delta'_{\mathrm{H}} = -\frac{16\mu_0 L_{\mathrm{q}}}{B_{\mathrm{p}}\pi} \frac{\eta_{\mathrm{H}} P_{\mathrm{tot}}}{w_{\mathrm{dep}}^2} F_{\mathrm{H}}(w^*, x_{\mathrm{dep}}, \mathcal{M}; \gamma, \varepsilon, \delta, \tau), \quad (5.32)$$

where F_H is again a geometrical function which is given by

$$F_H = \frac{1}{2\pi w} \int_{\Omega_{O-point}}^{\Omega_{X-point}} d\Omega \; \delta\tilde{T}(\Omega) \oint d\xi \frac{\cos(\Phi(\xi,\bar{x}))}{\partial\Omega/\partial\bar{x}}. \qquad (5.33)$$

Analogous to F_{CD}, also the geometrical function F_H is factorially written as

$$F_H(w^*, x_{dep}, \mathcal{M}; \gamma, \varepsilon, \delta, \tau) = N_H(w^*)G_H(w^*, x_{dep})M_H(w^*, \mathcal{M}), \qquad (5.34)$$

where $N_H(w^*)$ represents the geometrical function in case of a power source which is exactly positioned at $r_{dep} = r_s$ and unmodulated, $G_H(w^*, x_{dep})$ describes the effect of misalignment of the power and $M_H(w^*, \mathcal{M})$ again accounts for the effect of power modulation.

5.3 Consequences for NTM growth

In this section the effects of the symmetry breaking are discussed for each term appearing in the Rutherford equation. The results presented are obtained though numerical evaluation of the integrals given above, mostly but not exclusively using their representation in $\{\bar{x}, \xi\}$ coordinates. The calculations have been checked extensively for accuracy and convergence. In a number of cases the evaluations have been performed both in $\{\bar{x}, \xi\}$ coordinates as well as in flux coordinates $\{\Omega, \xi\}$, with identical results given the achieved accuracy. However, due to the divergence of terms in the flux coordinate representation, accurate and converged results are more difficult to obtain in that case.

The factors g_1 and c_{neo}

The extension of the Rutherford equation, to the case of asymmetric islands, in equation 5.18, introduced two coefficients, g_1 and c_{neo}, depending on the parameters of the perturbation, γ, ε, δ and τ. Here the trend of these coefficients in the parameter space is discussed. Figure 5.2(a) and 5.2(b) show for both the coefficients a slight increase when a deformation in amplitude is taken into account; this is represented by blue circles for the quasi-linear correction to the constant-ψ approximation (ε) and by red squares for the finite third order term in the equilibrium flux (γ). The discrepancy with the symmetric case is at most of the order of 1%. Phase deformations appear to be negligible. These results appear in accordance with the conclusions of [Lazzaro and Nowak, 2009]. Note that the last two points for $\gamma \neq 0$ have been calculated reducing the integration range, in order to avoid the perturbation due to the "second island chain". This might reduce the accuracy of these results without affecting the validity of the conclusions.

Efficiencies for NTM suppression by heating and current drive

The capability of the current drive and local heating to suppress NTMs is affected by perturbations of the island geometry trough the geometrical efficiency F_{CD} 5.25 and F_H
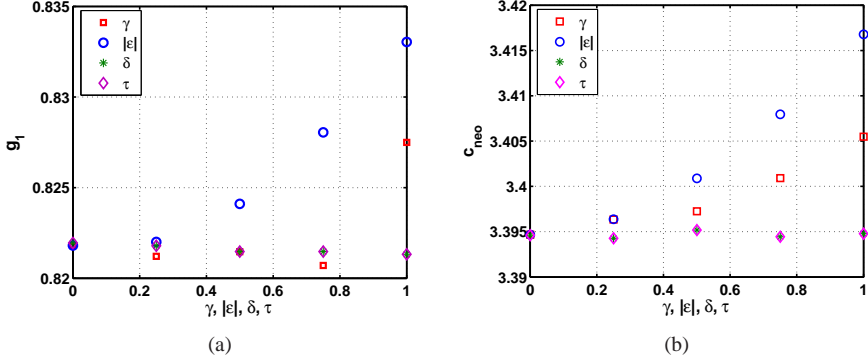
(a)　　　　　　　　　　　　　　　　(b)

Figure 5.2: Consequences of asymmetries on the generalized Rutherford equation: (a) the behavior of the coefficient $g_1(\gamma, \varepsilon, \delta, \tau)$ in equation (5.18) and (b) the behavior of the coefficient $c_{\mathrm{neo}}(\gamma, \varepsilon, \delta, \tau)$ in equation (5.22) are presented. Every dependency is considered separately. The value at $\gamma = \varepsilon = \delta = \tau = 0$ corresponds to the symmetric island case.

5.33, respectively. First the case of continuous EC power deposition at the exact mode resonant surface r_s is considered, in which case the functions $F_{\mathrm{CD,H}}$ reduce to $N_{\mathrm{CD,H}}$. Every perturbation of the symmetric case is implemented separately and kept constant, i.e. the normalized shape of the island is kept constant, while the normalized island width, w^*, varies over the displayed range. As shown in figure 5.3(a) and 5.3(b), all the effects appear to be negligible. Despite the marginal effect observed, it is interesting to observe how the up-down asymmetry modifies the normalized geometrical function $G_{\mathrm{CD,H}}$ when a misalignment with respect to the resonant radius is taken into account. In figure 5.4 and 5.5, the shape of the function $G_{\mathrm{CD,H}}$ clearly reflects the up-down asymmetry of the island with the function being broader on the side where the island is wider. This is particularly evident when the power is deposited mainly inside the magnetic island, i.e. when the island is considerably larger than the power deposition width. The asymmetry is larger for the current drive than for the heating. It is noticed that a simple phase shift cannot affect this function, since it is obtained integrating over the full angular domain. The last statement is not valid when the modulation of the EC power (with a phase mismatch) is introduced or when the combination of two or more effects is taken into account, i.e. when deformations both in amplitude and in phase are occurring. Here, a relevant example for the experimental suppression of tearing modes is discussed, namely the deposition of EC power with a duty cycle $\mathcal{D} = 50\%$, in phase with either the O-point or the X-point. The magnetic island ($w^* = 3$) is described with a quasi-linear correction for the constant-ψ approximation, i.e. $\varepsilon \neq 0$, such that the radial position of the O- and X-points is displaced symmetrically from the resonant surface. Note that the simple factorization proposed in equation (5.26) breaks down for $\phi \neq 0$. For this reason the factor $G_{\mathrm{CD,H}}M_{\mathrm{CD,H}}$ is indicated in the following with $G_{\mathrm{CD,H}}(w^*, x_{\mathrm{dep}}, \mathcal{D}, \phi)$.
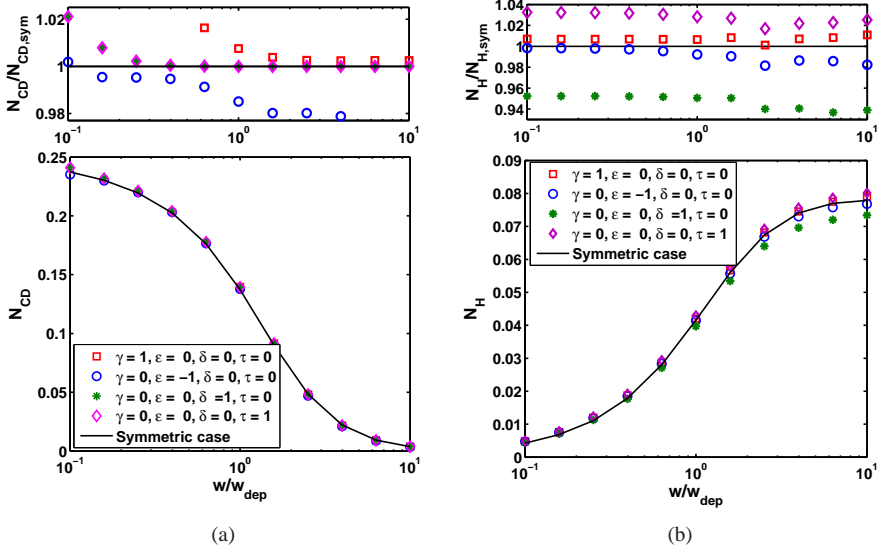
Figure 5.3: (a) The ECCD geometrical function N_{CD} defined in equation (5.25) and (b) the ECRH geometrical function N_H defined in equation (5.33). Both have been obtained in case of no misalignment and continuous power deposition. The solid black line refers to the reference case, $\gamma = \varepsilon = \delta = \tau = 0$, squares to $\gamma = 1, \varepsilon = \delta = \tau = 0$, circles to $\varepsilon = -1, \gamma = \delta = \tau = 0$, stars to $\delta = 1, \gamma = \varepsilon = \tau = 0$ and diamonds to $\tau = 1, \gamma = \varepsilon = \delta = 0$.

As described in [De Lazzari et al., 2009] for a symmetric island of this normalized size, the effect of modulation with no phase mismatch, $\phi = 0$, enhances the current drive efficiency at the resonant surface by 20% while the efficiency of the resonant heating is reduced by 10%. This is shown with blue solid lines in figure 5.6. The efficiency of the normalized, modulated geometrical functions $G_{CD,H}$ shows a decrease (in the absolute value) of about one order of magnitude for a phase displacement $\phi = \pi$ (red solid line). By effect of the perturbation, the curves appear shifted towards the displaced O-point for $\phi = 0$ (blue circles) while for $\phi = \pi$, they appear to shift towards the X-point (red squares). This has a particular relevance for the current drive, since the efficiency is found to be negative, i.e. the current drive destabilizes the island. It is noticed also how the power modulation reduces considerably the asymmetry of the current drive efficiency introduced by ε, along the radial coordinate, with respect to the continuous deposition (black solid line in figure 5.6(a)).
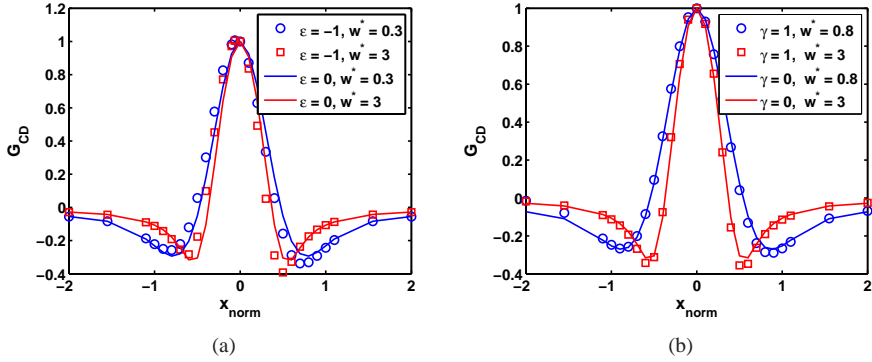
Figure 5.4: Detrimental effect of deposition misalignment on the heating normalized geometrical function $G_{\mathrm{CD}}(w^*, x_{\mathrm{dep}})$, varying the island size $w^* = w/w_{\mathrm{dep}}$: in figure (a) the reference case for a symmetric island (solid lines) is compared with the case of an asymmetric island with $\varepsilon = -1, \gamma = \delta = \tau = 0$ (circles for $w^* = 0.3|0.8$, squares for $w^* = 3$). In figure (b) the same as in (a) but for $\gamma = 1, \varepsilon = \delta = \tau = 0$. The displacement is normalized as $x_{\mathrm{norm}} = x_{\mathrm{dep}}/\max(w, w_{\mathrm{dep}})$.
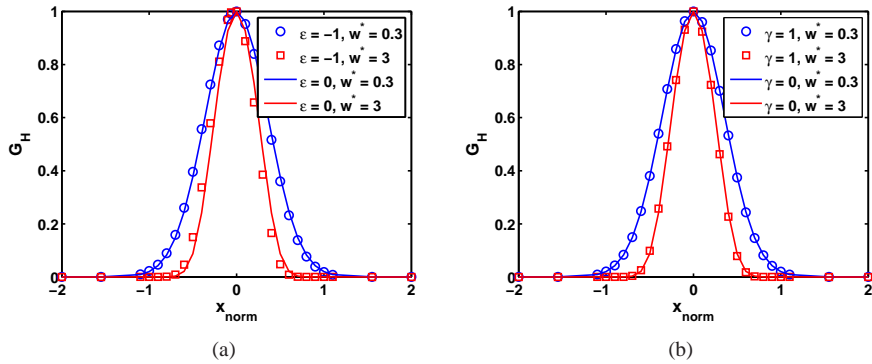
Figure 5.5: Detrimental effect of deposition misalignment on the heating normalized geometrical function $G_{\mathrm{H}}(w^*, x_{\mathrm{dep}})$, varying the island size $w^* = w/w_{\mathrm{dep}}$: in figure (a) the reference case for a symmetric island (solid lines) is compared with the case of an asymmetric island with $\varepsilon = -1, \gamma = \delta = \tau = 0$ (circles for $w^* = 0.3$, squares for $w^* = 3$). In figure (b) the same as in (a) but for $\gamma = 1, \varepsilon = \delta = \tau = 0$. The displacement is normalized as $x_{\mathrm{norm}} = x_{\mathrm{dep}}/\max(w, w_{\mathrm{dep}})$.
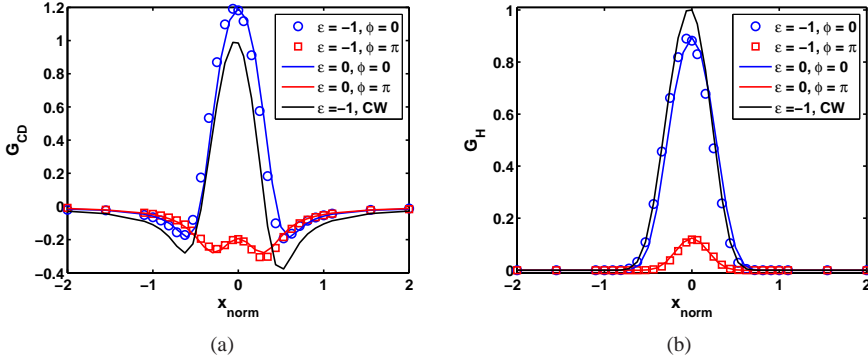
Figure 5.6: Effect of power modulation ($\mathcal{D} = 50\%$ duty cycle), combined with phase mismatch on the normalized geometrical functions $G_{\mathrm{CD,H}}(x_{\mathrm{dep}}, \mathcal{D}, \phi; \varepsilon)$, for ECCD (a) and for ECRH (b). The displacement is normalized as $x_{\mathrm{norm}} = x_{\mathrm{dep}}/\max(w, w_{\mathrm{dep}})$, the island size being $w = 3w_{\mathrm{dep}}$. . Each picture shows the reference case, calculated for a symmetric island at $\phi = 0$ (blue solid lines) and at $\phi = \pi$ (red solid lines), compared with the efficiency for an asymmetric island with $\varepsilon = -1$ (blue circles for $\phi = 0$ and red squares for $\phi = \pi$). The black dash-dotted line refers to the case of continuous power deposition on an asymmetric island. It is noticed for G_{CD}, that the asymmetry of this last curve, with respect to the rational surface ($x_0 = 0$), is strongly reduced when the power is modulated.

5.4 Discussion

The conclusion of the previous section, that the effect of all the asymmetries on the efficiency of NTM suppression by either heating or localized current drive is negligible as long as the power is deposited at the resonant surface, is in stark contrast with the results presented in [Lazzaro and Nowak, 2009]. In the latter work it was suggested that the efficiency of current drive might even change sign and become destabilizing for small islands with a phase asymmetry (finite δ). In order to understand this discrepancy one has to consider the flux surface average of the cosine of the island phase, i.e.

$$\langle \cos(\Phi(\xi, \bar{x})) \rangle = \frac{\oint \mathrm{d}\xi \frac{\cos(\Phi(\xi, \bar{x}))}{\partial \Omega / \partial \bar{x}}}{\oint \mathrm{d}\xi \frac{1}{\partial \Omega / \partial \bar{x}}}. \tag{5.35}$$

As can be seen in section 5.2, it provides the weight with which the current density or temperature perturbation at a given location contributes to stabilization of the mode. It is noted here that in the asymmetric cases $\langle \cos(\Phi(\xi, \bar{x})) \rangle$ depends also on sign($\bar{x}$): in the outer region, $\Omega > \Omega_{\mathrm{sep}}$, the behavior of this function for $\bar{x} > 0$, will generally differ from the one calculated for $\bar{x} < 0$. In the case of a symmetric island, i.e. $\gamma = \varepsilon = \delta = \tau = 0$,

analytical expressions exist for $\langle \cos \xi \rangle$ [Biskamp, 1993; Giruzzi et al., 1999], which have been used to benchmark our numerical results. In [Lazzaro and Nowak, 2009] the island phase in this term is simply approximated as $\Phi(\xi, \bar{x}) \approx \xi$. This is found to lead to a strong discrepancy when the phase deformation δ is taken into account. In detail, the approximation results in a too slow convergence of the $\langle \cos(\Phi(\xi, \bar{x})) \rangle$ to zero for large Ω, as shown in figure 5.7(a). When contributions from the external region in the integrals defining the geometrical efficiency function for current drive F_{CD} 5.25 become important (i.e. for $w^* \ll 1$), this results in a further negative contribution to the geometrical efficiency, as shown in figure 5.8. In this figure, the blue circles, represent the normalized efficiency of current drive in the notation of [Lazzaro and Nowak, 2009] $\eta_{\text{hel}} = w^{*2} F_{CD}(w^*, x_0 = 0, CW; \delta = 1.9)$ with $\Phi(\xi, \bar{x}) \approx \xi$, which is found to be negative for small values of w^*. Moreover, in [Lazzaro and Nowak, 2009] an additional approximation is made to the island geometry as represented by their equations (10) and (11), which are obtained using a Taylor expansion of $\cos(\xi - \delta \bar{x})$ around $\delta \bar{x} = 0$ up to second order in $\delta \bar{x}$. This approximation breaks down for large $\bar{x}$, while this region contributes significantly to the term from non-inductive current drive in case of $w^* \ll 1$.

(a)   (b)
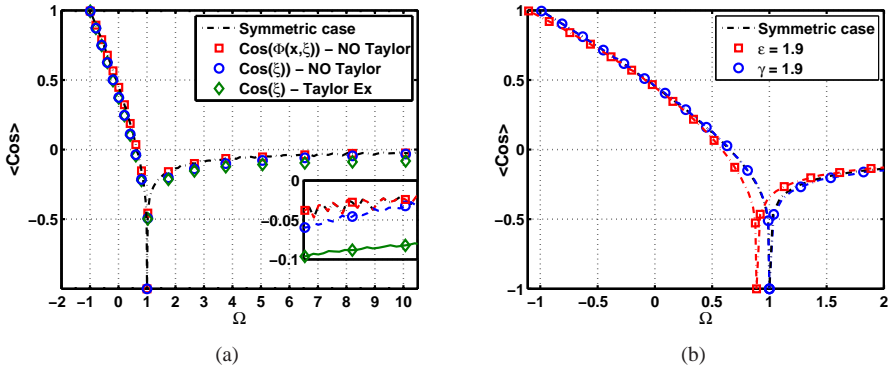
Figure 5.7: In figure (a) the trend of the flux averaged cosine $\langle \cos(\Phi(\xi, \bar{x})) \rangle$ is represented. The picture has been zoomed in to show how different approximations affect the asymptotic behavior at larger Ω. The black dash-dotted lines represent the symmetric case. The results obtained in case of a finite phase asymmetry $\delta = 1.9$ (i.e. $\delta = 1.9/w$ in the notation of [Lazzaro and Nowak, 2009]) are indicated as follows: squares are obtained with the full phase factor $\Phi(\xi, \bar{x}) = \xi - \delta \bar{x}$. Circles are calculated adding the approximation of $\Phi(\xi, \bar{x}) \approx \xi$. Diamonds are obtained as in [Lazzaro and Nowak, 2009], i.e. using also approximate expressions for the island geometry. In (b) the effect of finite up-down asymmetries is plotted. The results shown refer to $\varepsilon = 1.9$ (blue circles) and $\gamma = 1.9$, (red squares). The black dashed curve again shows the results for the symmetric case.
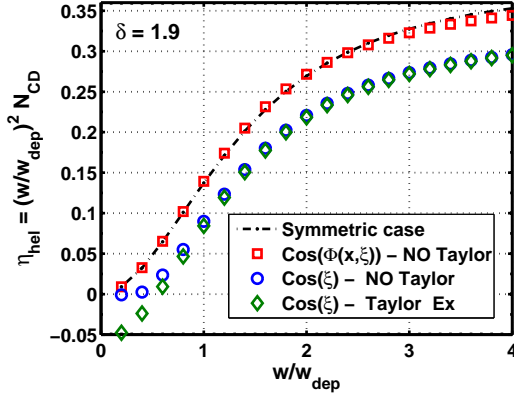
Figure 5.8: Trend of $\eta_{\mathrm{hel}} = w^{*2} N_{\mathrm{CD}}$, varying $w^* = w/w_{\mathrm{dep}}$, in the notation of [Lazzaro and Nowak, 2009]. It is reminded that $N_{\mathrm{CD}} = F_{\mathrm{CD}}(w^*; x_0 = 0, \mathrm{CW})$. The black dash-dotted lines represent current drive efficiency for the symmetric case. The results obtained in case of a finite phase asymmetry $\delta = 1.9$ (i.e. $\delta = 1.9/w$ in the notation of [Lazzaro and Nowak, 2009]) are indicated as follows: squares are obtained using the expression 5.25 derived in the present paper retaining the full phase factor $\Phi(\xi, \bar{x}) = \xi - \delta \bar{x}$. Circles are calculated adding the approximation of $\Phi(\xi, \bar{x}) \approx \xi$ in equation (5.25). Diamonds are obtained as in [Lazzaro and Nowak, 2009], i.e. using also approximate expressions for the island geometry.

As a result the asymptotic behaviour of $\langle \cos(\Phi(\xi, \bar{x})) \rangle$ for large Ω and the predicted normalized efficiency for NTM suppression becomes even more negative as illustrated (green diamonds) in figure 5.8, for the parameters used in Fig. 3 of [Lazzaro and Nowak, 2009]. The results presented in figure 5.7(a) and 5.8 even show that $\langle \cos(\Phi(\xi, \bar{x})) \rangle$ as well as η_{hel} and F_{CD} are identical up to the numerical accuracy of the calculation for the symmetric case and the case with a finite phase asymmetry δ even for this large value of $\delta = 1.9$. That $\langle \cos(\Phi(\xi, \bar{x})) \rangle$ really must be independent of any phase shearing as represented by δ or τ is understood as follows. Take the flux average of any function $A(\bar{x}, \xi)$ over a sheared flux surface as resulting from a finite δ and/or τ. Performing a change of coordinates as $\{\bar{x}, \xi\}$ to $\{\bar{x}, \xi' = \Phi(\xi, x)\}$ then results in an integral representing the corresponding average over a symmetric flux surface of the same function shifted by $\delta \bar{x} + \tau |\bar{x}|$. It follows that for any value of δ or τ the average of $\langle \cos(\Phi(\xi, \bar{x})) \rangle$ over a sheared flux surface is identical to the corresponding average $\langle \cos(\xi) \rangle$ in the symmetric island case. Similarly, for any function A with translational symmetry in ξ the flux surface average will be independent of the shearing of the flux surface. This holds, in particular, for the flux surface average of the power density or driven current in case of continuous wave application. These arguments result in the conclusion that a finite δ or τ asymmetry cannot affect the geometrical efficiency for tearing mode stabilization of

either heating or current drive in the unmodulated case. In case of power modulation in phase with the island rotation a finite effect of the shearing is still to be expected in particular for small w/w_{dep} as the power is deposited at different island phases for different values of $\bar{x}$.

The arguments given above do not apply to the cases with an up-down asymmetry. In these cases, illustrated in figure 5.7(b) (see also [Lazzaro and Nowak, 2009]), the effect on $\langle \cos(\Phi(\xi, \bar{x})) \rangle$ nevertheless is very small: in case of finite ε the whole curve is just seen to be slightly shifted to the left as the flux values at the O- and X-points are slightly decreased from their values of -1 and $+1$ in the symmetric case. While in case of a finite γ the curves virtually overlap in the interior region. The major effect then comes from the changes in the flux surface averaged power density and driven current. As long as the power is deposited at a radius close to the O-point position, the flux surface averaged driven current density is found to be peaked inside the island resulting in an effective stabilization. When the X- and O-point radii diverge, as in the case of a finite ε, a mismatch between the power deposition location and the O-point can result in more power being localized in the X-point region. In such cases a larger destabilizing (i.e. negative value of F_{CD}) effect may be found in case of a radial mismatch towards the X-point as can be seen also in the results as presented in figures 5.4(a) and 5.6(a). In fact, in the case of an asymmetric island size the normalized flux surface averaged current density and the consequent geometrical efficiency can be seen as an average of the same over two cases with different island sizes as discussed in [Urso et al., 2010]. In that paper an asymmetric deformation in amplitude is applied by dividing the island in two parts, where in one part for $r > r_{\mathrm{s}}$ the width is changed to γw with $0 < \gamma < 1$, while for the other part, $r < r_{\mathrm{s}}$, the island width w remains unchanged. As a consequence the efficiency for the resulting asymmetric island, $\eta_{\mathrm{ECCD,ASYM}} = \frac{w^2}{w_{\mathrm{dep}}} F_{\mathrm{CD}}$ in the notation of [Urso et al., 2010], can be equated to the average of the efficiency of two symmetric islands,

$$\eta_{\mathrm{ECCD,ASYM}}(w) = \frac{1}{2}(\eta_{\mathrm{ECCD,SYM}}(w) + \eta_{\mathrm{ECCD,SYM}}(\gamma w)), \qquad (5.36)$$

their width being w and γw, respectively. However in [Urso et al., 2010] this averaged efficiency is then compared to the efficiency for a symmetric island at double the size of the larger of the two island parts, which leads to the unsurprising conclusion that the latter is larger. However, in the context of our present work a consistent comparison with the symmetric case should be performed with respect to the averaged island width $w_{\mathrm{asym}} = \frac{1}{2}(w + \gamma w) < w$, resulting in a smaller value for $\eta_{\mathrm{ECCD,SYM}}(w_{\mathrm{asym}})$. This results in just a small difference between the symmetric and asymmetric island cases consistent with the conclusions of the present paper.

5.5 Conclusions

This paper addressed the effects of a number of asymmetries, affecting the geometry of a magnetic island and hence the temporal evolution of the mode. In detail, a finite third order approximation of the unperturbed flux function and a quasi-linear correction to the

constant-ψ approximation have been identified to break the up-down symmetry of the mode while a shear flow and a temperature gradient across the island have been found to produce a phase shift, proportional to the radial excursion from the resonant surface [Ren et al., 1999; Smolyakov et al., 2001; van der Plas and de Blank, 2007]. The model focused in particular on the consequences for the control and the suppression of an NTM by means of ECCD and ECRH. As a consequence the Rutherford equation has been reformulated consistently for the generalized topology of the magnetic island, accounting for the contributions of the bootstrap current, of the local current drive and of the resonant heating. The outcome of this study shows that the effect of asymmetries is negligible for the coefficients g_1 and c_{neo} appearing in the generalized Rutherford equation 5.18 in front of the tearing mode growth rate and the neoclassical drive term, respectively. The effect is small for both the current drive and the heating efficiency, $F_{CD,H}$ when the EC power is deposited at the rational surface. Deformations in amplitude do affect the normalized geometrical functions, $G_{CD,H}$ in a trivial manner: the maximum for the efficiency moves with the O-point along the radial coordinate, while the width of these functions reflects the asymmetry in the island width.

These conclusions appear to be partly in contrast to opposite conclusions reached in the previous literature [Lazzaro and Nowak, 2009; Urso et al., 2010]: a significant reduction of the efficiency for NTM stabilization by ECCD in case of an up-down asymmetric island size was claimed in [Urso et al., 2010], while in [Lazzaro and Nowak, 2009] this efficiency was even shown to become negative in case of a finite phase shift δ and an island much smaller than the EC deposition width. It is shown that the former claim is based on an improper comparison between the asymmetric and symmetric cases as made in [Urso et al., 2010], while the latter conclusion is shown to be the result of the approximations made in [Lazzaro and Nowak, 2009].

Acknowledgements

References

Biskamp D. *Nonlinear Magnetohydrodynamics*. Cambridge Press, 1993.

Chang Z, Callen JD, Fredrickson ED, Budny RV, Hegna CC, McGuire KM, Zarnstorff MC, and TFTR Group. Observation of nonlinear neoclassical pressure-gradient driven tearing modes in TFTR. *Phys. Rev. Lett.* **74**, 4663 (1995).

De Lazzari D and Westerhof E. On the merits of heating and current drive for tearing mode stabilization. *Nucl. Fusion* **49**, 075002 (2009). Erratum: *Nucl. Fusion* **50**, 079801 (2010).

Gantenbein G, Zohm H, Giruzzi G, Günter S, Leuterer F, Maraschek M, Meskat J, Yu Q, ASDEX Upgrade Team, and ECRH-Group (AUG)l. Complete suppression of neoclassical tearing modes with current drive at the electron-cyclotron-resonance frequency in ASDEX Upgrade Tokamak. *Phys. Rev. Lett.* **85**(6), 1242 (2000).

Gates AD, Lloyd B, Morris AW, Gabentein G, O'Brien M, Valovic M, Warrick CD, Wilson HR, the COMPASS-D team, and teams ECRH. Neoclassical islands on COMPASS-D . *Nucl. Fusion* **37**, 1593 (1997).

Giruzzi G, Zabiego M, Ganakon TA, Garbet X, Cardinali A, and Bernabei S. Dynamical modelling of tearing mode stabilization by RF current drive. *Nucl. Fusion* **39**, 107 (1999).

Hegna CC and Callen JD. On the stabilization of neoclassical magnetohydrodynamic tearing modes using localized current drive or heating. *Phys. Plasmas* **4**(8), 2940 (1997).

Isayama A, Kamada Y, Ozeki T, and Isei N. Measurement of magnetic island width in long-pulse, high-discharges in JT-60U. *Plasma Phys. Control. Fusion* **41**, 35 (1999).

Isayama A et al. Complete stabilization of a tearing mode in steady state high-β_p H-mode discharges by the first harmonic electron cyclotron heating/current drive on JT-60U. *Plasma Phys. Control. Fusion* **42**(12), L37 (2000).

JET Team. Observation of neoclassical tearing modes in JET. *Nucl. Fusion* **39**, 1965 (1999). Prepared by Huysmans, GTA.

La Haye RJ. Neoclassical tearing modes and their control. *Phys. Plasmas* **13**, 055501 (2006a).

La Haye RJ, Lao LL, Strait EJ, and Taylor TS. High beta tokamak operation in DIII-D limited at low densitycollisionality by resistive tearing modes. *Nucl. Fusion* **37**, 397 (1997).

La Haye RJ, Günter S, Humphreys DA, Lohr J, Luce TC, Maraschek ME, Petty CC, Prater R, Scoville JT, and Strait EJ. Control of neoclassical tearing modes in DIII–D. *Phys. Plasmas* **9**(5), 2051 (2002).

La Haye RJ, Brennan DP, Buttery RJ, and Gerhardt SP. Island in the stream: the effect of plasma flow on tearing stability. *Phys. Plasmas* **17**, 056110 (2010).

Lazzaro E and Nowak S. ECCD control of dynamics of asymmetric magnetic islands in a sheared flow. *Plasma Phys. Control. Fusion* **51**, 035005 (2009).

Meskat JP, Zohm H, Gabentein G, Günter S, Maraschek M, Suttrop W, Yu Q, and Team ASDEX Upgrade. Analysis of the structure of neoclassical tearing modes in ASDEX Upgrade. *Plasma Phys. Control. Fusion* **43**, 1325 (2001).

Ren C, Chu MS, and Callen JD. Magnetic island deformation due to sheared flow and viscosity. *Phys. Plasmas* **6**, 1203 (1999).

Rutherford PH. Nonlinear growth of tearing mode. *Phys. Fluids* **16**(11), 1903 (1973).

Sauter O. On the contribution of local current density to neoclassical tearing mode stabilization. *Phys. Plasmas* **11**(10), 4808 (2004).

Sauter O et al. Beta limits in long-pulse tokamak discharges. *Phys. Plasmas* **4**(5), 1654 (1997).

Smolyakov AI, Lazzaro E, Azumi M, and Kishimoto Y. Stabilization of magnetic islands due to the sheared plasma flow and viscosity. *Plasma Phys. Control. Fusion* **43**, 1661 (2001).

Udintsev VS, van Milligen BPh, Schüller FC, Krämer-Flecken A, Donné AJH, van Gorkom JC, Domier CW, and the TEXTOR-team. Plasma transport properties in the presence of MHD modes studied by ECE at TEXTOR. *Nucl. Fusion* **43**, 1424 (2003).

Urso L, Zohm H, Isayama A, Maraschek M, Poli E, ASDEX Upgrade Team, and JT-60 Team. ASDEX Upgrade–JT-60U comparison and ECRH power requirements for NTM stabilization in ITER. *Nucl. Fusion* **50**, 025010 (2010).

van der Plas EV and de Blank HJ. Temperature gradients in fast collisionless magnetic reconnection. *Phys. Rev. Lett.* **98**, 265002 (2007).

Westerhof E et al. Tearing mode stabilization by electron cyclotron resonance heating demonstrated in the TEXTOR tokamak and the implication for ITER. *Nucl. Fusion* **47**, 85 (2007).

Zohm H et al. Neoclassical MHD in ASDEX Upgrade and COMPASS-D. *Plasma Phys. Control. Fusion* **39**, B237 (1997).

6 Requirements on localized current drive for the suppression of neoclassical tearing modes

The work presented in this chapter refers to the paper by Bertelli, De Lazzari and Westerhof, submitted to *Nucl. Fusion*.

Abstract

A heuristic criterion for the full suppression of an NTM was formulated as $\eta_{\mathrm{NTM}} \equiv j_{\mathrm{CD,max}}/j_{\mathrm{BS}} \geq 1.2$ [Zohm et al., *J. Phys. Conf. Ser.*, **25** 234 (2005)], where $j_{\mathrm{CD,max}}$ is the maximum in the driven current density profile applied to stabilize the mode and j_{BS} is the local bootstrap current density. In this work we subject this criterion to a systematic theoretical analysis on the basis of the generalized Rutherford equation. Taking into account only the effect of j_{CD} inside the island, a new criterion for full suppression by a minimum applied total current is obtained in the form of a maximum allowed value for the width of the driven current, w_{dep}, combined with a required minimum for the total driven current in the form of $w_{\mathrm{dep}}\eta_{\mathrm{NTM}}$, where both limits depend on the marginal, and saturated island sizes. These requirements can be relaxed when additional effects are taken into account, such as a change in the stability parameter Δ' from the current driven outside the island, power modulation, the accompanying heating inside the island, or when the current drive is applied preemptively. When applied to ITER scenario 2, the requirement for full suppression either the 3/2 or 2/1 NTM becomes $w_{\mathrm{dep}} \lesssim 5$ cm and $w_{\mathrm{dep}}\eta_{\mathrm{NTM}} \gtrsim 5$ cm in agreement with [Sauter *et al.*, *Plasma Phys. Control. Fusion*, **52** 025002 (2010)]. Optimization of the ITER ECRH Upper Port Launcher design towards minimum required power for full NTM suppression requires an increase in the toroidal injection angle of the lower steering mirror of several degrees compared to its present design value, while for the upper steering mirror the present design value is close to the optimum.

6.1   Introduction

The suppression of Neoclassical Tearing Modes (NTMs) is likely to be an essential requirement for the achievement of the main goals of ITER [Shimada et al., 2007]. NTMs are driven unstable by a dip in the current density profile inside the magnetic island which results from the annihilation of the pressure gradient driven bootstrap current as a consequence of the pressure flattening inside the magnetic island [Sauter et al., 1997]. The main strategy for their suppression then is to fill this dip in the current density profile by another current generated either inductively through heating inside the island or non-inductively through direct current drive [Hegna and Callen, 1997; La Haye, 2006a]. Because of their good localization electron cyclotron resonance heating (ECRH) and current drive (ECCD) are the preferred tools to achieve NTM stabilization [Prater, 2004]. In particular, ECCD has been applied successfully in several tokamaks to suppress both $m = 3$, $n = 2$ and $m = 2$, $n = 1$ NTMs where m and n are the poloidal and toroidal mode number, respectively [Gantenbein et al., 2000; Isayama et al., 2000; La Haye et al., 2002]. Also on ITER, the suppression of NTMs is expected to come from ECCD. In fact, it is one of the main tasks of the ITER ECRH Upper Port Launcher, whose design has been optimized specifically for this task [Henderson et al., 2008; Ramponi et al., 2008].

What the precise requirements on such a system should be in order to achieve full NTM suppression remains an open question. In the ITER ECRH design studies, the parameter η_{NTM} defined as the ratio of the maximum in the driven current density profile over the bootstrap current density at the mode rational surface

$$\eta_{\mathrm{NTM}} \equiv \frac{J_{\mathrm{CD,max}}}{J_{\mathrm{BS}}}, \tag{6.1}$$

was introduced. Assuming that $\eta_{\mathrm{NTM}} \geq 1.2$ is a sufficient requirement for NTM suppression, a design requirement was imposed that the ITER ECRH system should be able to achieve this number over a range of discharge scenarios for both the $m = 3$, $n = 2$ and $m = 2$, $n = 1$ modes [Zohm et al., 2005]. Different experiments, however, report widely different values of η_{NTM} required for the full suppression of NTMs [Petty et al., 2004; Isayama et al., 2009]. Theoretical considerations [Sauter et al., 2010], based on the generalized Rutherford equation (GRE) [Rutherford, 1973; La Haye, 2006a], show that the required value of η_{NTM} depends amongst others on the marginal island size and the dominant physical effect limiting the neoclassical growth of the tearing mode for island sizes below this marginal size (finite parallel transport or ion polarization current) as well as on the EC driven current density profile width. Fitting of model predictions from the GRE to the experimental data from different tokamaks, has been used to establish the value of a number of constants in the GRE and from there to extrapolate to ITER conditions [La Haye et al., 2006b; Urso et al., 2010]. This method, however, does not discriminate between experimental uncertainties in the various parameters that enter the GRE, like the bootstrap current density, the maximum EC driven current density and the width of the EC driven current density profile, and the theoretical uncertainties in the coefficients appearing in the model itself. Moreover, the effect of the inescapable heating that accompanies the EC current drive is generally neglected in these analyses. Whereas the effect of

heating in ITER is expected to be small compared to the effect of non-inductive current drive, this is not the case in present experiments [Kislov et al., 1997; Westerhof et al., 2007; De Lazzari et al., 2009]. Since the effects of heating and non-inductive current drive scale completely different with respect to the size of the magnetic island, the effects of the two should be properly separated when scaling current experiments to ITER [Hegna and Callen, 1997; De Lazzari et al., 2009].

This paper aims to provide a systematic theoretical formulation for the requirements on the heating and current drive on the basis of the generalized Rutherford equation. Section 2 presents and discusses the generalized Rutherford equation as used in this paper. An equation for the requirement on η_{NTM} to achieve full suppression of an NTM is presented. In Section 3 the resulting numerical values for η_{NTM} are presented covering the relevant two dimensional parameter space defined by the saturated NTM island size and the width of the EC power deposition and driven current density profile. The possible location of present day experiments in this space and the resulting conclusion for the latter are discussed. Also the power requirements for the immediate, full suppression of a seed island (preemptive ECCD) are presented. In Section 4, these results are used to formulate practical requirements for the ITER ECRH system to achieve full NTM suppression. An optimization of the ITER ECRH Upper Port Launcher is then presented, starting from its present design. It is shown that a significant reduction in the power requirement for full NTM suppression can be obtained by a moderate change in the toroidal injection angle. Finally, the main conclusions of the work are summarized in Section 5.

6.2 Theoretical framework

The generalized Rutherford equation

The non-linear evolution of neoclassical tearing modes is commonly described by the generalized Rutherford equation (GRE), which gives the time rate of change of the full width w of the magnetic island as the sum of a series of terms each originating from a specific perturbation of the parallel current density with the proper helicity [Rutherford, 1973; La Haye, 2006a]. Including only the most relevant terms for the present work, the GRE is written as

$$0.82 \frac{\tau_r}{r_{\mathrm{s}}} \frac{\mathrm{d}w}{\mathrm{d}t} = r_{\mathrm{s}} \Delta_0' + r_{\mathrm{s}} \delta \Delta_0' + r_{\mathrm{s}} \Delta_{\mathrm{BS}}' + r_{\mathrm{s}} \Delta_{\mathrm{CD}}' + r_{\mathrm{s}} \Delta_{\mathrm{H}}' \tag{6.2}$$

where $\tau_r \equiv \mu_0 r_{\mathrm{s}}^2 / \eta$ is the local resistive time scale for the resistivity η at the rational surface r_{s} of the mode (μ_0 is the permeability of free space). The terms on the right hand side provide the effect of the linear stability index, the variation of Δ_0' due to the perturbation of the equilibrium current, the perturbation of the bootstrap current, the localized non-inductive current drive, and the localized heating, respectively. It is important to realize that the last three terms all derive from the generic form of the contribution in the GRE arising from a non-inductive helical current δJ in the flux surface averaged, generalized

Ohm's law for the helical electric field perturbation: $(1/R)\langle \partial \psi_1 / \partial t \rangle = \eta_0 (J_{1,\parallel} - \delta J)$, where R is the major radius, ψ_1 the perturbation of the helical flux function creating the magnetic island, η_0 the equilibrium plasma resistivity at the rational surface, and $J_{1,\parallel}$ the associated total perturbation of the parallel current density. The flux surface average operator $\langle . \rangle$, as indicated by the brackets, is defined as

$$\langle A \rangle \equiv \frac{\oint A(\mathrm{d}l / |\nabla \psi|)}{\oint (\mathrm{d}l / |\nabla \psi|)},$$

where the integral is along the closed line segment with constant helical flux ψ. Following Ref. [De Lazzari et al., 2009] this generic contribution is written as

$$
\begin{aligned}
r_s \Delta'_{\delta J} &= -\frac{16 \mu_0 L_q r_s}{B_p \pi w} \int_{-\infty}^{+\infty} \mathrm{d}\bar{x} \oint \mathrm{d}\xi \, \delta J \cos \xi \\
&= -\frac{16 \mu_0 L_q r_s}{B_p \pi w} \int_{-1}^{+\infty} \mathrm{d}\Omega \, \delta J \oint \mathrm{d}\xi \frac{\cos \xi}{\mathrm{d}\Omega / \mathrm{d}\bar{x}}
\end{aligned}
\tag{6.3}
$$

where $L_q \equiv q/(\mathrm{d}q/\mathrm{d}r)$ is the shear length, $q = m/n$ the safety factor calculated at the rational surface, B_p the poloidal magnetic field, $\bar{x} \equiv (r - r_s)/w$ the normalized radial displacement from the rational surface, $\xi \equiv m\theta - n\phi$ the helical angle, and $\Omega \equiv 8\bar{x}^2 - \cos \xi$ the normalized perturbed helical flux function describing the geometry of the island.

The neoclassical instability drive comes from the cancellation of the bootstrap current inside the magnetic island, that is to say $\delta J_{BS} = -J_{BS}$ inside the magnetic island, and thus equals

$$
\begin{aligned}
r_s \Delta'_{BS} &= +\frac{16 \mu_0 L_q r_s}{B_p \pi w} J_{BS} \int_{-1}^{+1} \mathrm{d}\Omega \oint \mathrm{d}\xi \frac{\cos \xi}{\mathrm{d}\Omega / \mathrm{d}\bar{x}} \\
&= +\frac{16 \mu_0 L_q r_s}{B_p \pi} \frac{4}{3w} f(w, w_{marg}) J_{BS}
\end{aligned}
\tag{6.4}
$$

where the factor $4/3$ derives from the analytical evaluation of the double integral and the factor $f(w, w_{marg})$ has been introduced to describe the limitation of the neoclassical drive for small island sizes below a marginal island size w_{marg}. The marginal island size is defined here as the island size at which the NTM growth rate reaches its maximum value (in the absence of a possible non-inductive current applied towards its stabilization or the associated heating). As in [Sauter et al., 2010] two alternate choices for this limitation $f(w, w_{marg})$ will be considered. The first choice,

$$f_{tra}(w, w_{marg}) = \frac{w^2}{w^2 + w_{marg}^2} \tag{6.5}$$

derives from the incomplete flattening of the pressure gradient inside the magnetic island as consequence of a finite parallel transport time scale [Fitzpatrick, 1995]. In this case the marginal island size is found to scale as $w_{marg} \propto (\chi_\perp / \chi_\parallel)^{1/4}$, where $\chi_\perp$ and $\chi_\parallel$ are

the perpendicular and parallel heat diffusivity, respectively. In the following this choice is referred to as 'transport' model (label 'tra'). In the second choice, the limitation comes from the stabilizing ion polarization effect [Mikhailovskii, 2003], in which case the factor f is written as

$$f_{\mathrm{pol}}(w, w_{\mathrm{marg}}) = 1 - \frac{w_{\mathrm{marg}}^2}{3w^2}. \tag{6.6}$$

In this case the marginal island size is expected to scale with the ion banana width. In the following this choice is referred to as 'polarization' model (label 'pol'). In the experiments both effects may act simultaneously resulting in a behaviour intermediary between f_{tra} and f_{pol}. However the actual values for w_{marg} are poorly known. Typical values for the marginal island size, consistent with experimental observation, are in the range of 1 to 6 cm [Sauter et al., 2010].

For the heating and current drive terms, the expressions derived in [De Lazzari et al., 2009] will be used. As is commonly done, a fast rotation of the island is assumed and the power deposition and current drive profiles are averaged over a complete rotation period. The stabilizing contribution from a non-inductively driven current $\delta J = \langle J_{\mathrm{CD}} \rangle = 2\pi R \eta_{\mathrm{CD}} \langle p_{\mathrm{EC}} \rangle$, defined in terms of the global current drive efficiency $\eta_{\mathrm{CD}} \equiv I_{\mathrm{CD}}/P_{\mathrm{tot}}$, i.e. the ratio of the driven current over the total absorbed power, and the flux surface averaged power density $\langle p_{\mathrm{EC}} \rangle$, is written as

$$
\begin{aligned}
r_{\mathrm{s}} \Delta'_{\mathrm{CD}} &= -\frac{16\mu_0 L_{\mathrm{q}} r_{\mathrm{s}}}{B_{\mathrm{p}} \pi w} \int_{-1}^{\infty} \mathrm{d}\Omega \left(2\pi R \langle p_{\mathrm{EC}} \rangle \eta_{\mathrm{CD}} \oint \mathrm{d}\xi \frac{\cos \xi}{\mathrm{d}\Omega/\mathrm{d}\bar{x}} \right) \\
&= -\frac{16\mu_0 L_{\mathrm{q}}}{B_{\mathrm{p}} \pi} \frac{\eta_{\mathrm{CD}} P_{\mathrm{tot}}}{w_{\mathrm{dep}}^2} F_{\mathrm{CD}}(w/w_{\mathrm{dep}}, \bar{x}_{\mathrm{dep}}, D_{\mathrm{mod}}, \phi_{\mathrm{mod}}) \\
&= -\frac{16\mu_0 L_{\mathrm{q}} r_{\mathrm{s}}}{B_{\mathrm{p}} \pi} \frac{\pi^{3/2} J_{\mathrm{CD,max}}}{w_{\mathrm{dep}}} F_{\mathrm{CD}}(w/w_{\mathrm{dep}}, \bar{x}_{\mathrm{dep}}, D_{\mathrm{mod}}, \phi_{\mathrm{mod}})
\end{aligned}
\tag{6.7}
$$

where F_{CD} is a dimensionless geometrical function depending on the ratio of the island width w over the full, Gaussian width of the power deposition profile w_{dep}, as well as on the location of the power deposition $\bar{x}_{\mathrm{dep}} = (r_{\mathrm{dep}} - r_{\mathrm{s}})/w$, and the duty cycle D_{mod} and phase ϕ_{mod} of a possible power modulation. The final expression is obtained, substituting the total driven current as

$$I_{\mathrm{CD}} = \pi^{3/2} r_{\mathrm{s}} w_{\mathrm{dep}} J_{\mathrm{CD,max}}, \tag{6.8}$$

assuming an identical Gaussian profile for the power deposition and driven current density $\propto \exp[-4(\bar{x} - \bar{x}_{\mathrm{dep}})^2/w_{\mathrm{dep}}^2]$. In the following, only a perfectly aligned power deposition ($\bar{x}_{\mathrm{dep}} = 0$) and either a continuous power ($D_{\mathrm{mod}} = 1$) or a modulated power ($D_{\mathrm{mod}} \neq 1$) ideally centred around the island O-point will be considered, i.e. $\phi_{\mathrm{mod}} = 0$. Following the work of De Lazzari et al. [De Lazzari et al., 2009], one can now write an expression for the geometrical function F_{CD}, in the form

$$F_{\mathrm{CD}}(w/w_{\mathrm{dep}}, \bar{x}_{\mathrm{dep}} = 0, D_{\mathrm{mod}}, \phi_{\mathrm{mod}} = 0) = N_{\mathrm{CD}}(w/w_{\mathrm{dep}}) M_{\mathrm{CD}}(w/w_{\mathrm{dep}}, D_{\mathrm{mod}}),$$
$$\tag{6.9}$$

where the function N_{CD} is well approximated by the rational function

$$N_{\mathrm{CD}} = \frac{0.25 + 0.24(w/w_{\mathrm{dep}})}{1 + 0.64(w/w_{\mathrm{dep}})^3 + 0.43(w/w_{\mathrm{dep}})^2 + 1.5(w/w_{\mathrm{dep}})} \tag{6.10}$$

and a good approximation for the factor M_{CD}, representing the effect of power modulation, is

$$M_{\mathrm{CD}} = (w_{\mathrm{dep}}/w)^3 [m_1(w/w_{\mathrm{dep}})^2 + m_2] + m_3; \tag{6.11}$$

with

$$m_1 = 2.25 D_{\mathrm{mod}}^4 - 3.44 D_{\mathrm{mod}}^3 - 0.99 D_{\mathrm{mod}}^2 + 2.2 D_{\mathrm{mod}} - 0.02, \tag{6.12}$$

$$m_2 = 0.01 \left(0.33 D_{\mathrm{mod}}^5 - 1.02 D_{\mathrm{mod}}^4 + 0.87 D_{\mathrm{mod}}^3 - 0.28 D_{\mathrm{mod}}^2 + 0.1 D_{\mathrm{mod}}\right), \tag{6.13}$$

$$m_3 = 1.34 D_{\mathrm{mod}}^4 - 3.54 D_{\mathrm{mod}}^3 + 1.1 D_{\mathrm{mod}}^2 + 2.09 D_{\mathrm{mod}} + 0.01. \tag{6.14}$$

Coefficients m_1 and m_2 have been adjusted with respect to those in [De Lazzari et al., 2009], such that $M_{\mathrm{CD}}(D_{\mathrm{mod}} = 1) = 1$. These modifications do not affect the fitting results. The corresponding arguments of F_{CD} will be suppressed in the remainder of the paper.

In the case of localized heating, one may write $\delta J = -(\eta_1/\eta_0) J_{0,\|}$, where η_1 is the perturbation to the resistivity and $J_{0,\|}$ the parallel equilibrium current density. Its stabilizing contribution is written similar to the current drive contribution (6.7) as [De Lazzari et al., 2009]

$$r_{\mathrm{s}} \Delta'_{\mathrm{H}} = -\frac{16 \mu_0 L_{\mathrm{q}}}{B_{\mathrm{p}} \pi} \frac{\eta_{\mathrm{H}} P_{\mathrm{tot}}}{w_{\mathrm{dep}}^2} F_{\mathrm{H}}(w/w_{\mathrm{dep}}, \bar{x}_{\mathrm{dep}}, D_{\mathrm{mod}}, \phi_{\mathrm{mod}}) \tag{6.15}$$

where η_{H} represents a current generation efficiency through heating which is defined as [De Lazzari et al., 2009]

$$\eta_{\mathrm{H}} \equiv \frac{3 w_{\mathrm{dep}}^2}{8 \pi R n_e \chi_{\perp} k_B} \frac{J_{\mathrm{s}}}{T_{\mathrm{s}}} \tag{6.16}$$

where n_e is the electron density, and J_{s} and T_{s} are the inductive part of the current density and the electron temperature at the rational surface, respectively. Analogously to F_{CD}, the geometrical function F_{H} is well approximated by a rational function,

$$F_{\mathrm{H}}(w/w_{\mathrm{dep}}, \bar{x}_{\mathrm{dep}} = 0, D_{\mathrm{mod}} = 1, \phi_{\mathrm{mod}} = 0) = \frac{0.077(w/w_{\mathrm{dep}})^2 + 0.088(w/w_{\mathrm{dep}})}{(w/w_{\mathrm{dep}})^2 + 0.8(w/w_{\mathrm{dep}}) + 2.17}.$$

$$\tag{6.17}$$

For the heating term, power modulation will not be considered. The corresponding arguments of F_{H} will be suppressed in the remainder of the paper.

Finally, one needs to know the linear stability index Δ'_0. In principle this can be calculated from a detailed knowledge of the plasma equilibrium, but the calculation is

so sensitive to the details of, in particular, the current density profile that a reasonable value cannot be obtained in this way from experimentally available data. However, by observing that for a saturated NTM the neoclassical drive and the linear stability index must cancel, an indirect expression in terms of the bootstrap term can be obtained:

$$\Delta_0' = -\Delta_{\mathrm{BS}}'(w = w_{\mathrm{sat}}), \tag{6.18}$$

where w_{sat} is the saturated island size. It is noted, that without local heating or current drive the main characteristics of the Rutherford equation are determined by the two parameters w_{marg} and w_{sat} [Sauter et al., 2010]: the maximum growth rate is reached at $w = w_{\mathrm{marg}}$ and the growth stops once $w = w_{\mathrm{sat}}$ is reached.

This is not yet the whole story: the linear stability index is also affected by the non-inductively driven current. On a local resistive time scale the equilibrium current density profile adapts to the presence of this non-inductively driven current changing the linear stability index. This effect is represented by the term $\delta\Delta_0'$ in the GRE equation (6.2). In the absence of a magnetic island the effect of a well localized non-inductively driven current has been evaluated using a perturbation analysis resulting in the expression [Westerhof, 1990]

$$r_{\mathrm{s}}\delta\Delta_0' = r_{\mathrm{s}}\frac{\mu_0 L_{\mathrm{q}}}{B_{\mathrm{p}}} \; \mathcal{P} \int_{-\infty}^{+\infty} dx \frac{1}{x} \frac{\partial \delta J_{\mathrm{CD}}}{\partial x}, \tag{6.19}$$

where $\mathcal{P}$ indicates that the possible singularity in the integrand has to be treated by evaluating the principal value integral. However, in the presence of a finite size island Δ_0' is to be evaluated by the jump in the derivative of the perturbed helical flux function over the entire island. While it will be assumed that this does not affect Δ_0', this cannot be maintained for its perturbation coming from a very localized driven current. Excluding the current driven within the interval $x = [-w/2 : +w/2]$ the equation for $\delta\Delta_0'$ becomes

$$r_{\mathrm{s}}\delta\Delta_0' = r_{\mathrm{s}}\frac{\mu_0 L_{\mathrm{q}}}{B_{\mathrm{p}}} \; \left(\int_{-\infty}^{-w/2} + \int_{+w/2}^{+\infty} \right) dx \frac{1}{x} \frac{\partial \delta J_{\mathrm{CD}}}{\partial x}. \tag{6.20}$$

Using the Gaussian profile for J_{CD} as defined above, and assuming again perfect alignment of the driven current on the rational surface, i.e. $\bar{x}_{\mathrm{dep}} = 0$, one obtains

$$\begin{aligned} r_{\mathrm{s}}\delta\Delta_0' &= -\frac{4\mu_0 L_{\mathrm{q}}}{B_{\mathrm{p}}\pi} \frac{\eta_{\mathrm{CD}}P_{\mathrm{tot}}D_{\mathrm{mod}}}{w_{\mathrm{dep}}^2} \mathrm{erfc}\left(\frac{w}{w_{\mathrm{dep}}}\right) \\ &= -\frac{4\mu_0 L_{\mathrm{q}}r_{\mathrm{s}}}{B_{\mathrm{p}}\pi} \frac{\pi^{3/2} J_{\mathrm{CD,max}}D_{\mathrm{mod}}}{w_{\mathrm{dep}}} \mathrm{erfc}\left(\frac{w}{w_{\mathrm{dep}}}\right) \end{aligned} \tag{6.21}$$

where D_{mod} has been inserted to account for the reduction of the total driven current due to power modulation and where

$$\mathrm{erfc}(x) \equiv \frac{2}{\sqrt{\pi}} \int_x^\infty \mathrm{e}^{-t^2} dt = 1 - \mathrm{erf}(x) \tag{6.22}$$

is the complementary error function. Note, that for perfect alignment ($\bar{x}_{\mathrm{dep}} = 0$) and no modulation ($D_{\mathrm{mod}} = 1$) the expressions for Δ'_{CD} equation (6.7) and $\delta\Delta'_0$ equation (6.21) reduce to the same value in the limit of $w/w_{\mathrm{dep}} \to 0$. Thus the total stabilizing effect from a relatively broad driven current density profile can be substantially bigger then estimated from considering only the effect of driven current inside the island. However, the time scales on which these terms take effect is essentially different: while Δ'_{CD} is established on a fast collisional time scale as soon as the power is applied, $\delta\Delta'_0$ is only established on a much slower current diffusion time scale.

General formulation of the requirements for mode stabilization

A typical curve of the growth rate $\mathrm{d}w/\mathrm{d}t$ as a function of the normalized island size w/w_{marg} is sketched in figure 6.1 for a case with $w_{\mathrm{sat}}/w_{\mathrm{marg}} = 10.0$. The two full lines represent the growth rate for the two cases limiting the bootstrap driven term at small islands: the incomplete flattening inside the island due to a finite parallel transport time scale (labelled 'tra'), or the ion polarization effect (labelled 'pol'). When some heating and or current drive power is introduced with $w_{\mathrm{dep}}/w_{\mathrm{marg}} = 1.5$, the curve is seen to shift downward (dashed lines in figure 6.1). A new, smaller stable island size is found at which $\mathrm{d}w/\mathrm{d}t$ vanishes. When the power is increased further, the whole curve can be shifted below $\mathrm{d}w/\mathrm{d}t = 0$. At the minimum required power for full stabilization the maximum of the curve of the growth rate just touches the line $\mathrm{d}w/\mathrm{d}t = 0$. The calculation of this minimum required power or driven current density is discussed below.

The required power, or driven current density to keep the mode stable at a given island size is obtained from

$$r_{\mathrm{s}}\Delta'_0 + r_{\mathrm{s}}\delta\Delta'_0(w) + r_{\mathrm{s}}\Delta'_{\mathrm{BS}}(w) + r_{\mathrm{s}}\Delta'_{\mathrm{CD}}(w) + r_{\mathrm{s}}\Delta'_{\mathrm{H}}(w) = 0. \tag{6.23}$$

Substituting the individual terms from the equations given above, and removing common fore factors, one obtains an expression for the ratio of the the maximum in the driven current density $J_{\mathrm{CD,max}}$ over the bootstrap current density J_{BS} required to keep the mode stable at this size. Denoting this ratio as $\eta_{\mathrm{NTM}}(w)$ one finds

$$\eta_{\mathrm{NTM}}(w) = \frac{4w_{\mathrm{dep}}}{3\pi^{3/2}} \left(\frac{\frac{1}{w}f(w, w_{\mathrm{marg}}) - \frac{1}{w_{\mathrm{sat}}}f(w_{\mathrm{sat}}, w_{\mathrm{marg}})}{F_{\mathrm{CD}} + \frac{w_{\mathrm{dep}}^2}{w_{\mathrm{marg}}^2}\bar{\eta}_{\mathrm{H}}F_{\mathrm{H}} + \frac{D_{\mathrm{mod}}}{4}\mathrm{erfc}\left(\frac{w}{w_{\mathrm{dep}}}\right)} \right), \tag{6.24}$$

where the function f can be interpreted either as f_{tra} according to equation (6.5) or as f_{pol} according to equation (6.6). The three terms in the denominator originate from the stabilizing effects of current drive inside the island, heating inside the island, and the changes to the mode stability index from the current driven outside the island, respectively. Note, that a normalized ratio of the inductive over the non-inductive current drive has been introduced as

$$\bar{\eta}_{\mathrm{H}} \equiv \frac{w_{\mathrm{marg}}^2}{w_{\mathrm{dep}}^2} \frac{\eta_{\mathrm{H}}}{\eta_{\mathrm{CD}}} \tag{6.25}$$
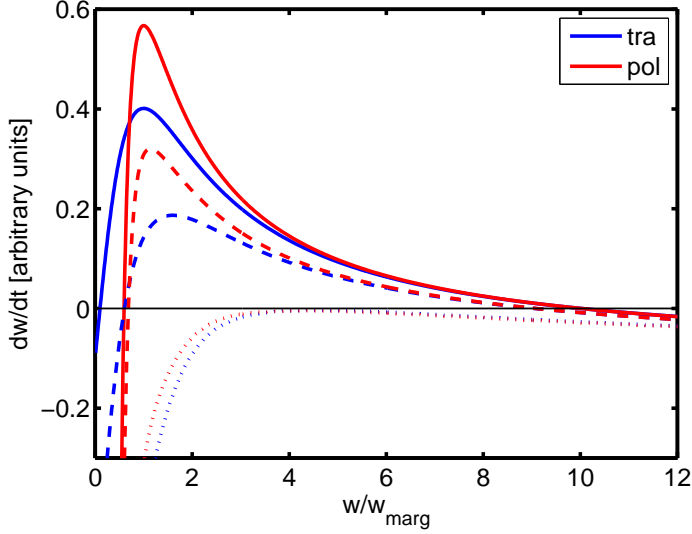
Figure 6.1: The evolution of the island width, $\mathrm{d}w/\mathrm{d}t$ (in arbitrary units), as a function of the island width normalized to the marginal island size, w/w_{marg}. The parameters are given in the text. The solid curves indicate the evolution of the island width without heating and/or current drive whereas the dash (dotted) curves indicate the case introducing heating and/or current drive power for a partial (full) suppression.

which brings out explicitly the correct dependence on w_{dep} of the heating contribution. The requirement for full suppression of the NTM now immediately follows as the maximum of $\eta_{\mathrm{NTM}}(w)$ over all possible values of w: i.e.

$$\eta_{\mathrm{NTM}} = \mathrm{Max}\left[\frac{4w_{\mathrm{dep}}}{3\pi^{3/2}} \left(\frac{\frac{1}{w}f(w, w_{\mathrm{marg}}) - \frac{1}{w_{\mathrm{sat}}}f(w_{\mathrm{sat}}, w_{\mathrm{marg}})}{F_{\mathrm{CD}} + \frac{w_{\mathrm{dep}}^2}{w_{\mathrm{marg}}^2}\bar{\eta}_{\mathrm{H}}F_{\mathrm{H}} + \frac{D_{\mathrm{mod}}}{4}\mathrm{erfc}\left(\frac{w}{w_{\mathrm{dep}}}\right)} \right) ; 0 \leq w \leq w_{\mathrm{sat}} \right].$$

(6.26)

Note, that given a normalized ratio of inductive over non-inductive current drive $\bar{\eta}_{\mathrm{H}}$ this final result depends on just two dimensionless parameters, namely, the saturated island width and the power deposition width, both normalized by the marginal island size: i.e. $\bar{w}_{\mathrm{sat}} \equiv w_{\mathrm{sat}}/w_{\mathrm{marg}}$ and $\bar{w}_{\mathrm{dep}} \equiv w_{\mathrm{dep}}/w_{\mathrm{marg}}$.
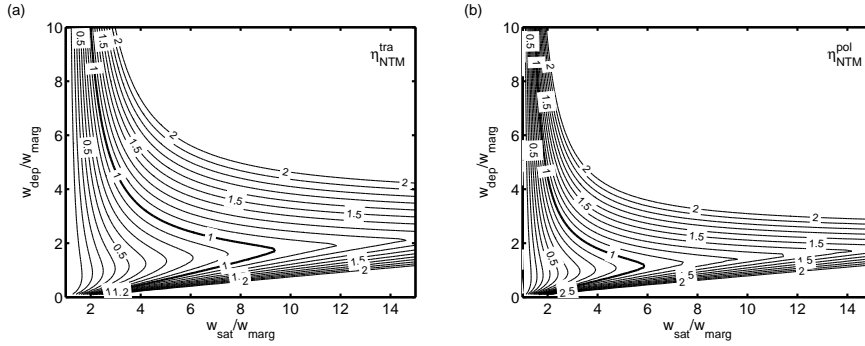
Figure 6.2: Contours of (a) $\eta_{\mathrm{NTM}}^{\mathrm{tra}}$ and (b) $\eta_{\mathrm{NTM}}^{\mathrm{pol}}$ keeping only the effect of current drive inside the island in case of CW current drive, i.e. keeping only F_{CD} with $D_{\mathrm{mod}} = 1$ in the denominator of equation (6.26) determining η_{NTM}. All contours are drawn equidistantly with a spacing of 0.1 up to a value of 2, with the thick line accentuating the level of 1.

6.3 Analysis of the η_{NTM} criterion

In this section, we show and analyze numerical results of the NTM suppression figure of merit, η_{NTM}, given by equation (6.26). As shown in the previous section, η_{NTM} finally only depends on two dimensionless parameters: $\bar{w}_{\mathrm{sat}}$ and $\bar{w}_{\mathrm{dep}}$. A complete picture can thus be obtained by calculating η_{NTM} over a region of parameter space covering most current and future experiments and plotting the results in terms of contours of constant η_{NTM} in the space spanned by $\bar{w}_{\mathrm{sat}}$ and $\bar{w}_{\mathrm{dep}}$. The results presented below cover the region $\bar{w}_{\mathrm{sat}} = [1 : 15]$ and $\bar{w}_{\mathrm{dep}} = [0 : 10]$. In the existing literature η_{NTM} has mostly been analysed keeping only the stabilizing effect of the non-inductively driven current inside the magnetic island, i.e. keeping only F_{CD} in the denominator of equation (6.26) determining η_{NTM} [Zohm et al., 2005; Sauter et al., 2010]. In line with this common practice, figure 6.2 shows the 2D contours of constant η_{NTM} over the space studied taking into account only the current drive inside the island for continuous power application (CW).

The following conclusions can be drawn from figure 6.2(a). For large saturated island sizes ($\bar{w}_{\mathrm{sat}} > 7$) the optimum value for $\eta_{\mathrm{NTM}}^{\mathrm{tra}}$ is close to unity and is found for $\bar{w}_{\mathrm{dep}} \approx 2$. On the other hand, for moderate saturated island sizes ($\bar{w}_{\mathrm{sat}} < 7$) the optimum value for $\eta_{\mathrm{NTM}}^{\mathrm{tra}}$ is smaller than unity (decreasing with decreasing $\bar{w}_{\mathrm{sat}}$) and is found for $\bar{w}_{\mathrm{dep}} \approx 1$. The same conclusions can be drawn for $\eta_{\mathrm{NTM}}^{\mathrm{pol}}$ (figure 6.2(b)), except that in both cases mentioned above an about 25% narrower power deposition and a slightly higher value of $\eta_{\mathrm{NTM}}^{\mathrm{pol}}$ is required. In all cases η_{NTM} increases dramatically when $\bar{w}_{\mathrm{dep}}$ is either increased or decreased. This strong dependence of η_{NTM} indicates that it cannot be used as the sole criterion to guide and optimize the design of an ECRH system for NTM control. An additional criterion must be imposed on $\bar{w}_{\mathrm{dep}}$. In fact, for a fixed toroidal
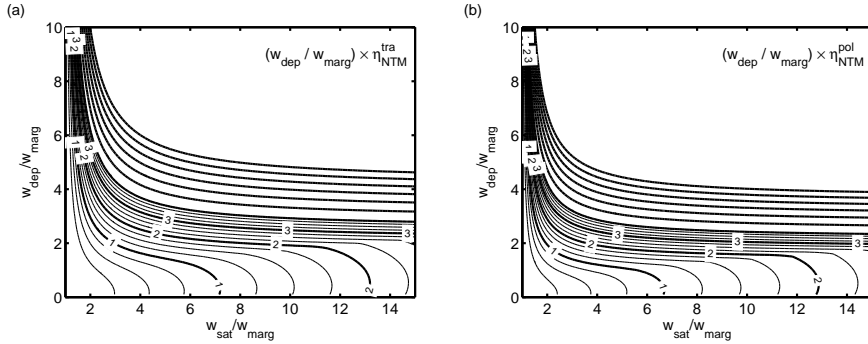
Figure 6.3: Contours of (a) $\bar{w}_{\mathrm{dep}}\eta_{\mathrm{NTM}}^{\mathrm{tra}}$ and (b) $\bar{w}_{\mathrm{dep}}\eta_{\mathrm{NTM}}^{\mathrm{pol}}$ keeping only the effect of current drive inside the island in case of CW current drive. The thick contours are drawn equidistantly with a spacing of 1 up to a value of 10 (0.25 for the thin lines).

injection angle of the ECRH, the product of $\bar{w}_{\mathrm{dep}}$ and η_{NTM} is a constant being related to the ratio of the total driven current over the total bootstrap current annihilated by an island of marginal size w_{marg}. When formulating the requirement in terms of this product, $\bar{w}_{\mathrm{dep}}\eta_{\mathrm{NTM}}$, figure 6.3 shows that, at a given $\bar{w}_{\mathrm{sat}}$, the required value remains almost constant when the deposition width $\bar{w}_{\mathrm{dep}}$ is decreased below the value at which the minimum in η_{NTM} was found under the same conditions in figure 6.2. In particular, for large saturated island sizes ($\bar{w}_{\mathrm{sat}} > 7$) an almost optimum value for $\bar{w}_{\mathrm{dep}}\eta_{\mathrm{NTM}}^{\mathrm{tra}}$ is close to two and is found for $\bar{w}_{\mathrm{dep}} \simeq 2$ while for moderate saturated island sizes ($\bar{w}_{\mathrm{sat}} < 7$) the optimum value for $\bar{w}_{\mathrm{dep}}\eta_{\mathrm{NTM}}^{\mathrm{tra}}$ is close to unity and is found for $\bar{w}_{\mathrm{dep}} \simeq 1$. A similar behavior is found for the case considering the limitation of NTM growth by the ion polarization effect, except that again a slightly narrower deposition is required. In the remainder of this section, the results will be shown in terms of $\bar{w}_{\mathrm{dep}}\eta_{\mathrm{NTM}}$ rather than simply η_{NTM}.

So far, only the stabilizing effect of a driven current inside the island obtained by CW power application has been considered. When one also includes the effect from the driven current outside the island on the tearing mode stability index, i.e. the erfc term in the denominator of equation (6.26) determining η_{NTM}, the requirement for full NTM stabilization changes considerably (figure 6.4(a)): while for narrow deposition widths $\bar{w}_{\mathrm{dep}} \lesssim 1$ there is hardly any change, for a broader deposition $\bar{w}_{\mathrm{dep}} \gtrsim 2$ the required value of $\bar{w}_{\mathrm{dep}}\eta_{\mathrm{NTM}}^{\mathrm{tra}}$ is significantly reduced. An even further reduction in the required value of $\bar{w}_{\mathrm{dep}}\eta_{\mathrm{NTM}}^{\mathrm{tra}}$ in case of broad deposition profiles is obtained by power modulation. This is shown in figure 6.4(b) for a case with a 50% duty cycle of modulated ECCD, i.e. $D_{\mathrm{mod}} = 0.5$. As pointed out already in [Perkins et al., 1997; Giruzzi et al., 1999; Yu et al., 2004; Maraschek et al., 2007], an advantage from power modulation is only obtained in case of broad deposition profiles. When the NTM growth is supposed to be limited by the polarization effect rather than by the finite parallel transport, the same
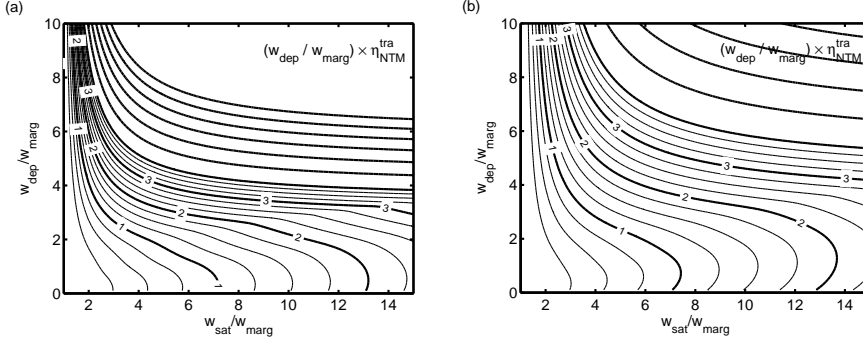
Figure 6.4: Contours of $\bar{w}_{\mathrm{dep}}\eta_{\mathrm{NTM}}^{\mathrm{tra}}$ including both the effect of current drive inside the island as well as the effect of the current outside the island on the tearing stability index in case of (a) CW current drive and (b) modulated current drive with a duty cycle of 50%.

qualitative behavior is observed in response to either the $\delta\Delta_0'$ term or to power modulation. Quantitatively, the required values of $\bar{w}_{\mathrm{dep}}\eta_{\mathrm{NTM}}^{\mathrm{pol}}$ are about 20% higher. The most important message to be taken from these results, is that for a given value of $\bar{w}_{\mathrm{dep}}\eta_{\mathrm{NTM}}$ the requirement on the maximum deposition width can be considerably relaxed when the favourable effects from either the equilibrium profile modifications or a power modulation are accounted for. In the latter case even by almost a factor of 2.

Finally, we analyze the contribution of localized heating inside the island on the requirement for NTM suppression (6.26). Although in the current experiments the heating contribution is not dominant and in theoretical works often is neglected, it appears relevant to analyze the behavior of $\bar{w}_{\mathrm{dep}}\eta_{\mathrm{NTM}}$ for different relative values of the heating contribution. In figure 6.5 2D contours of $\bar{w}_{\mathrm{dep}}\eta_{\mathrm{NTM}}^{\mathrm{tra}}$ are again shown as a function of $\bar{w}_{\mathrm{sat}}$ and $\bar{w}_{\mathrm{dep}}$ for the case of a normalized current generation efficiency (6.25) of (a) $\bar{\eta}_{\mathrm{H}} = 0.3$ and (b) $\bar{\eta}_{\mathrm{H}} = 1.0$. The effect of the heating comes in addition to the effect of the driven current in both Δ_{CD}' as well as $\delta\Delta_0'$. Comparing with figure 6.4(a) it is seen that the localized heating mostly affects the requirements at small $\bar{w}_{\mathrm{dep}}$, reducing the required value of $\bar{w}_{\mathrm{dep}}\eta_{\mathrm{NTM}}^{\mathrm{tra}}$ considerably. It is important to note that the values of $\bar{\eta}_{\mathrm{H}}$ are just examples in order to illustrate the effect of the heating contribution on $\bar{w}_{\mathrm{dep}}\eta_{\mathrm{NTM}}$.

As mentioned in the introduction, widely different values for the NTM stabilization requirement in terms of η_{NTM} have been obtained on the basis of the analysis of available experimental results: the analyses of both JT-60U and AUG experiments with saturated island sizes in the range of $\bar{w}_{\mathrm{sat}} = 2 - 3$ have yielded a requirement of $\eta_{\mathrm{NTM}} = 0.3 - 0.6$ [Isayama et al., 2009; Urso, 2009], while a requirement of $\eta_{\mathrm{NTM}} = 2 - 3$ is obtained from the analysis of DIII-D experiments with a saturated island size of $\bar{w}_{\mathrm{sat}} = 4 - 5$ [Petty et al., 2004]. In both data sets the deposition width is typically between 1 and 2 times w_{marg}. Thus the parameter range of the JT-60U and AUG experiments is covered by the lower left hand corners of the figures presented above. In particular, figure 6.2
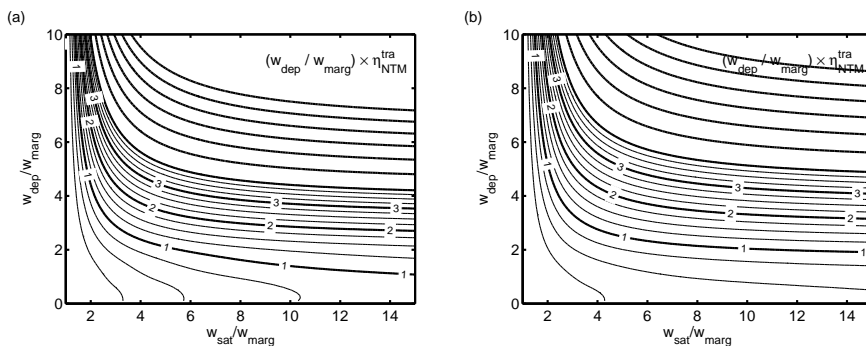
Figure 6.5: Contours of $\bar{w}_{\mathrm{dep}}\eta_{\mathrm{NTM}}^{\mathrm{tra}}$ taking into account the effect of localized heating inside the magnetic island. A normalized current generation efficiency is used with the value of (a) $\bar{\eta}_{\mathrm{H}} = 0.3$ and (b) $\bar{\eta}_{\mathrm{H}} = 1.0$. The effect of the heating comes in addition to the effect of the driven current in both Δ'_{CD} as well as $\delta\Delta'_0$.

where predicted η_{NTM} values are consistent with the experimental values quoted. However, the parameter range of the DIII-D experiments lies only slightly to the right of this corner at values of $\bar{w}_{\mathrm{dep}}$ where η_{NTM} is still close to 1, considerably smaller than the required value reported in [Petty et al., 2004]. More dedicated experiments will be required to extend the data base from present experiments in order to verify the detailed predictions made above. In particular, the data base needs to be extended to larger values of $\bar{w}_{\mathrm{sat}}$ in order to come closer to the relevant parameter range for future experiments like ITER.

Preemptive ECCD

Under preemptive ECCD is understood the application of localized ECCD at a rational surface well before an NTM is actually excited [Pletzer and Perkins, 1999; Nagasaki et al., 2003; La Haye et al., 2005; La Haye, 2006a]. Preemptive ECCD can act in two ways. First, by the effect of $\delta\Delta'_0$ the classical stability index is made more negative, thus increasing the linear stability of the mode and making the plasma more resilient against the creation of a seed island. Second, when a seed island is created nevertheless, the localized ECCD inside the island will immediately take effect and can suppress the seed island before it has had the time to grow. Since the physics processes responsible for the seeding are still poorly quantifiable, it is difficult to assess the requirements for the prevention of the seeding itself. However, the power requirements for the immediate, full suppression of the seed island are easily formulated in the context of the present theoretical analysis:
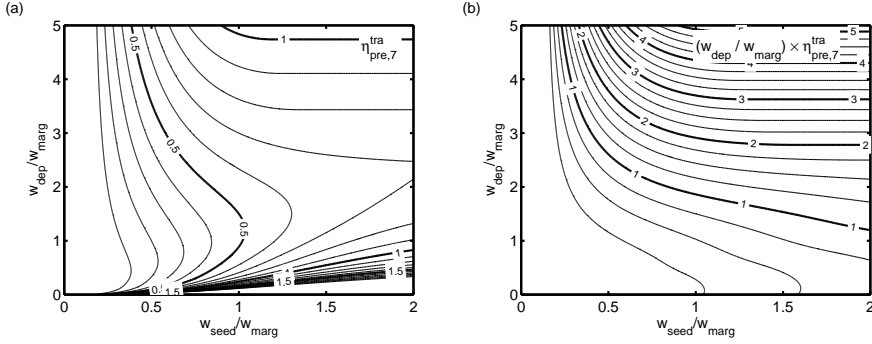
Figure 6.6: Contours of (a) $\eta_{\mathrm{pre},7}^{\mathrm{tra}}$ and (b) $\bar{w}_{\mathrm{dep}}\eta_{\mathrm{pre},7}^{\mathrm{tra}}$. For the case with a saturated island size of $w_{\mathrm{sat}} = 7w_{\mathrm{marg}}$, the requirement for full NTM suppression by pre-emptive ECCD is given as a function of the seed island size and the ECCD power deposition width. The effect of localized heating is neglected, i.e. $\bar{\eta}_{\mathrm{H}} = 0.0$. Contours are drawn with an equidistant spacing of 0.1 (a) and 0.25 (b).

in analogy to the requirement for full suppression of a saturated NTM (6.26) one obtains

$$\eta_{\mathrm{pre},\bar{w}_{\mathrm{sat}}} = \mathrm{Max}\left[\frac{4w_{\mathrm{dep}}}{3\pi^{3/2}}\left(\frac{\frac{1}{w}f(w,w_{\mathrm{marg}}) - \frac{1}{w_{\mathrm{sat}}}f(w_{\mathrm{sat}},w_{\mathrm{marg}})}{F_{\mathrm{CD}} + \frac{w_{\mathrm{dep}}^2}{w_{\mathrm{marg}}^2}\bar{\eta}_{\mathrm{H}}F_{\mathrm{H}} + \frac{1}{4}\mathrm{erfc}\left(\frac{w}{w_{\mathrm{dep}}}\right)}\right); 0 \le w \le w_{\mathrm{seed}}\right],$$

(6.27)

where $\eta_{\mathrm{pre},\bar{w}_{\mathrm{sat}}}$, indicates the minimum required ratio of the driven current density over the bootstrap current density in case the island would grow to the given saturated island size $\bar{w}_{\mathrm{sat}}$ without ECCD. Note, that preemptive ECCD would typically be performed with CW power application such that $D_{\mathrm{mod}} = 1$ has been assumed in (6.27). As long as w_{seed} is smaller than the island at which $\eta_{\mathrm{NTM}}(w)$ (6.24) reaches its maximum, this would considerably relax the requirement for the full suppression of NTMs.

In figure 6.6, $\eta_{\mathrm{pre},\bar{w}_{\mathrm{sat}}}^{\mathrm{tra}}$ is given for a saturated island size of $w_{\mathrm{sat}} = 7w_{\mathrm{marg}}$ and considering the transport model for the limitation of the neoclassical NTM drive at small island sizes. This figure is to be compared to a cross section of figure 6.4(a) at $w_{\mathrm{sat}} = 7w_{\mathrm{marg}}$, which shows a requirement for full suppression of a saturated NTM as $\bar{w}_{\mathrm{dep}} \lesssim 1$ and $\bar{w}_{\mathrm{dep}}\eta_{\mathrm{NTM}}^{\mathrm{tra}} \gtrsim 1$. From this comparison, the following conclusion can be drawn: as long as the seed stays smaller than w_{marg}, the requirement for preemptive ECCD allows either a reduction of the driven current (proportional to $\bar{w}_{\mathrm{dep}}\eta_{\mathrm{pre},\bar{w}_{\mathrm{sat}}}$) by about 50%, or to relax the requirement on w_{dep} by about a factor of 2. It is noted that, where the curves become horizontal in the figure, the seed island size exceeds the

island size at which $\eta_{\mathrm{NTM}}^{\mathrm{tra}}(w)$ (6.24) reaches its maximum. Consequently, in that parameter regime the advantage of preemptive ECCD disappears. This is the case for large deposition widths or seed island sizes larger than about double the marginal island size. When the saturated island size is increased (decreasing the effect of the second term in the numerator of (6.27)), the requirement on preemptive ECCD increases and the relative advantage of ECCD is found to decrease slightly. Similarly, for small saturated island sizes the advantage is expected to disappear when seed islands up to w_{marg} will need to be suppressed.

A smaller required value of $\bar{w}_{\mathrm{dep}}\eta_{\mathrm{pre},\bar{w}_{\mathrm{sat}}}$ of course translates into a smaller power requirement for the ECCD. It is indeed also observed experimentally that the power requirement for full suppression of the NTM by preemptive ECCD is considerably smaller than the power requirement for the full suppression of a saturated NTM [Nagasaki et al., 2003, 2005]. It has even been noted that in case of incomplete suppression of NTMs the mode is suppressed to a smaller island size by preemptive ECCD than by late ECCD applied after the mode has reached its saturated island size [Nagasaki et al., 2005]. In the context of our current analysis a possible explanation is suggested by the additional stabilizing effect of $\delta\Delta_0'$ which is present from the outset in the case of preemptive ECCD as long as it is has been applied sufficiently in advance of the island seeding, but which initially is absent in the case of late ECCD. The measurements then could even indicate a possible hysteresis in this term.

6.4   Application to ITER

The control of NTMs and sawteeth in ITER is achieved by means of the ECRH upper port launcher (UPL) which can deliver up to 20MW continuous wave (CW) at 170 GHz. The system consists of four antennas (or launchers) each containing eight waveguides and two steering mechanisms, a lower steering mirror (LSM) and an upper steering mirror (USM). The maximum total injected power from either the set of four LSMs or USMs is 13.3 MW. A detailed description of the launcher subsystems can be found in the work by Henderson et al. [Henderson et al., 2008]. The configuration allows to access the relevant flux surfaces associated with NTM destabilization. Mirrors are steered along the poloidal direction, while the toroidal injection angle β is kept constant. The toroidal injection angle β is defined as the angle between the initial wave vector and its projection in the poloidal plane [Prater et al., 2008]. In case of a typical ITER equilibrium, the steering range of the LSM covers the region from $0.55 \lesssim \rho_{\mathrm{tor}} \lesssim 0.85$ while the USM covers the region from $0.3 \lesssim \rho_{\mathrm{tor}} \lesssim 0.8$, ρ_{tor} being the square root of the normalized toroidal flux [Ramponi et al., 2008]. According to the present design $\beta^{\mathrm{LSM}} = 18°$ and $\beta^{\mathrm{USM}} = 20°$. These values were optimized to obtain the highest values of η_{NTM} [Ramponi et al., 2007].

In this section the results obtained so far in this paper will be applied to ITER. In particular the ITER standard scenario 2 [Prater et al., 2008; Sauter et al., 2010] is considered. The relevant parameters for the NTMs on the $q = 3/2$ and $q = 2/1$ surfaces are taken from [Ramponi et al., 2008; Sauter et al., 2010] and summarized in table 6.1.

Table 6.1: Relevant parameters for $3/2$ and $2/1$ modes.

q	ρ_{tor}	w_{sat} [cm]	J_{BS} [MAm^{-2}]
3/2	0.62	25	0.094
2/1	0.75	32	0.073

The saturated island width is 25 cm and 32 cm for the $3/2$ and $2/1$ modes, respectively, while the marginal island size is considered to be in the range between $2 \leq w_{\text{marg}} \leq 6$ cm for both modes. Note that the values given here refer to the average minor radius in the mid-plane, which in the case of the elongated ITER plasma differs by a factor $1/\sqrt{\kappa}$, where $\kappa = 1.7$ is the elongation, from a radial coordinate defined as $\sqrt{S/\pi}$, where S is the surface in the poloidal plane enclosed by the given flux surface, as used in some other studies. It is also remarked that in ITER, the heating contribution to η_{NTM} is negligible in the relevant range $15° \leq \beta \leq 25°$, being $\bar{\eta}_{\text{H}} \lesssim 0.1$.

Using these parameters for $q = 3/2$ and $q = 2/1$ modes and $w_{\text{marg}} = 2$ cm, the normalized saturated island sizes become $\bar{w}_{\text{sat}} = 12.5$ and $\bar{w}_{\text{sat}} = 16$, respectively. Looking at the relevant parameter regime in figure 6.3(a), this suggests the requirement $\bar{w}_{\text{dep}} \lesssim 2.5$ and $\bar{w}_{\text{dep}}\eta_{\text{NTM}} \gtrsim 2.5$. Similarly, for $w_{\text{marg}} = 4$ cm, the relevant parameter range becomes $\bar{w}_{\text{sat}} = 6$ to 8, in which case figure 6.3(a) suggests the requirement $\bar{w}_{\text{dep}} \lesssim 1.25$ and $\bar{w}_{\text{dep}}\eta_{\text{NTM}} \gtrsim 1.25$. In this way a single unnormalized criterion is obtained for the range of $w_{\text{marg}} = 2$ to 4 cm, which reads,

$$w_{\text{dep}} \lesssim 5 \text{ cm} \quad \text{and} \quad w_{\text{dep}}\eta_{\text{NTM}} \gtrsim 5 \text{ cm}, \tag{6.28}$$

which agrees with the criterion obtained in [Sauter et al., 2010]. For $w_{\text{marg}} = 6$ cm this criterion can be slightly relaxed. Since the product of $w_{\text{dep}}\eta_{\text{NTM}}$ for a given bootstrap current, stands for the total driven current, it is convenient to reformulate this criterion as $I_{\text{CD}} \gtrsim (\pi^{3/2}\sqrt{\kappa}r_{\text{s}}w_{\text{dep}}J_{\text{BS}})|_{w_{\text{dep}}=5\,\text{cm}}$. It is observed that in the current design for the ITER ECRH system the focus on the optimization of only η_{NTM} has resulted in deposition widths considerably smaller than the optimum value of 5 cm [Ramponi et al., 2007, 2008]. Note that in [Ramponi et al., 2007] the widths are given in terms of $\sqrt{S/\pi}$ rather than the average mid-plane radius. As a consequence, the new criterion for NTM stabilization in ITER, as derived above, is in particular cases not met. In those cases the current optimization is lacking the proper trade off between the width and total driven current density. As shown in figure 6.2, an over-focused beam leads to a strong increase in the η_{NTM} requirement. In the light of these conclusions, a reassessment of the ITER design is found to be necessary.

Optimization of the ITER ECRH Upper Port Launcher

Since, for a given equilibrium of the plasma, both the driven current density and the power deposition width are determined by the injection parameters, an optimization anal-

ysis can be achieved by calculating these quantities as a function of the toroidal injection angle β, for LSM and USM configurations. For every value of β the poloidal injection angle α, defined as the angle between a horizontal plane and the poloidal projection of the initial wave vector [Prater et al., 2008], is tuned in order to keep the location of the power deposition constant at the resonant surface. The calculation of the EC driven current and the width of the current density profile have been obtained with a single beam for either LSM or USM, with properties as defined in [Ramponi et al., 2007]. The computation has been performed by means of a beam-tracing code, TORBEAM [Poli et al., 2001]. The code computes the current drive by an analytical solution to the adjoint equation [Lin-Liu et al., 2003]. An optimum β angle minimizes the required power when it satisfies the two criteria given above, namely a small value for $w_{\mathrm{dep}} \leq 5$ cm and the maximum achievable current drive. This optimum is then compared to the toroidal angles β^{LSM} and β^{USM} as in the present ITER ECRH system design. In the following discussion a number of figures will be shown, representing four cases: subscripts (a) and (b) address the $3/2$ mode for LSM and USM, respectively, while (c) and (d) represent the same configurations for the $2/1$ mode.

Figure 6.7, presents the total driven current per unit power and the corresponding deposition width for $q = 3/2$ and $q = 2/1$, according to LSM and USM configurations, as a function of β. All the plots show a large, nearly flat region of w_{dep} between $15° \leq \beta \leq 21°$ where, in turn, I_{CD} grows approximately linearly. This trend indicates the possibility to increase the total driven current without affecting significantly the width of the current profile, by a modest increase of the angle β from its current design value.

A detailed optimization requires nonetheless the estimation of the power requirement for mode stabilization, based on the full criterion given in equation (6.26). For a given launcher configuration and equilibrium (i.e. for given values of $\bar{w}_{\mathrm{dep}}$ and $\bar{w}_{\mathrm{sat}}$), the minimal power for the stabilization in ITER is determined by ,

$$P_{\mathrm{NTM}} = \eta_{NTM}(\bar{w}_{\mathrm{dep}}, \bar{w}_{\mathrm{sat}}) \frac{J_{\mathrm{BS,ITER}}}{\gamma_{\mathrm{CD,ITER}}}, \quad \gamma_{\mathrm{CD,ITER}} \equiv J_{\mathrm{CD,max}}/P_{\mathrm{tot}} \qquad (6.29)$$

where $\gamma_{\mathrm{CD,ITER}}$ is the maximum in the driven current density profile for unit power, obtained from the beam tracing calculation and the value of $\bar{w}_{\mathrm{sat}}$ and $J_{\mathrm{BS,ITER}}$ depend on the mode under consideration. In analogy with the work of Sauter et al. [Sauter et al., 2010], a set of values for the marginal island width has been chosen: $w_{\mathrm{marg}} = 2, 4$ and 6 cm, covering the range of predicted values of w_{marg} as found in the literature. The result appears in figure 6.8 where the trend for the power requirement is plotted for $\eta_{\mathrm{NTM}}^{\mathrm{tra}}$ and $\eta_{\mathrm{NTM}}^{\mathrm{pol}}$. The calculation takes into account only the stabilizing effect of J_{CD} inside the island as is generally done in the literature. For $w_{\mathrm{marg}} = 4$ cm and 6 cm (dashed and dotted lines, respectively), the minimum power in all the cases is found for β larger than the currently designed angles. In particular for the LSM an increase in β by about $4°$ results in a significant reduction of the power. In the case $w_{\mathrm{marg}} = 2$ cm (solid lines) the minimum power is reached at approximately $21°$. For USM the current design is generally close to the optimum.

In order to complete the analysis for the angle optimization, additional effects need to be taken into account. In a recent work by Bertelli et al. [Bertelli and Westerhof, 2009],
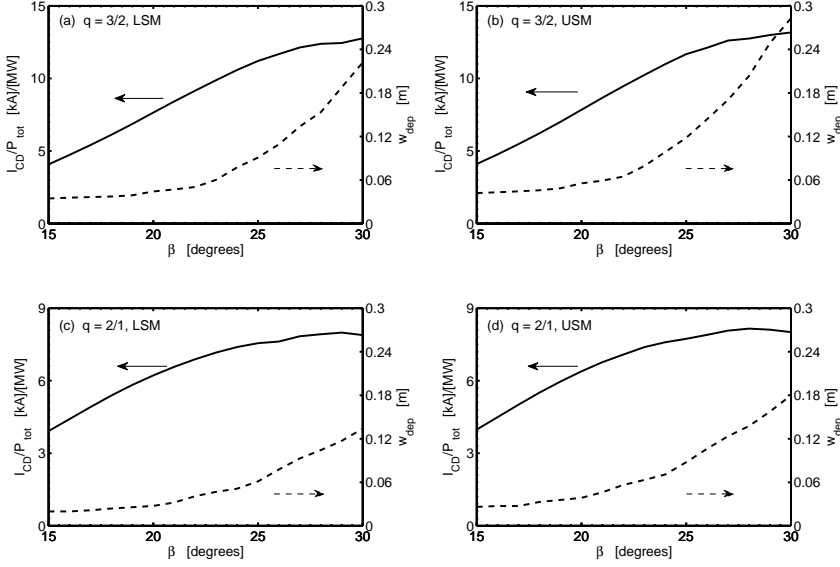
Figure 6.7: Total driven current per unit power I_{CD}/P_{tot} (solid lines) and the relative power deposition width w_{dep} (dashed lines) as a function of the toroidal injection angle β. Arrows indicate for every curve, the correspondent ordinate axis.

the (anomalous) radial transport is shown to affect the driven current density causing a non-negligible broadening of the profile. This is caused by the high temperature predicted for ITER, which leads to a long collisional time for the resonant electrons. Using the effective diffusion coefficient D_{eff} as in Bertelli and Westerhof [2009], an expression for the corrected width is found as $w_{CD} = \sqrt{w_{dep}^2 + 4D_{eff}\tau/\kappa}$, where the factor 4 was added for consistency with the full Gaussian width used in this paper and the factor κ accounts for the difference between the average mid-plane radial coordinate used here and the $\sqrt{S/\pi}$ used in [Bertelli and Westerhof, 2009]. The effective electron collision time related to the EC current generation τ is defined as $\tau \equiv \tau_{coll}(v_{res}/v_{th})^3$, where τ_{coll} is the electron collision time [Wesson, 2004] and v_{res}, v_{th} indicate the velocity of the resonant electrons and the electron thermal velocity, respectively. In the case of ITER, the ratio of the velocities $v_{res}/v_{th} \approx 2.5$, such that we refer to $\tau \equiv \tau_{2.5}$ [Prater et al., 2008; Bertelli and Westerhof, 2009]. The broadening of w_{CD} implies a reduction of the maximum in the driven current density and therefore an increase in the required power. It should be noted that when the correction to the current profile width is taken into account, w_{CD} replaces w_{dep} in all the equations related to Δ'_{CD} (7-14) and with $\delta\Delta'_0$ (6.21). In
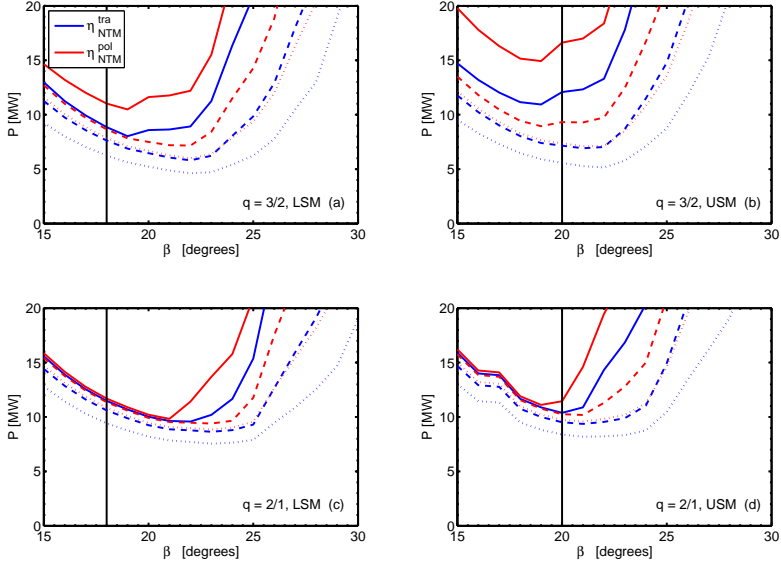
Figure 6.8: Power requirements for the stabilization of $q = 3/2$ and $q = 2/1$ modes in ITER scenario 2, as a function of the toroidal injection angle β. Only the stabilizing effect of a CW driven current inside the island, Δ'_{ECCD}, is taken into account. Each picture shows the trend of the power for $w_{\mathrm{marg}} = 2$ cm (solid lines), $w_{\mathrm{marg}} = 4$ cm (dashed lines) and $w_{\mathrm{marg}} = 6$ cm (dotted lines). For every value of w_{marg} the power has been determined for the "transport model" (6.5) and the "polarization model" (6.6). Black vertical lines denote the values of the toroidal angle for the current design of the ITER ECRH system, $\beta = 18°$ for LSM and $\beta = 20°$ for USM.

addition to the radial transport, two extra stabilizing effects need to be considered, namely the contribution of the non-inductivly driven current on the linear stability $\delta\Delta'_0$, derived in (6.21), and the possibility of power modulation.

This is illustrated, for $w_{\mathrm{marg}} = 2$ cm, in figure 6.9 and for $w_{\mathrm{marg}} = 4$ cm, in figure 6.10. In these two sets of figures, only results obtained in the case of the transport model are considered. Unlike figure 6.8, the marginal island width is kept constant, while the different curves are obtained by adding extra physics in the calculation of η_{NTM} and the resulting required power. The reference case, denoted with solid lines, accounts only for the stabilizing effect of current drive inside the island with no radial transport, and no modulation. In the remaining curves the additional effects are added one by one. At first the effect of the radial diffusion at a rate of $D_{\mathrm{eff}} = 0.3$ m^2/s is added (dashed
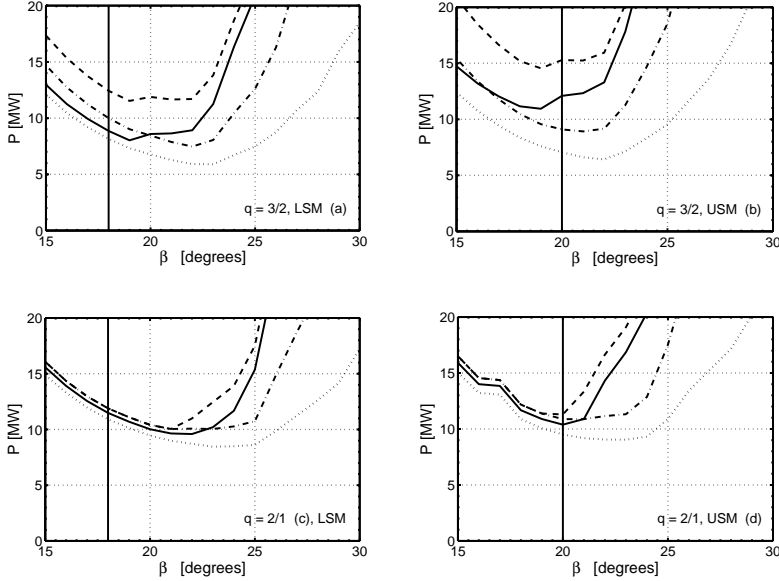
Figure 6.9: Power requirements for the stabilization of $q = 3/2$ and $q = 2/1$ modes in ITER scenario 2, as a function of the toroidal injection angle β, for $w_{\mathrm{marg}} = 2$ cm. Solid lines indicate the reference case (figure 6.8) taking into account only Δ'_{ECCD} in case of CW current drive and neglecting radial diffusion, i.e. $D_{\mathrm{eff}} = 0$ m^2/s. The second set of curves (dashed lines) introduces a finite radial transport, $D_{\mathrm{eff}} = 0.3$ m^2/s. The third case (dot-dashed lines) considers in addition the effect of $\delta\Delta'_0$. In the last set of curves (dotted lines), power modulation is introduced with $D_{\mathrm{mod}} = 0.5$ while all other parameters are as in the previous case.

lines), with the consequent broadening of w_{dep}. This results in a sizable increase in the power requirement in particular for the case of the $3/2$ mode. The power requirement for the $2/1$ mode is hardly affected as long as $\beta \lesssim 20°$, which is understood, since in these cases the power deposition width was originally significantly smaller than the required minimum value of 5 cm (6.28).

The inclusion of the $\delta\Delta'_0$ effect, denoted with dashed-dotted lines, can have a large stabilizing effect, increasing with larger values of β. For the case of $w_{\mathrm{marg}} = 2$ cm, a reduction of the minimum required power of 40% is found for the $3/2$ mode. However, for the $2/1$ mode and in case of $w_{\mathrm{marg}} \geq 4$ cm, the improvement in minimum power is negligible.

The largest achievable improvement for all cases is observed with modulation of the
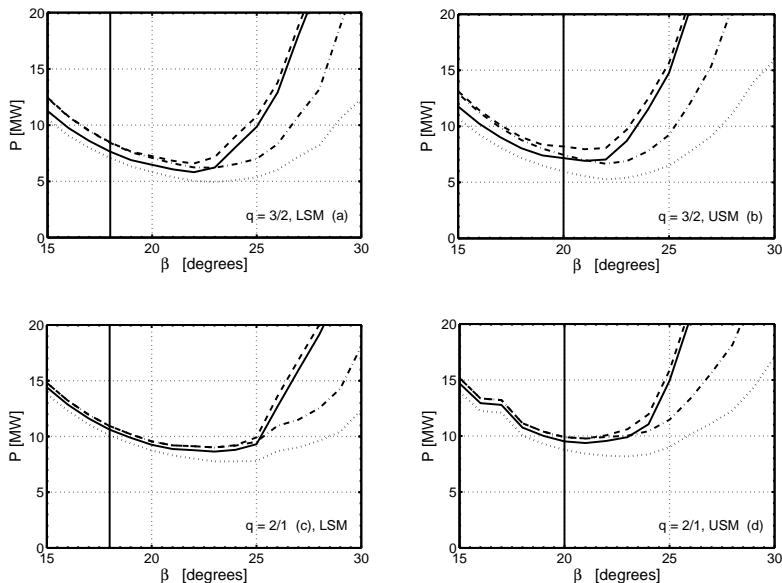
Figure 6.10: The same as in figure 6.9, for $w_{\mathrm{marg}} = 4\mathrm{cm}$.

power, $D_{\mathrm{mod}} = 0.5$ (dotted lines). In this case the optimum is obtained at $\beta \approx 23°$ in case of the LSM and $\beta \approx 22°$ in case of the USM. For these values of β, the power deposition width is increased by a factor of 2 for LSM while for USM it is increased by approximately 25% (see figure 6.7).

From the analysis shown so far, the best compromise for all LSM scenarios is $\beta = 22°$ while for USM the current design appears a good choice. If the size of the marginal island for ITER were confirmed to be $w_{\mathrm{marg}} \approx 4$ cm, as suggested in the "Progress in the ITER physics basis" [Shimada et al., 2007], a further increase in β would be profitable suggesting $\beta = 23°$ for LSM and $\beta = 22°$ for USM. If the design has to be optimized taking full advantage of ECCD modulation, these angles could be even increased by one extra degree. For LSM, increasing the angle by $\simeq 5°$, is expected to yield a reduction of the required power of the order of 20% in the modulated ECCD case. For USM the increase of the angle by $\simeq 2°$, corresponds to a predicted reduction of about 10%.

6.5 Summary and conclusions

In this paper the requirements for full NTM suppression have been addressed, by means of an analytical expression of η_{NTM} obtained from the GRE in (6.2), where the linear

stability index has been approximated with the bootstrap term evaluated at the saturated island width, $\Delta'_0 = -\Delta'_{BS}(w = w_{sat})$. Concerning the bootstrap term, two possible models determining the scaling of w_{marg} have been considered, the first based on the finite parallel transport, the second on the ion polarization effect. For each model an analytical expression for η_{NTM} was calculated, η^{tra}_{NTM} and η^{pol}_{NTM}, as a function of the power deposition width and the saturated island width normalized to the marginal island size. This purely analytical approach is thought to have two merits. First, it does not rely on fitting of individual terms in the GRE, to experimental data which does not properly discriminate between uncertainties in the determination of various physical quantities appearing in these terms, such as the bootstrap current density or the driven current and its profile width, and the uncertainties in the (geometric) coefficients appearing in front of these terms in the GRE. Since most terms in the numerator and in the denominator of the equation for η_{NTM} (6.26) originate from the same term for a generic helical current perturbation (6.3), these latter coefficients cancel out in the expression for η_{NTM}, such that the theoretical uncertainties in these coefficients do not affect η_{NTM}. Second, it provides a simple, yet complete description of η_{NTM}, taking into account also additional terms such as the localized heating and the effect of the driven current on the linear stability. The theoretical limits of the model are therefore the limits of the GRE itself.

A systematic study of the η_{NTM} requirement has been performed over the relevant parameter space, defined by the power deposition width and the saturated island width normalized to the marginal island size. The strong dependence of η_{NTM} on w_{dep} has led to the conclusion that a more appropriate condition is based on a combination of $\bar{w}_{dep}$ and $\bar{w}_{dep}\eta_{NTM}$. A crude estimation of this condition for NTM suppression is given in section 6.3, taking into account only the stabilizing effect of the non-inductively driven current inside the island. This criterion distinguishes between two regions in parameter space, depending on the size of w_{sat}. For large saturated island sizes ($\bar{w}_{sat} > 7$) a minimum required value for $\bar{w}_{dep}\eta^{tra}_{NTM}$ is close to two and is found for $\bar{w}_{dep} \lesssim 2$. For moderate saturated island sizes ($\bar{w}_{sat} < 7$) the minimum value for $\bar{w}_{dep}\eta^{tra}_{NTM}$ is close to unity and is found for $\bar{w}_{dep} \lesssim 1$. An analogous conclusion is drawn for η^{pol}_{NTM} except that a slightly narrower deposition is required. A further decrease of power deposition width does not lead to any significant reduction of the required driven current. Increasing $\bar{w}_{dep}$ however, leads to a rapid increase of the required driven current. A smaller value of $\bar{w}_{sat}$ implies generally a lower required current.

The inclusion of additional stabilizing effects namely $\delta\Delta'_0$ and the power modulation is found to provide a remarkable reduction, up to a factor 2, in the power requirement. The use of power modulation appears beneficial only for broad profiles, $\bar{w}_{dep} \gtrsim 2$. In contrast, a finite value for the normalized current generation efficiency, $\bar{\eta}_H$, from localized heating inside the island leads to a reduction in the required driven current mostly in case of relatively narrow deposition profiles, $\bar{w}_{dep} \lesssim 2$.

Available data from experimental results obtained in JT-60 and AUG [Isayama et al., 2009; Urso, 2009] show good consistency with the model, while the required values for η_{NTM} reported from DIII-D [Petty et al., 2004] are about a factor of 2 in excess of current predictions. However, these data refer only to the lower left hand corner of the

diagrams presented and do not reach the parameter regime expected for ITER. Dedicated experiments are required to extend the database and test the predictions made by the present analysis.

In case the driven current is applied preemptively, full suppression of a seed island with a maximum size equal to the marginal island is found to require up to a factor of 2 lower driven current or to allow a factor of 2 broader deposition profile than the full suppression of saturated NTM. The advantage of preemptive ECCD is smaller in case of small saturated island sizes and vanishes when significantly larger seed islands occur. In the second part of the paper the criterion derived for NTM stabilization has been applied to ITER scenario 2. The analysis points out that the focus of the previous design optimization on only the η_{NTM} criterion has led to an over-focused power deposition. This suggests a reassessment of the present design values for the toroidal injection angle β in the ITER ECRH system, which are for LSM $\beta = 18°$ and for USM $\beta = 20°$. The optimum condition must satisfy (6.28), yielding the maximum possible driven current while keeping the current density width close to or below 5 cm. Analyzing the trend of I_{CD} and w_{dep} as functions of β, this optimum is found near $\beta \simeq 21°$ for either LSM or USM. In this range, the contribution of the heating term to η_{NTM} is found to be negligible. Further optimization of the power requirement, including the effect owing to the broadening of the current density profile as a consequence of finite radial diffusion and the stabilizing effects related to $\delta\Delta_0'$, indicates an optimum angle of $21° - 22°$ for the LSM while the current design value of $\beta = 20°$ is a good optimum for the USM. Power modulation has the potential to significantly reduce the required power. Taking full advantage of this reduction requires a further increase of the toroidal injection angle to $\beta = 23°$ for the LSM and for $\beta = 22°$ for the USM. This implies a reduction of the power requirement of approximately 25% for the LSM and 10% for the USM compared to the present design.

Acknowledgments

References

Bertelli N and Westerhof E. Consequences of finite transport on the effectiveness of ECCD for neoclassical tearing mode stabilization in ITER. *Nucl. Fusion* **49**, 095018 (2009).

De Lazzari D and Westerhof E. On the merits of heating and current drive for tearing mode stabilization. *Nucl. Fusion* **49**, 075002 (2009). Erratum: *Nucl. Fusion* **50**, 079801 (2010).

Fitzpatrick R. Helical temperature perturbations associated with tearing modes in tokamak plasmas. *Phys. Plasmas* **2**(3), 825 (1995).

Gantenbein G, Zohm H, Giruzzi G, Günter S, Leuterer F, Maraschek M, Meskat J, Yu Q, ASDEX Upgrade Team, and ECRH-Group (AUG)l. Complete suppression of neoclassical tearing modes with current drive at the electron-cyclotron-resonance frequency in ASDEX Upgrade Tokamak. *Phys. Rev. Lett.* **85**(6), 1242 (2000).

Giruzzi G, Zabiego M, Ganakon TA, Garbet X, Cardinali A, and Bernabei S. Dynamical modelling of tearing mode stabilization by RF current drive. *Nucl. Fusion* **39**, 107 (1999).

Hegna CC and Callen JD. On the stabilization of neoclassical magnetohydrodynamic tearing modes using localized current drive or heating. *Phys. Plasmas* **4**(8), 2940 (1997).

Henderson MA et al. Overview of the ITER EC upper launcher. *Nucl. Fusion* **48**, 054013 (2008).

Isayama A et al. Complete stabilization of a tearing mode in steady state high-β_p H-mode discharges by the first harmonic electron cyclotron heating/current drive on JT-60U. *Plasma Phys. Control. Fusion* **42**(12), L37 (2000).

Isayama A et al. Neoclassical tearing mode control using electron cyclotron current drive and magnetic island evolution in JT-60U. *Nucl. Fusion* **49**, 055006 (2009).

Kislov DA, Alikaev VV, Esipchuk Yu V, Kakurtn AM, Kislov A Ya, Martynov DA, Notkin GE, Razumova KA, Sushkov AV, and Volkov VV. The m=2, n=1 mode suppression by ECRH on the T-10 tokamak. *Nucl. Fusion* **37**(3), 339 (1997).

La Haye RJ. Neoclassical tearing modes and their control. *Phys. Plasmas* **13**, 055501 (2006a).

La Haye RJ, Günter S, Humphreys DA, Lohr J, Luce TC, Maraschek ME, Petty CC, Prater R, Scoville JT, and Strait EJ. Control of neoclassical tearing modes in DIII–D. *Phys. Plasmas* **9**(5), 2051 (2002).

La Haye RJ, Humphreys DA, Ferron JR, Luce TC, Perkins FW, Petty CC, Prater R, Strait EJ, and AS Welander. Higher stable beta by use of pre-emptive electron cyclotron current drive on DIII-D. *Nucl. Fusion* **45**, L37 (2005).

La Haye RJ, Prater R, Buttery RJ, Hayashi N, Isayama A, Maraschek ME, Urso L, and Zohm H. Cross-machine benchmarking for ITER of neoclassical tearing mode stabilization by electron cyclotron current drive. *Nucl. Fusion* **46**, 451 (2006b).

Lin-Liu YR, Chan VS, and Prater R. Electron cyclotron current drive efficiency in general tokamak geometry. *Phys. Plasmas* **10**, 4064 (2003).

Maraschek M et al. Enhancement of the stabilization efficiency of a neoclassical magnetic island by modulated electron cyclotron current drive in ASDEX Upgrade tokamak. *Phys. Rev. Lett.* **98**, 025005 (2007).

Mikhailovskii AB. Theory of magnetic islands in tokamaks with accenting neoclassical tearing modes. *Contrib. Plasma Phys.* **43**, 125 (2003).

Nagasaki K, Isayama A, Ide S, and the JT-60 Team. Stabilization effect of early ECCD on a neoclassical tearing mode in the JT-60U tokamak. *Nucl. Fusion* **43**, L7 (2003).

Nagasaki K, Isayama A, Hayashi N, Ozeki T, Takechi M, Oyama N, Ide S, Yamamoto S, and the JT-60 Team. Stabilization of neoclassical tearing mode by ECCD and its evolution simulation on JT-60U tokamak. *Nucl. Fusion* **45**, 1608 (2005).

Perkins FW, Harvey RW, Makowski M, and Rosenbluth MN. In *Proceedings of the 24th EPS Conference on Controlled Fusion and Plasma Physics*, volume 21A, page 1017, 1997.

Petty CC, La Haye RJ, Luce TC, Humphreys DA, Hyatt AW, Lohr J, Prater R, and Strait EJand MR Wade. Complete suppression of the m = 2/n = 1 neoclassical tearing mode using electron cyclotron current drive in DIII-D. *Nucl. Fusion* **44**, 243 (2004).

Pletzer A and Perkins FW. Stabilization of neoclassical tearing modes using a continuous localized current drive. *Phys. Plasmas* **6**, 1589 (1999).

Poli E, Peeters AG, and Pereverzev GV. TORBEAM, a beam tracing code for electron-cyclotron waves in tokamak plasmas. *Comp. Phys. Comm.* **136**, 90 (2001).

Prater R. Heating and current drive by electron cyclotron waves. *Phys. Plasmas* **11**(5), 2349 (2004).

Prater R et al. Benchmarking of codes for electron cyclotron heating and electron cyclotron current drive under ITER conditions. *Nucl. Fusion* **48**, 035006 (2008).

Ramponi G, Farina D, Henderson MA, Poli E, Saibene G, and Zohm H. ITER ECRH-ECCD system capabilities for extended physics applications. *Fusion Sci. Tech.* **52**, 193 (2007).

Ramponi G, Farina D, Henderson MA, Poli E, Sauter O, Saibene G, Zohm H, and Zucca C. Physics analysis of the ITER ECW system for optimized performance. *Nucl. Fusion* **48**, 054012 (2008).

Rutherford PH. Nonlinear growth of tearing mode. *Phys. Fluids* **16**(11), 1903 (1973).

Sauter O, Henderson MA, Ramponi G, Zohm H, and Zucca C. On the requirements to control neoclassical tearing modes in burning plasmas. *Plasma Phys. Control. Fusion* **52**, 025002 (2010).

Sauter O et al. Beta limits in long-pulse tokamak discharges. *Phys. Plasmas* **4**(5), 1654 (1997).

Shimada M et al. Progress in the ITER physics basis. *Nucl. Fusion* **47**, s1 (2007).

Urso L. *Modelling and experiments on NTM stabilisation at ASDEX Upgrade*. PhD thesis, Ludwig-Maximilians-Universität München, 2009.

Urso L, Zohm H, Isayama A, Maraschek M, Poli E, ASDEX Upgrade Team, and JT-60 Team. ASDEX Upgrade–JT-60U comparison and ECRH power requirements for NTM stabilization in ITER. *Nucl. Fusion* **50**, 025010 (2010).

Wesson J. *Tokamaks*. Oxford University Press, third edition, 2004.

Westerhof E. Tearing mode stabilization by local current density perturbations. *Nucl. Fusion* **30**(6), 1143 (1990).

Westerhof E et al. Tearing mode stabilization by electron cyclotron resonance heating demonstrated in the TEXTOR tokamak and the implication for ITER. *Nucl. Fusion* **47**, 85 (2007).

Yu Q, Zhang XD, and Günter S. Numerical studies on the stabilization of neoclassical tearing modes by radio frequency current drive. *Phys. Plasmas* **11**, 1960 (2004).

Zohm H, Heidinger R, Henderson MA, Poli E, Ramponi G, Saibene G, and Verhoeven AGA. Comparison of the performance of different options for the ITER ECRH Upper Launcher. *J. Phys.: Conf. Ser.* **25**, 234 (2005).

7 Conclusions and Outlook

This thesis addresses the stabilization of (neoclassical) tearing modes by localized heating and current drive. The problem has a significant relevance for the stability of a plasma and for the performance of a future fusion reactor. The theoretical modeling was based on the generalized Rutherford equation (GRE), describing the time evolution of the magnetic island. This equation is derived by matching a linear exterior solution of the helical flux perturbation to an equation for the interior solution obtained by averaging the diffusion equation for the helical current perturbation over the interior region. The GRE allows a detailed study of the effect of ECRH and ECCD on the tearing mode evolution and accurate predictions concerning the power requirements for full suppression. In the following section the results of the thesis are reviewed. In the last part of the chapter possible future developments in both model development and experimental validation are commented.

7.1 Conclusions

This section follows closely the structure presented in the introduction to this thesis, where a number of questions have been raised on each of the topics treated in the dissertation. In the first place, the comparison of the stabilizing contributions of the local heating and the current drive has been addressed aiming at a further understanding of the model. The study has first been performed under the "customary" approximations for the island topology (Chapter 4) while in a second step an extension to a generalized, asymmetric topology has been made (Chapter 5). Chapter 6 is devoted to the requirements for the full suppression of the mode. The resulting predictions are found to be in reasonable agreement with the existing experimental data. The application to ITER resulted in particular recommendations for improvements of the ECRH system design.

About the merits of localized heating and current drive

Localized heating and current drive are acknowledged to stabilize NTMs by generating a current perturbation either inductively, through a temperature perturbation (ECRH), or non-inductively by direct current drive (ECCD). Experimental measurements have shown that the heating is the dominant effect for medium size limiter tokamaks (TEXTOR, T-10) while the ECCD appears to be more effective for mid-to-large size divertor tokamaks (AUG, DIII-D, JT-60). This has motivated the study of the relative merits of ECCD and ECRH as performed in Chapter 4, with the results as reported below.

- To determine the relevant merits of ECCD and ECRH, the contributions to the Rutherford equation of ECCD and ECRH are described with a parallel structure: they are written as the product a common fore-factor, a current generation efficiency $\eta_{CD,H}$, and a geometrical factor $F_{CD,H}$. The current generation efficiency

represents the efficiency with which the EC power is converted into a current either non-inductively, by driving a current directly, or inductively, trough a temperature perturbation. The geometrical factor depends on the NTM width and the deposition properties, namely the power deposition width w_{dep}, the relative location x_{dep} with respect to the rational surface and the modulation duty cycle, D (in chapter 6 referred to as D_{mod}). It is shown that F_{CD} is larger than F_{H}, for $w/w_{\mathrm{dep}} < 2$, while F_{H} is the largest in the region where $w/w_{\mathrm{dep}} > 2$. The product $\eta_{\mathrm{CD,H}}F_{\mathrm{CD,H}}$ determines the efficiency of current drive and heating for each tokamak experiment.

- For small-medium size tokamaks like TEXTOR or T-10, the current generation efficiency η_{CD} is found to be of the same order as η_{H}. As a consequence the relative merits of ECCD and ECRH are determined only by $F_{\mathrm{CD,H}}$. Since the size of a typical magnetic island is of the same order or larger than the deposition width these modes fall in the (dynamical) range where ECRH is found to be dominant. ASDEX-Upgrade shows an intermediate behavior, where localized heating can still play a role for large islands.

- The case of large tokamaks like ITER is generally characterized by $\eta_{\mathrm{CD}} \gg \eta_{\mathrm{H}}$. As a consequence, even when $w > 2w_{\mathrm{dep}}$, localized heating is predicted to play a marginal role.

- The appendix of chapter 4 shows the application of the results to the TEXTOR experiments on tearing mode suppression by ECRH and ECCD. It is shown that the model is generally in good agreement with the experimental data. In particular, the modeling confirms that the dominant stabilizing mechanism in TEXTOR comes from the heating. One aspect not explained by the current model is the asymmetric response of the island suppression to a radial mismatch of the power deposition. The contribution of the non-inductive driven current on the linear stability, or the eventual modification in the magnetic equilibrium owing to the heating outside the island might explain this non-symmetric trend.

Asymmetries of islands and their impact on the GRE

The experimental evidence for asymmetric islands found in several experiments performed in AUG, DIII-D, JT-60 and in TEXTOR motivated the extension of the model presented in chapter 5. This was achieved by relaxing the basic assumptions which are leading to the well known symmetric shape for the magnetic island in a plasma slab. In addition, the consequences for the island geometry of a number of effects such as a finite flow shear and a finite temperature gradient across the island have been considered. The resulting asymmetric mode has been studied in order to determine the role of asymmetries in the growth and suppression of neoclassical tearing modes, with particular attention to the local current drive (ECCD) and resonant heating (ECRH) terms. A comparison is made with existing literature in which unexpectedly large effects of these asymmetries are claimed. The outcome of this work can be summarized as follows:

- The topology of a tearing mode can be deformed by considering a finite third order term in the unperturbed flux function or a quasi-linear correction to the constant-ψ approximation. Both effects break the up-down symmetry of the mode leading to an "amplitude deformation". When the shear flow and the temperature gradient across the island are considered, a phase shift proportional to the radial excursion from the resonant surface is produced [Ren et al., 1999; Smolyakov et al., 2001; van der Plas and de Blank, 2007]. As a consequence of the deformation in the island topology, the Rutherford equation must be modified consistently as shown in equation (5.4).

- The effect of the asymmetries on the evolution of an NTM appears to be mostly negligible. This is found to be valid for the coefficients g_1 and c_{neo} appearing in the generalized Rutherford equation 5.18 and for the stabilizing contributions provided by electron cyclotron waves to neoclassical tearing modes. It is shown that phase shifts over the island do not affect the stabilizing terms from ECCD and ECRH in case of CW power application. Also the effect on the island width of an up-down asymmetry is small, except that the consequences of a radial mismatch change in a predictable way: on the side of the larger island width the ECCD and ECRH terms are less sensitive to the effects of a radial displacement of the power deposition.

- A significant reduction of the efficiency for NTM stabilization by ECCD in case of an up-down asymmetric island size was claimed in [Urso et al., 2010], while in [Lazzaro and Nowak, 2009] this efficiency was even shown to become negative in case of a finite phase shift and an island much smaller than the EC deposition width. It could be shown that the former claim is based on an improper comparison between the asymmetric and symmetric cases as made in [Urso et al., 2010], while the latter conclusion was a numerical artifact, due to incorrect approximations.

The requirements for full suppression of NTMs

The requirement for full NTM suppression is often described in the literature with the ratio of the maximum driven current density over the bootstrap current density at the rational surface, $\eta_{\text{NTM}} = j_{\text{CD}}/j_{\text{BS}}$. Theoretical calculations give $\eta_{\text{NTM}} > 1.2$ as the criterion for complete NTM suppression. Experimentally, complete suppression was reached for $0.3 \lesssim \eta_{\text{NTM}} \lesssim 3$. This large variation motivated a systematic study of the requirement for full NTM suppression as reported in Chapter 6. An analytical expression for η_{NTM} has been obtained from the GRE, depending only on the saturated island width w_{sat} and on the power deposition width w_{dep}, both normalized to the marginal island size w_{marg}. A new criterion for the full suppression of the mode is formulated by means of an analysis of η_{NTM} over the full parameter space. An application of this criterion to ITER suggests that a further optimization of the ITER ECRH system is possible. The main findings of this study are listed below.

- The results show a strong dependence of η_{NTM} on the normalized power deposition width, $\bar{w}_{\text{dep}} = w_{\text{dep}}/w_{\text{marg}}$, which has led to the conclusion that a more

appropriate criterion is based on a combination of $\bar{w}_{\mathrm{dep}}$ and $\bar{w}_{\mathrm{dep}}\eta_{\mathrm{NTM}}$. In particular, for large saturated island sizes ($\bar{w}_{\mathrm{sat}} > 7$) a minimum required value for $\bar{w}_{\mathrm{dep}}\eta_{\mathrm{NTM}}$ has been found close to two, with $\bar{w}_{\mathrm{dep}} \lesssim 2$. For moderate saturated island sizes ($\bar{w}_{\mathrm{sat}} < 7$) the minimum value for $\bar{w}_{\mathrm{dep}}\eta_{\mathrm{NTM}}$ has been found to be close to unity, with $\bar{w}_{\mathrm{dep}} \lesssim 1$. A further decrease of power deposition width does not lead to any significant reduction of the required driven current. Increasing $\bar{w}_{\mathrm{dep}}$ however, leads to a rapid increase of the required driven current. A smaller value of $\bar{w}_{\mathrm{sat}}$ implies generally a lower required current.

- As anticipated in the introduction to this subsection, the available experimental estimates of η_{NTM} from various tokamaks are rather different. A value of $\eta_{\mathrm{NTM}} = 0.3 - 0.6$ with saturated island sizes in the range of $\bar{w}_{\mathrm{sat}} = 2 - 3$ was reported for JT-60U and AUG, while for DIII-D $\eta_{\mathrm{NTM}} = 2 - 3$ with $\bar{w}_{\mathrm{sat}} = 4$ – 5 is calculated. Note that these experiments all occupy a similar position in the parameter space defined by the normalized saturated island size and deposition width. The predictions from the present analysis are in agreement with the observations from JT-60U and AUG, whereas for DIII-D the value for η_{NTM} is found to be considerably smaller than the experimental estimate.

- Application of the analysis to ITER points out that the focus of the ITER ECRH system design optimization on only the η_{NTM} criterion has led to an over-focused power deposition in particular when the lower steering mirror is exploited. Our analysis shows that the optimization towards a minimum power requirement for NTM suppression requires an increase of the toroidal injection angle for the lower steering mirror of $4°$ from its present design value of $\beta = 18°$ to the optimum value of $\beta = 22°$. The current design value of $\beta = 20°$ is a good optimum for the upper steering mirror.

7.2 Outlook

The Generalized Rutherford Equation as provided in this thesis, can describe the nonlinear island evolution as observed in the experiments, at least qualitatively, reasonably well. This makes the GRE well suited for modeling in the context of the design of feedback control loops for NTMs. From the point of view of the physics, a number of interesting effects neglected in the GRE, still require further investigations. The examination of merits and limits of this approach, leads to outline a few questions that might represent the most immediate future developments in relation to this thesis. The most immediate extension in the theoretical modeling is possibly the study of the time dependency of ECCD and ECRH.

Further improvements in the understanding of the NTM stabilization might require a more critical review of the theory. In the first place the GRE is generally applied in regimes where the basic assumptions underlying the model are questionable. This occurs in the limit of large islands where the width is comparable to the resonant radius so that the "small amplitude" and the constant-ψ approximations do not hold, or in the limit of

small islands, where a number of poorly understood effects (as described in chapter 3), can play a significant role. In addition the Rutherford equation neglects effects related with toroidicity and any other feature far from the resonant surface. A second problem is related to the experimental uncertainty concerning some important parameters such as the bootstrap current density, the driven current density and the power deposition width. The lack of accurate estimations and of a careful error analysis results in a problematic validation of the existing model. The combination of these two issues makes it rather difficult to discriminate whether discrepancies observed between GRE predictions and experimental measurements is due to a lack in the physics described by the model or can be understood as being due to the experimental uncertainties. From this argument, the future developments in the topic might probably follow two directions. From a experimental point of view, in the regime where the basic assumptions are satisfied, the GRE can still provide important predictions, with a particular attention to the power requirement for the full NTM suppression. In this regime, a detailed error analysis might be relevant for the validation of the model. From a numerical point of view, the limits in the validity of the GRE might be benchmarked with 3D non-linear MHD simulations accounting for a more complete description of the mode stability. In the following, a more detailed description of these future challenges is presented.

Time dependence of the ECCD and ECRH terms in the Rutherford equation

A further extension of the model concerning the ECCD and ECRH terms in the GRE appears of particular interest. According to the present model, the time scale for the mode rotation τ_{rot} is assumed to be much shorter than both the collision time τ_{col} and the typical time scale for the evolution of the mode τ_{isl}. As a consequence, the effect of the driven current and the localized heating can be averaged over a rotation period. When the last is comparable to the collision time (the time scale for the generation and decay of the driven current), a variation of Δ'_{CD} is expected owing to the fluctuation of the generated current. This fluctuation averages out as long as the NTM evolution is slow compared to the rotation period. When this approximation does not hold the evolution of the mode will be affected.

Experimental benchmark of GRE and η_{NTM}

A glance at the recent literature indicates a general interest towards an experimental benchmark of the GRE aiming to achieve accurate predictions of the required power to achieve full NTM stabilization. The current status of benchmarking of the GRE against experiments [La Haye et al., 2006b; Sauter et al., 2010; Urso et al., 2010], consists of the fitting of individual terms in the GRE, to experimental data from different tokamaks. This is generally used to extrapolate, using the fitted coefficients to the conditions for ITER stability. As explained in chapter 6, this method does not properly distinguish between uncertainties in the physical quantities appearing in these terms, such as the bootstrap current density or the driven current and its profile width, and the uncertainties in the geometric coefficients appearing in front of these terms in the GRE. As a consequence,

although this method might provide a qualitative benchmark to the Rutherford equation, it cannot be considered a consistent validation of the theoretical model. The analytical expression for η_{NTM}, as proposed in chapter 6, being unaffected by the theoretical uncertainties related with the geometrical coefficients, is thought to be a more appropriate solution. An experimental benchmark of this expression, especially in the ITER relevant region, might therefore be an interesting road to follow.

Benchmark of the GRE with a fully non-linear resistive MHD code

Another interesting development might address the limits in the validity of the GRE, obtained by comparing the model with the predictions of a non-linear MHD code. Such a code solves for every time step the reduced resistive MHD equations accounting for the correct helical flux function and the toroidal geometry of the tokamak. This tool opens the possibility to focus on the transition between the linear and the non-linear regime in the evolution of a tearing mode. The further implementation of a localized current and a temperature perturbation related with an external source, are expected to simulate the effect of ECCD and ECRH. In the range of validity of the Rutherford equation, it is interesting to stress that the benchmark proposed is twofold: it is meant at the same time to be a benchmark of the non-linear MHD code in the range where the approximations underlying the derivation of the GRE are verified and a study of the limits of the Rutherford model.

References

La Haye RJ, Prater R, Buttery RJ, Hayashi N, Isayama A, Maraschek ME, Urso L, and Zohm H. Cross-machine benchmarking for ITER of neoclassical tearing mode stabilization by electron cyclotron current drive. *Nucl. Fusion* **46**, 451 (2006b).

Lazzaro E and Nowak S. ECCD control of dynamics of asymmetric magnetic islands in a sheared flow. *Plasma Phys. Control. Fusion* **51**, 035005 (2009).

Ren C, Chu MS, and Callen JD. Magnetic island deformation due to sheared flow and viscosity. *Phys. Plasmas* **6**, 1203 (1999).

Sauter O, Henderson MA, Ramponi G, Zohm H, and Zucca C. On the requirements to control neoclassical tearing modes in burning plasmas. *Plasma Phys. Control. Fusion* **52**, 025002 (2010).

Smolyakov AI, Lazzaro E, Azumi M, and Kishimoto Y. Stabilization of magnetic islands due to the sheared plasma flow and viscosity. *Plasma Phys. Control. Fusion* **43**, 1661 (2001).

Urso L, Zohm H, Isayama A, Maraschek M, Poli E, ASDEX Upgrade Team, and JT-60 Team. ASDEX Upgrade–JT-60U comparison and ECRH power requirements for NTM stabilization in ITER. *Nucl. Fusion* **50**, 025010 (2010).

van der Plas EV and de Blank HJ. Temperature gradients in fast collisionless magnetic reconnection. *Phys. Rev. Lett.* **98**, 265002 (2007).

List of publications

Journal papers

[1] On the merits of heating and current drive for tearing mode stabilization
D. De Lazzari and E. Westerhof
Nucl. Fusion **49**, 075002 (2009). Erratum: Nucl. Fusion **50**, 079801 (2010)

[2] A closed loop control system for stabilization of MHD events on TEXTOR
B.A. Hennen, E.Westerhof, J.W. Oosterbeek, P.W.J.M. Nuij, D. De Lazzari, G.W. Spakman, M. de Baar, M. Steinbuch, and the TEXTOR team
Fusion Eng. Des. **84**, 928 (2009)

[3] The role of asymmetries in the growth and suppression of neoclassical tearing modes
D. De Lazzari, and E. Westerhof
Plasma Phys. Control. Fusion **53**, 035020 (2011)

[4] Modeling of tearing mode suppression experiments in TEXTOR based on the generalized Rutherford equation
B. Ayten, D. De Lazzari, M.R. de Baar, B.A. Hennen, E. Westerhof and the TEXTOR Team
Nucl. Fusion **51**, 043007 (2011)

[5] Requirements on localized current drive for the suppression of neoclassical tearing modes
N. Bertelli, D. De Lazzari, E. Westerhof
Submitted to *Nucl. Fusion*

Conference proceedings

[1] ECRH experiments on tearing mode physics at TEXTOR
E. Westerhof et al.
In *proceedings of the 15th Joint Workshop on Electron Cyclotron Emission and Electron Cyclotron Resonance Heating (EC-15)*, p104 (2008)

[2] Physics and real time control of tearing modes in TEXTOR
M.R. de Baar, E. Westerhof, W.A. Bongers, I.G.J. Classen, C. Domier, A.J.H. Donné, B.A. Hennen, G.M.D. Hogeweij1, R.J.E. Jaspers, A. Lazaros, D. De Lazzari, N.C. Luhmann Jr., P.W.J.M. Nuij, J.W. Oosterbeek, H.K. Park, F.C. Schüller, G.W. Spakman, M. Steinbuch, and the TEXTOR-Team
In *proceedings of the 22nd IAEA Fusion Energy Conf.*, Ex p9-12 (2008)

[3] On the merits of heating and current drive for tearing modes stabilization
D. De Lazzari, E. Westerhof, B. Ayten and the TEXTOR team

In *proceedings of the 36th EPS Conference on Plasma Physics*, Vol.**33E**, P-1.124 (2009)

[4] A closed loop control system for stabilization of MHD events on TEXTOR
B.A. Hennen, E.Westerhof, J.W. Oosterbeek, P.W.J.M. Nuij, D. De Lazzari, G.W. Spakman, M. de Baar, M. Steinbuch, and the TEXTOR team
In *proceedings of the 25th Symposium on Fusion Technology (SOFT-25)*, (2009)

[5] Feedback control of tearing modes through ECRH with launcher mirror steering and power modulation using a line-of-sight ECE diagnostic
B. Hennen, E. Westerhof, P. Nuij, B. Ayten, M. de Baar, W. Bongers, A. Bürger, D. De Lazzari, H.Oosterbeek, D.Thoen, M. Steinbuch and the TEXTOR team
In *proceedings of the* 16*th Joint Workshop on Electron Cyclotron Emission and Electron Cyclotron Resonance Heating (EC*-16*)*, (2010)

[6] Simulation of tearing mode suppression experiments in TEXTOR based on the generalized Rutherford equation
B. Ayten, D. De Lazzari, M.R. De Baar, B. Hennen, E. Westerhof, and the TEXTOR Team
In *proceedings of the* 37*th EPS Conference on Plasma Physics*, (2010)

Contributions to conferences, workshops

[1] Modeling of NTM Stabilisation by ECCD
D. De Lazzari, E. Westerhof
Poster at the 20th NNV/CPS Symposium on Plasma Physics and Radiation Technology, 4-5 March 2008, Lunteren (The Netherlands)

[2] Implementing RF heating and current drive in NTM models
D. De Lazzari, B. A. Hennen, E. Westerhof
Oral presentation at the working session of EFDA Integrated Modelling Taskforce (ITM), 16-18 April 2008 Culham, Abingdon (UK)

[3] On merits of heating and current drive for tearing mode stabilization
D. De Lazzari, E. Westerhof
Oral presentation at the US-Japan Workshop on MHD Control, Magnetic Islands and Rotation, 23-25 November 2008, Austin (Texas)

[4] Modeling of magnetic islands stabilization by electron cyclotron waves
D. De Lazzari, E. Westerhof
Poster at Physics@FOM, 20-21 January 2009, Veldhoven (The Netherlands)

[5] Stabilization of magnetic islands in fusion plasmas by localized heating and current drive
D. De Lazzari, E. Westerhof

Oral presentation at the 21st NNV/CPS symposium on Plasma Physics and Radiation Technology, 3-4 March 2009, Lunteren (The Netherlands)

[6] The role of asymmetries in the growth and suppression of neoclassical tearing modes
D. De Lazzari, E. Westerhof
Poster presentation at the Theory of fusion plasmas Joint Varenna -Lausanne international workshop, August 30 - September 3, 2010, Varenna, Italy

[7] Requirements for the suppression of neoclassical tearing modes
N. Bertelli, D. De Lazzari, and E. Westerhof
Poster presentation at the 23st NNV/CPS symposium on Plasma Physics and Radiation Technology, 15-16 March 2011, Lunteren (The Netherlands)

[8] Requirements for the suppression of neoclassical tearing modes
N. Bertelli, D. De Lazzari, and E. Westerhof
Oral presentation at the Workshop on Control of burning plasma 21-25 March 2011, Lorentz Center, Leiden (The Netherlands)

[9] Suppression of neoclassical tearing modes: the limits of the model
N. Bertelli, D. De Lazzari, and E. Westerhof
Poster presentation at the Workshop on Advanced Magnetohydrodynamics 11-15 April 2011, Lorentz Center, Leiden (The Netherlands)

Summary

Stabilization of magnetic islands in tokamaks by localized heating and current drive

This thesis deals with the theory of active stabilization of the so-called Neoclassical Tearing modes (NTMs) in fusion reactors. Hot fuel, in the form of a fully ionized gas (referred to as "plasma"), is confined by a magnetic field with the topology of toroidally nested magnetic surfaces. The NTM is a spontaneous break of this magnetic configuration, leading to a non-symmetric topology characterised by a chain of magnetic islands. Within a magnetic island temperature and pressure are flattened. The NTM onset occurs when the plasma pressure exceeds a certain limit. Since the fusion power is proportional to the pressure squared, NTMs limit the performance of the reactor. Active stabilization of such instabilities can yield an enhanced performance of the fusion reactor of up to 50%. For this reason, it is important to study the mechanisms responsible for their growth and achieve a reliable control strategy.

Control and suppression of NTMs is achieved experimentally by depositing highly localized radio-frequency power, in the range of electron cyclotron frequency (EC), at the island location. Qualitatively, the effect of the localized EC power on magnetic islands is twofold: it makes the island formation more difficult, and it compensates for the effect of the temperature flattening inside the island region by a local increase of the temperature and by inducing a current inside the island. These effects are referred to as Electron Cyclotron Resonance Heating (ECRH) and Electron Cyclotron Current Drive (ECCD), respectively.

The thesis addresses the stabilizing contribution of ECRH and ECCD, on the temporal evolution of a magnetic island. This model relies on the equation for the evolution of the magnetic island width, the generalized "Rutherford" equation (GRE), which depends on the different driving and stabilizing mechanisms.

There are three main open questions that this work tries to answer: the relative merits of ECRH and ECCD, the role of asymmetries in the magnetic island topology and finally the determination of a criterion for full NTM suppression.

The research focused at first on the relative merits of each method. The conditions determining the relative importance of ECRH and ECCD are found to depend on the product of two factors, the efficiency with which ECRH or ECCD generates a current inside the magnetic island and a geometrical factor showing essentially different scalings for either ECRH or ECCD. For a fusion reactor like ITER the main stabilizing mechanism for a magnetic island is found to be the ECCD, while ECRH becomes relevant in smaller devices.

In the following step an extension of the model allowed to treat asymmetries in the island shape and to discuss their effect on the ECCD and ECRH contribution to the island evolution. This study demonstrates that these deformations have a small or negligible impact on the tearing mode evolution. Opposing claims in the existing literature could be shown to be based on inappropriate approximations or comparisons.

The last part of the thesis is devoted to the determination of the requirements for the suppression of a magnetic island. This is usually described by the parameter η_{NTM}, defined as the ratio between the local driven current density, responsible for the stabilization of the mode and the local bootstrap current density, the drive of the NTM instability. An extensive analysis allowed to formulate a general criterion for the full NTM suppression in the form of a combined criterion for the maximum allowed width of the EC power density profile and a minimum required EC driven current. The results of this analysis have been used to suggest an improvement of the design of ITER-ECRH system. A moderate increase of the angle with which EC waves are injected into the plasma of up to $5°$ from its present design value is shown to reduce the power requirement by up to 25%.

In conclusion, the theoretical work presented in this thesis has provided a comprehensive analysis of the stabilization of a magnetic island by means of the localized heating and driven current. The proposed model verifies and improves criteria for the design of ITER-ECRH system. Finally, it provides a sound theoretical basis for the design of NTM feedback control loops.

Acknowledgements

The research for this thesis was done with the support of a large number of people. In this section I would like to take the opportunity to thank all of them.

First and foremost I would like to thank my promotor, Niek Lopes Cardozo. His original point of view and the suggestions he provided me made a considerable contribution to the thesis. I am also grateful to my second promotor, Wim Goedheer, for the useful discussion and remarks. This thesis would not have been possible without the careful, patient support of Egbert Westerhof. He has been my direct supervisor in this project and has helped me understanding the physics of magnetic islands and their stabilization. Furthermore he was of great value in correcting and improving papers and finally this thesis.

I would like to thank the Core Committee for carefully reading the manuscript and sharing their comments and suggestions. In particular, I would like to thank Marco de Baar, whose remarks substantially improved the first two chapters of this thesis. Also I would like to extend my gratitude to Guido Huysmans for the time spent during my visit in CEA Cadarache. I wish I could have given a larger contribution to his project.

I am convinced that doing research as a team effort is a more stimulating, fruitful and funny work. For this reason I would like to thank Bart Hennen, Bircan Ayten and Nicola Bertelli for the opportunity to collaborate with them. With respect to the thesis, I am also grateful to Jan-Willem Blockland for the useful discussions and for the help in the layout of the manuscript.

During the first 18 months of my project in Jülich Forschungszentrum, I experienced a very friendly environment. A large contribution to this atmosphere was due to Tony Donné, who could keep the entire group around the table by telling great "on the road stories". At the same time I cannot forget the humor (and the suggestions) of my former mentor, Roger Jaspers, who was asking me how many papers I had published, approximately every three months. During the following year, this turned out to be a useful "approach" to my project. I would like to thank as well Geert Willem Spakman, Ephrem Delabie, Johan Oosterbeek, Andreas Bürger, Jurrian Boom and Jarich Konig for the nice conversations during lunch and coffee breaks.

At the end of 2009 I left my secondment to "turn back" to Rijnhuizen. During this moving I have been helped by Karijn Heling and Peggy Reimus in the "impossible mission" of finding a new apartment in Utrecht. I would like to thank both of them. At FOM-Rijnhuizen I had a couple of nice surprises. At first I discovered to be settled in the most beautiful office I could imagine, in the heart of Rijnhuizen castle. Secondly I soon met a number of nice, crazy PhD fellows, Jakub Zielinski, Kiril Bystrov and Alexey

Kuznetsov. In their company I spent a number of coffee breaks and learned how "to get properly messy".

It is a great feeling to realize that, wherever you go, you have the possibility to make a lot of friends. Among the Jülich crew I would like to mention Rosanna, Giuseppe, Greta, Alex, Eylem and Lidiya. Thank you for all the enjoyable time we had together. In Utrecht I had the pleasure to meet many nice people. Among them I want to thank two good friends, "Il Maestro Sbrizzi" and "Lo Sgubo". A special thanks goes to Gergana. You are the first person I have met in the UC campus and still one of my closest friends. I would like finally to thank all the "old" Italian friends. Thank you because every time I enter the usual pub at the usual time, I feel at home.

To conclude these acknowledgments I would like to show my gratitude to a few people which have a particular part in this adventure. In first place I would like to thank Nicola Bertelli, an outstanding researcher and an excellent friend, who accompanied me during most part of my work at FOM. I deeply appreciate your commitment and I learned a lot from our long, sometimes animated, discussions. Secondly I would like to thank Monica for her patience and the support she gave me in the last period of my thesis. You are certainly the most beautiful thing that happened to me since last year. Most importantly, this thesis is dedicated to my family, both nearby and far away. Thank you for having supported me in a number of ways, throughout all my life. You are with me, always.

Curriculum vitae

Diego De Lazzari was born on 26 June 1981 in Treviso, Italy. After having achieved the "Maturitá Scientifica" in 2000 at Liceo Scientifico "G. Berto" in Mogliano Veneto, Italy, he studied at Padova University, Italy where he graduated as M.Sc. in Physics in 2005. The Master project was held at the Laboratoire de Physique des Interations Ioniques et Moléculaires, "Université de Provence, on "Study of a diagnostic based on Lamb Shift Radiation to measure the local electric field in a plasma". In June 2007 he started a PhD project at FOM-Institute for Plasma Physics Rijnhuizen of which the results are presented in this dissertation. The first part of the project, until December 2009, was carried out at the Institut für Plasmaphysik, Forshungszentrum Jülich, Germany.